pH-Sensitive Core-Shell Nanoparticles for Intracellular Drug Delivery

By
Yuhua Hu

M. S. in Chemical Engineering Practice
Massachusetts Institute of Technology, 2003

M. S. Biochemical Engineering
Tsinghua University, 2001

B. S. Chemical Engineering
Tsinghua University, 1999

SUBMITTED TO THE DEPARTMENT OF CHEMICAL ENGINEERING IN PARTIAL FULFILLMENT OF THE REQUIREMENTS FOR THE DEGREE OF DOCTOR OF PHILOSOPHY IN CHEMICAL ENGINEERING
AT THE
MASSACHUSETTS INSTITUTE OF TECHNOLOGY

JUNE 2008

Signature of Author_____
Department of Chemical Engineering
April 10th, 2008

Certified by_____
Darrell J. Irvine
Eugene Bell Career Development Associate Professor in Tissue Engineering
Thesis Supervisor

Certified by_____
Patrick S. Doyle
Associate Professor of Chemical Engineering
Thesis Supervisor

Accepted by_____
William M. Deen
Carbon P. Dubbs Professor of Chemical Engineering
Chairman, Committee for Graduate Students

pH-Sensitive Core-Shell Nanoparticles for Intracellular Drug Delivery

By
Yuhua Hu

Submitted to the Department of Chemical Engineering
on June, 2008 in Partial Fulfillment of the Requirements for the
Degree of Doctor of Philosophy in Chemical Engineering
at The
Massachusetts Institute of Technology

ABSTRACT

Therapeutics such as proteins, DNA, or siRNA, can only exert their function in the cell cytosol or nucleus. However, most of them are cell membrane impermeable molecules that can only be taken up by cells via endocytosis or phagocytosis. Such drug molecules are thus confined in endolysosomes, where reduced pH and degradative enzymes may destroy them without therapeutic gain. Efficient escape of drug molecules to the cytosol before destruction in endolysosomes is a major challenge for intracellular drug delivery. To address this issue, we designed a pH-sensitive core-shell nanoparticle to segregate the functions of the particle into an endosome-disrupting pH-responsive core that would absorb protons at endolysosomal pH, and a shell whose composition could be tuned to facilitate particle targeting, cell binding, and drug binding.

Two-stage surfactant-free emulsion polymerization of 2-diethylamino ethyl methacrylate (DEAEMA) (core) and 2-amino ethyl methacrylate (AEMA) (shell) in the presence of a crosslinker was used for the synthesis of monodisperse core-shell hydrogel nanoparticles of 200 nm in diameter. The protonation of tertiary amine groups on the polyDEAEMA core on moving from extracellular to endolysosomal pH resulted in reversible swelling of the nanoparticles with a 2.8-fold diameter change.

With the aid of pH-sensitivity of these nanoparticles, efficient cytosolic delivery of calcein (with ~95% efficiency) was achieved by disrupting endolysosomes via proton sponge effect. The primary amine rich shell was found to facilitate cell and drug binding, and provided negligible cytotoxicity by sequestering the proton sponge component from any direct interactions with cells. These particles demonstrated a useful means to deliver therapeutic molecules to the cytosol of cells of interest efficiently. The applications of nanoparticles showed significant improvement in delivering a model antigen vaccine protein ovalbumin (OVA) to primary dendritic cells for T cell activation, and promising knockdown of mRNA by delivering siRNA to epithelial cells for gene silencing.

To extend this approach to a fully biodegradable system, nanoparticles with a cleavable crosslinker bis (acryloyl) cystamine (BAC) were synthesized. Preliminary explorations of this approach showed that such particles can degrade in the presence of glutathione *in vitro*, a reducing peptide present at mM concentrations in the cytosol of mammalian cells. This design could potentially serve as a drug releasing mechanism to further improve delivery efficiency.

Thesis Supervisor: Darrell J. Irvine
Title: Eugene Bell Career Development Associate Professor in Tissue Engineering
Thesis Supervisor: Patrick S. Doyle
Title: Associate Professor of Chemical Engineering

Acknowledgments

I would like to express my heartfelt gratitude to the many supportive people at MIT, without whom this thesis would not have been possible.

First, I wish to thank my advisor, Professor Darrell J. Irvine, whose endless enthusiasm and creative ideas are my constant source of energy and confidence. I would like to acknowledge my co-advisor, Professor Patrick S. Doyle, for his great help and support for my staying in the Chemical Engineering Department. I am very grateful to my thesis committee members, Professor Paula T. Hammond, Professor K. Dane Wittrup, and Dr. Richard C. Mulligan, for their numerous suggestions and helpful advice.

I must not forget the undergraduate students Tamara Litwin, Joshua Kutz, and Arpun Nagarasa, for their interest and direct contributions to this project on the nanoparticle synthesis and degradation studies. I would also like to acknowledge the fellow graduate students in the Immunobioengineering Lab: Brandon Kwong, for his professional training in OT I T cell priming assay and ELISA assay, and friendly collaboration in the animal facilities; Anna Bershteyn, for her helpful technical support in CryoEM images; Yana Wang, for her generous sharing in human blood isolation work with many detailed and useful discussions; Yuki Hori, Vinay Mahajan, Bonnie Huang, Cathy Huang, for their great collaboration and sharing of cell lines; Maria Foley, Marc Natter, Xingfang Su, and previous group members Dr. Yen-chen Huang, Dr. Junsang Doh, Dr. Siddhartha Jain, and Dr. Agnieszka N. Stachowiak for

their helpful discussions and suggestions. I feel very grateful to have our lab manger Sheree Beane and secretary Jazy Ma, who frequently went out of their way to help me with organizational difficulties.

In this project, Nicki Waston from the Whitehead Institute performed professional service on TEM; Kazuyoshi Murata from the WI-MIT BioImaging Center helped to obtain CryoEM images with high quality; and Dr. James L. Liu from the Cancer Research Center provided supportive collaboration in the siRNA delivery studies. I would like to express my thanks to all of them for their direct contributions to this thesis.

MIT's life could be sometimes stressful and tough, with all the competitiveness and perfectionism. Luckily, I have had extensive care, support, and help from my family and friends, who shared with me many wonderful and unforgettable moments throughout my time here. I would like to devote this thesis to them with my sincere gratitude.

Ying Cao was my roommate at Tang Hall when I arrived at MIT in summer 2001. Since then, we have established a lifelong friendship that many might envy. In the past seven years, she has put up with all my frustration and emotion, and has provided me endless support and encouragement. I cannot express how grateful I am for having a friend like her. I would also like to thank many of my Chinese friends, Hong He, Dalong Shi, Chang Li, Xiaowei He, Jing Zhou, Jie Lu, and Jacky Liang. With them I shared the first journey to the United States, as well as the sadness of leaving our lovely home and country. With them I shared the excitement of

exploring a new life at MIT, the difficulties of surviving in a totally new culture and society, and the happiness of many achievements and accomplishments. I would like to express my gratitude to all my other Chinese friends and the Chinese community here at MIT and Boston for giving me numerous support and help during my stay here.

I had a lot of fun hanging out with my classmates and friends from Chemical Engineering Department. In particular, I would like to mention Joanna Yu, Ramin Haghgooie, and Mike Rappel, with whom I went to practice school together in summer 2002; Daryl Powers and Anna Pisania, with whom I worked in the same lab for about two years; and Wanda Lau, who I met through Mike and went to many memorable events together. Their friendship accompanied my life here at MIT.

I would also like to thank all the friends I have met in different clubs and activities: the Chinese Student and Scholar Association, the MIT Rowing Club, the MIT Figure Skating Club, the Student Arts Association, the MIT Outing Club, the Boston Dragon Boat Festival Committee, and the Tsinghua Alumni Association at Boston. I cannot express how grateful I am for having been through so many interesting things with all those wonderful people! These fun activities formed the bedrock of my social experiences at MIT, and I could write pages about the great times and colorful life that we enjoyed together.

In the summer of 2006, while hiking in the beautiful Acadia National Park, I met my great boyfriend Dr. Christopher H. Rycroft. With him, I have shared a wonderful time together for the past two years with many unforgettable hiking trips in

the US, UK, and Peru. Chris has expressed a lot of interest in my project and has provided many valuable suggestions to this thesis. I am very grateful for his extreme patience and encouragement during the most stressful time when I was writing the thesis and trying to decide my future career. In addition, I would like to mention another two special polar bear friends Snowy and Snowball, who have been my most sweet companions, and who even made it to my thesis defense.

Throughout my time at MIT, my family has provided unwavering encouragement. I have exchanged thousands of phone calls and emails with my mother Zhaoming MA, my father Mingnan Hu, and my sisters Yuhong Hu and Yubing Hu. For good or for bad, they are the ones who always stand behind me, and let me know that I am not alone. In particular I would like to thank my grandfather Zhongming Ma. Although he was never able to finish even high school in the old time, he was one of most knowledgeable people I have ever met in my entire life. His legendary life, the best explanation of 'live and learn', has always been the spirit that promotes me to accomplish more, among which this thesis is one.

Finally, I would like to give my special appreciation to Mary, who walked along with me at the hardest time during my stay at MIT, and probably the most frustrating moment in my whole life. Without her, I might have given up my pursuit of a PhD degree at MIT three years ago. Proudly, I am now finishing up, and I will never forget how much guidance and support I have got from her and others during this process. I will probably forget what I have been through, however, I will keep all the courage and confidence and effort through my entire life!

Table of Contents

List of Figures

List of Tables

1 Introduction and Thesis Scope

1.1 Intracellular Drug Delivery

In recent years, many potentially powerful therapeutic strategies for the treatment of disease require the delivery of drugs into the cytosolic or nuclear compartments of cells. Examples include gene therapy mediated by plasmid DNA,[1-3] gene silencing or RNA interference via oligonucleotides,[4] anti-tumor toxin delivery,[5-7] and therapeutic protein delivery.[8, 9] Each of these examples requires the delivery of membrane-impermeable molecules into the cytosol, which has pushed the field of drug delivery into a new era of investigation at the intracellular or molecular level.

1.1.1 Typical Pathways for Intracellular Drug Delivery

Cells may take up macromolecular drugs via endocytosis, macropinocytosis, or phagocytosis, but these processes confine the internalized compounds to closed vesicles (endosomes or phagosomes), where the pH is progressively lowered to 5.5-6.5.[1] The fusion of these vesicles with lysosomes, intracellular compartments carrying the degradation machinery of the cell at a pH as low as 4.5,[10, 11] often leads to rapid destruction of therapeutic molecules with little or no release into the cytosol. For effective intracellular delivery, membrane-impermeable drug molecules are first introduced to the body through a specific route, such as intravenous, intramuscular or subcutaneous injection. The therapeutic molecules together with their carrier should then locate the desired tissue, bind to the cell surface and enter the cell quickly. The

drug molecules must then escape the endosome and enter the cytoplasm efficiently before being destroyed. For DNA delivery, the gene must transfer to the nucleus to obtain protein expression. Degradation of drug carriers in the cell can be a useful strategy to minimize the potential of cytotoxicity (Figure 1.1).

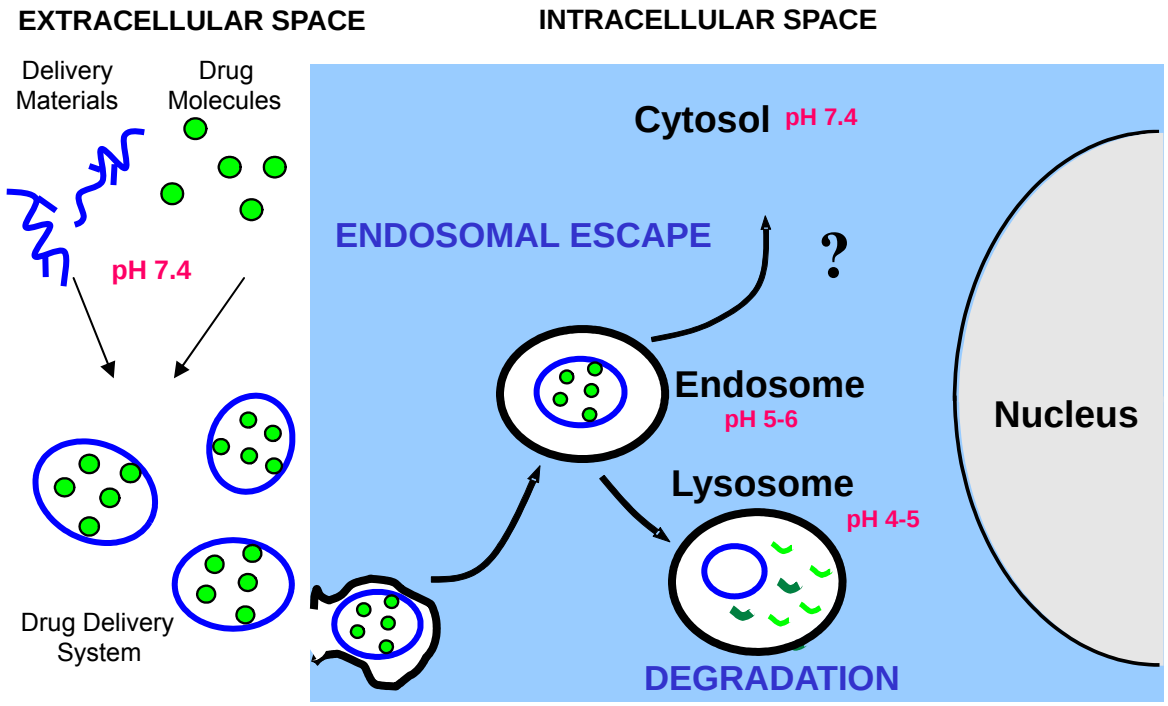

Figure 1.1 Schematic of the typical pathway for intracellular drug delivery. Drug molecules and delivery materials form a drug delivery system, which may be taken up by cells through endocytosis or phagocytosis. The drug delivery system then has to escape from endolysosomes before being denatured, locating in the cell cytosol.

1.1.2 Barriers and Current Strategies

As discussed above, there are several barriers along the pathway for efficient delivery of drug molecules to the cell cytosol: 1) biodistribution and targeting of the drug

delivery system to a specific area or cell types upon administration, 2) cellular uptake, 3) endolysosomal escape, and 4) drug unpacking and degradation of the delivery system. Strategies to overcome these barriers are under investigation.

A practical drug delivery system should be able to locate the disease area and target specific cell types. This capability would decrease the biodistribution time of the drug delivery system in the body after administration, and avoid immune response or side effects of treating healthy cells with drugs. Conjugation of targeting moieties would not only offer the advantage of enhancing specific binding to the cell membrane, but would also improve the cellular uptake via receptor-mediated endocytosis (RME).[12]

Many studies have proven that particle size is a critical parameter for the interaction between particles and cells both *in vitro* and *in vivo*. For instance, DNA is an extremely large molecule, and DNA-nanospheres in the size range of 200-750 nm can transfect some cell lines with limited efficiency.[13] It is essential to condense DNA into a nanostructure around 50-200 nm.[14] Cationic lipids, liposomes, and polymers have been used to condense DNA[15-17] through electrostatic attraction between the cations and the negatively charged phosphate backbone of DNA. Particle surface charge is another critical parameter for cellular uptake. Advantages can be gained if the nanoparticle carries a positive charge, since the cell membrane possesses a slight negative charge.[14]

Once endocytosis occurs, the extremely low pH (around 4-5) environment and the digestive enzymes present in maturing endolysosomes degrade the entrapped drug molecules and associated complexes. There are two approaches to protect the drug delivery system. One is to burst the endosome/lysosome membrane and release the drugs and their carriers to the cytosol before degradation. Some endosomolytic and lysosomotropic agents, such as chloroquine,[18, 19] glycerol,[20] or fusogenic peptides[21] have

been used in human cells for this purpose. Polyethylenimine (PEI) and starburst dendrimers have been found to function as 'proton sponges' for promoting early release of DNA[22-24]. Poly(ortho ester)[25] and poly-L-histidine grafted polymers[26, 27] were used for the same purpose. The other approach is to use poly acids possessing pH-sensitive pendant groups that are protonated at reduced pH. The resulting uncharged, hydrophobic polymer chain will interact with and disrupt the endosomal membrane, carrying drug molecules to the cytosol.[28]

After endolysosomal escape, drugs are expected to be released into the cytosol or nucleus efficiently. Failure to properly unpack these drug cargos from their carriers can lead to a low effective dosage of drugs in the cytosol.[29, 30] In addition, the degradation of drug carriers is of interest for safe *in vivo* application. Research focusing on the use of hydrolysis or enzymatic degradation to break down polymeric carriers and release drug molecules is ongoing.[31-33]

In summary, an ideal intracellular drug delivery system would (i) selectively reach the desired tissue and cells, (ii) easily be taken up by cells; (iii) successfully escape from endolysosomes; and (iv) efficiently release drug molecules to the cell cytosol and break down delivery materials into non-toxic components. Therefore, a biocompatible, biodegradable nanostructured delivery system of endolysosomal escaping capability, and of well-defined sizes and shapes with specific surface functionalities is needed.

1.1.3 Delivery Systems and Challenges

It is possible to obtain intracellular delivery through some physical methods, such as the microinjection/gene gun[34, 35] and hydrodynamics,[36] but there is concern that these

techniques cause tissue damage.[37] Most efforts have focused on developing drug delivery vehicles that coat or encapsulate drugs and deliver them efficiently to the desired target. Although viruses are relatively efficient gene transfer vehicles, repeated administration primes a potential anti-vector immune response that rapidly abolishes transgene expression. Another major concern with viral vectors is fears of viral integration in the host genome, which can lead to transformation of cells (cancer), and pre-existing immunity to the vector, which may prevent even the first dose from working.[14] Therefore a number of different non-viral systems have been investigated for intracellular drug delivery and gene therapy, which include calcium phosphate co-precipitates,[38] DEAE-dextran,[37] liposomes or lipids.[16, 17] Polymeric materials are promising drug delivery systems because size, charge density, and chemistry can be uniquely tailored to achieve a desired functionality. Furthermore, polymers are usually stable and can be engineered to have extended circulation time in the body.[37]

Although in the past two decades gene therapy trials have been initiated worldwide, little has been achieved in terms of curing disease. One of the major challenges of polymeric delivery systems is inefficiency in the escape of internalized DNA from intracellular compartments (*e.g.* endosomes) into the cytosol. Polymer-based delivery systems such as poly(lactide-co-glycolide) (PLGA)[39] have been able to encapsulate DNA and provide sustained release as the polymer degrades. A major issue with PLGA and related encapsulation polymers is that the acidic microclimate within the delivery particles degrades DNA.[33, 40] In addition, delivery systems made by these materials possess a very poor ability to escape from endolysosomes. Most of the entrapped DNA or drugs is eventually degraded by low pH or digested by the enzymes of lysosomes before it can be successfully released to the cytosol.[39] Therefore, endosomal escape,

which is a major bottleneck of the potency of current intracellular delivery systems, has been a focus for many researchers.

PEI has provided promising delivery efficiency by endosome disruption via the 'proton sponge' effect. However, the efficient release of DNA[29, 30] and trafficking to the nucleus is still a problem, due to the strong electrostatic binding between these polycationic materials and the negatively charged DNA. More importantly, the toxicity of PEI has limited its use, particularly for *in vivo* application.[41, 42]

Hoffman and coworkers have developed a series of poly acids (poly (2-ethylacrylic acid) (PEAA), poly (2-butylacrylic acid) (PBAA), and poly (2-propylacrylic acid) (PPAA)).[28, 43] This family of polymers become hydrophobic and exhibits membrane-disrupting properties when the pH drops below their pK_a. Acid-labile bonds such as acetal have been used as linkages between the backbone of these polymeric carriers and drugs. Its degradation in low pH facilitates drug release. However, it could be used for drug delivery only if drug molecules could be attached to the polymer backbone with acid-degradable side-chains in a friendly environment without degradation.

To enable delivery of membrane-impermeable molecules (such as antigen protein or siRNA) into the cytosol of cells, much research has been directed at the development of synthetic chaperones that can facilitate transport of hydrophilic molecules to the cytosol with minimal cytotoxicity.[44] Approaches include the use of membrane-penetrating peptides,[45, 46] pathogen-derived pore-forming proteins,[47, 48] and 'endosome escaping' polymers or lipids that disrupt the endosomal membrane in response to the pH reduction which occurs in these compartments.[17, 24, 43, 49-53] While many of these approaches show promise, strategies that can promote highly efficient delivery of molecules into the

cytosol while avoiding unacceptable cytotoxicity are still sought. In addition, many of the chaperone molecules that efficiently aid transport of macromolecules into the cytosol are formulated with drug cargos by physical complexation of the chaperone and drug (*e.g.*, polyplexes or lipoplexes of cationic polymers/lipids with DNA), forming nanoparticles whose size, stability, and properties are highly dependent on formulation parameters including the identity of the drug cargo, the drug-to-chaperone weight ratio, and the characteristics of the surrounding environment (pH, ionic strength, and presence/absence of serum proteins).[24, 54, 55] Lack of control over chaperone/drug particle size and stability is of concern because particle size is a critical determinant of cellular uptake *in vitro* and biodistribution and toxicity *in vivo*.[24]

It was therefore our aim to develop a drug delivery system which can protect drugs from degradation prior to release, while maintaining a hydrophilic environment. When endocytosis occurs, the drug delivery system should be able to respond to the environmental pH change, and disrupt the endolysosomal membrane rapidly. It should also possess the ability to facilitate the rapid release of drug molecules right after endosomal escape.

1.2 Potential Applications

Cytosolic delivery of membrane-impermeable molecules into dendritic cells (DCs), immune cells critically involved in the initiation of adaptive immune responses,[56-59] is of particular interest. DCs bind peptides derived from pathogens to their major histocompatibility complex (MHC) molecules, and present these peptide-MHC complexes at their surface for recognition by naïve T cells (Figure 1.2). Importantly, presentation of

antigens to cytotoxic T cells is greatly amplified (up to 1000-fold) by delivery of antigens to the cytosol, where the DC intracellular machinery can load them efficiently onto class I MHC molecules for presentation to $CD8^+$ T cells.[60, 61] Likewise, certain immunostimulatory molecules, such as mimics of viral RNA that trigger potent anti-viral immune responses, operate by binding to proteins in the cytosol of DCs.[62] Finally, efficient cytosolic drug delivery in DCs could be used to deliver plasmid DNA or gene silencing reagents in order to amplify or suppress adaptive immune responses for vaccines or immunotherapy.[63] However, transfection of DCs is notoriously inefficient.[64-66] As DCs would engulf particles easily through endocytosis or phagocytosis easily, it is suggested that efficient endosomal escape could help improve the intracellular delivery to DCs.

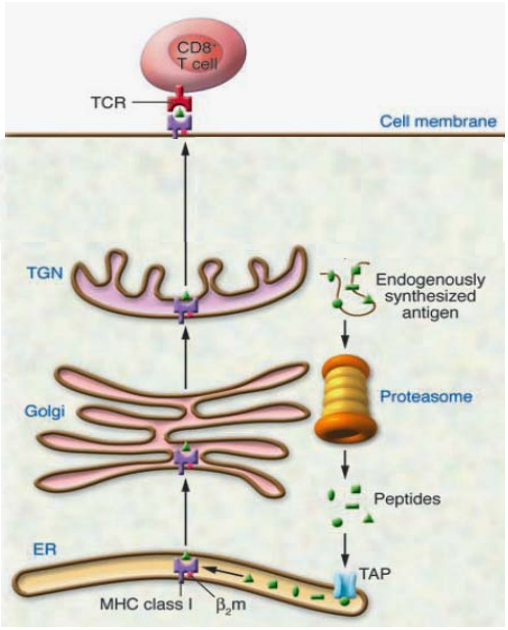

Figure 1.2 Schematic of $CD8^+$ T cell priming through cross presentation of Class I MHC.[67]

A second major application for intracellular drug delivery is in the area of gene silencing through RNA interference (RNAi). RNAi is an evolutionarily-conserved process by which double-stranded small interfering RNA (siRNA) induces sequence-specific, post-transcriptional gene silencing.[68] The RNAi pathway is initiated by the enzyme dicer, which cleaves long double-stranded RNA to short double-stranded fragments of 20 to 25 base pairs. One of the two strands of each fragment, known as the guide strand, is then incorporated into the RNA-induced silencing complex (RISC) and base-pairs with complementary sequences. When the guide-strand basepairs with a messenger RNA (mRNA) molecule and induces degradation of the mRNA, a post-transcriptional gene silencing happens (illustrated in Figure 1.3). RNAi is thought to have enormous potential for the treatment of a great variety of diseases, by allowing selective knockdown of deleterious gene functions. However, the promise of RNAi will only be a clinical reality when safe and efficient RNA delivery systems are established.

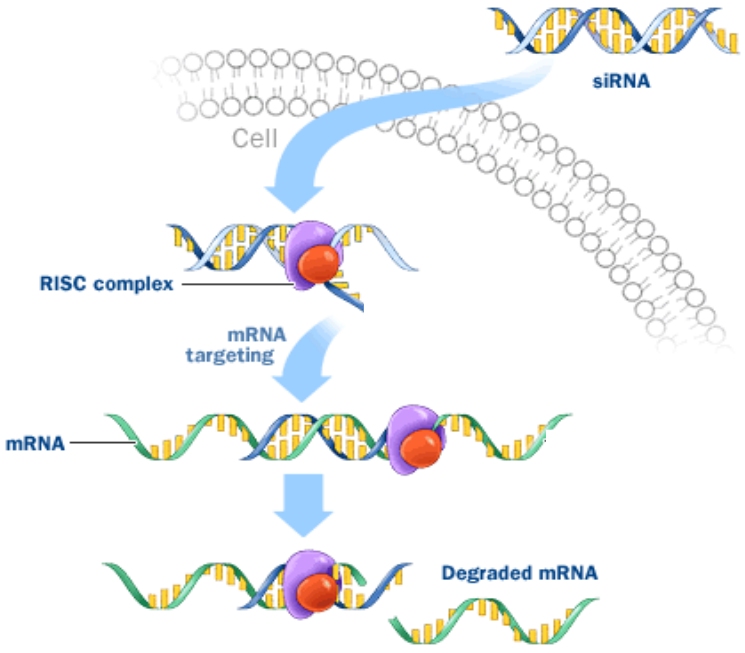

Figure 1.3 Schematic of post transcriptional gene silencing via RNA interference.[69]

1.3 Thesis Scope

1.3.1 Environmental-Responsive Hydrogels

A hydrogel is a material capable of imbibing and retaining a large amount of water without dissolving because of its crosslinked network structure. Polymers bearing hydrophilic groups such as –OH, -CONH, -COOH, $-SO_3H$, and $–NH_2$ can be crosslinked to form hydrogels. The swelling properties of ionic hydrogels are unique due to the ionization of their pendant functional groups. First, they exhibit the ability to respond to changes in environmental parameters, such as pH, temperature, pressure, and ionic strength of the external electrolyte. Second, small changes in these parameters can cause sudden dramatic changes in the degree of swelling.[70] In the case of a pH-sensitive hydrogel, the equilibrium degree of swelling can be changed suddenly by several orders of magnitude near the pK_a or pK_b of the hydrogels (Figure 1.4). Examples of monomers used for pH sensitive gels include acrylic acid, p-styrene sulfonic acid, crotonic acid, vinyl pyridine, and aminoethyl methacrylate. This behavior of the hydrogel can be explored in the development of drug delivery systems that respond to environmental pH change. We thus took advantage of the swelling ability of cationic gels and applied it for endosomal disruption at low pH.

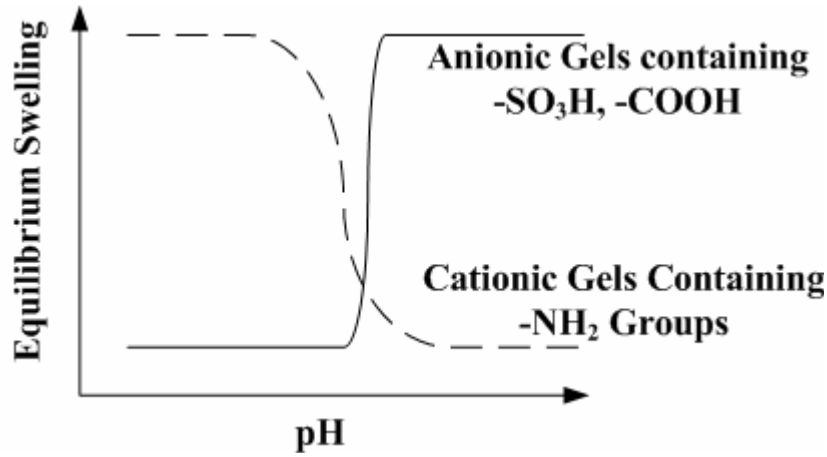

Figure 1.4 Schematic of equilibrium swelling versus pH for ionic hydrogel.[70]

The candidate cationic monomers for drug delivery should be non-toxic, biocompatible, and ideally biodegradable. In addition, they should have the potential of being modified for multiple functions such as cell/tissue targeting. Siegel *et al.* have done extensive research on the swelling ability of the family of aminoethyl methacrylate.[71] It has been reported that hydrogels made from diethyl aminoethyl methacrylate (DEAEMA) and poly (ethylene glycol) monomethacrylate (PEGMA) have a pK_b around 6.7.[72, 73] This is a desirable pK_b to respond to endolysosomal pH. We thus adopted DEAEMA as the basic monomer for the synthesis of a pH-sensitive gel.

1.3.2 Design of pH-Sensitive Core-Shell Nanoparticles

We first synthesized and studied poly(DEAEMA-co-PEGMA) bulk hydrogels. The chemical compositions of the hydrogel system were extensively examined to obtain a detailed understanding of their effects on the pH-sensitivity and reversible swelling

behavior, and a desirable transition pH which could provide efficient response to endolysosomal environment.

We then designed and tested an alternative strategy for cytosolic delivery, using monodisperse crosslinked pH-sensitive hydrogel nanoparticles as chaperones for delivery of molecules to the cytosol. Compared to traditional polymeric delivery systems, which are usually formed by the electrostatic attraction between polymers and drugs, hydrogel nanoparticles provide predefined size, structure and stability.

We pursued a core-shell particle structure, to physically and compositionally segregate the functions of the particle into an endosome-disrupting pH-responsive core that would absorb protons at endolysosomal pH, and a shell whose composition could be separately tuned to facilitate particle targeting, cell binding, and/or drug binding. The shell also shielded any hydrophobic and insoluble components in the core, leading to minimum cytotoxicity.

We further extended this concept of pH-sensitive core-shell nanoparticles to biodegradable nanoparticles crosslinked by a cleavable crosslinker by taking advantage of disulfide reduction happens in any mammalian cells by glutathione (GSH). Modifying DEAEMA with PEGMA improved the hydrophilicity and solubility of the breakdown components, and formed nontoxic micelles upon degradation in cytosol.

We utilized emulsion polymerization for the synthesis of these nanoparticles, which enables (1) a broad palette of chemical groups to be easily incorporated and (2) controlled fabrication of monodisperse nanoparticles of a predefined size.

1.3.3 Endosomal Escape and Intracellular Drug Delivery

The pH-sensitivity of nanoparticles was explored in biological systems, by considering the delivery of the small molecule calcein to dendritic cells. Microscopy and flow cytometry were used to detect the endocytosis of nanoparticles and their localization in cells. We have sought a detailed understanding on the mechanism of efficient cytosolic delivery of calcein through intracellular trafficking of nanoparticles with the aid of other molecular biology approaches.

Nanoparticles were further applied as a drug delivery system to promote the delivery of a protein vaccine antigen ovalbumin (OVA) to primary dendritic cells. The delivery efficiency and function were evaluated by the immune response of $CD8^+$ T cells. siRNA delivery was also tested with the aid of nanoparticles. The knockdown of target mRNA was examined and compared with a commercially available delivery agent.

1.3.4 Thesis Outline

The experimental work was carried out to fulfill the objectives discussed in sections 1.3.1 to 1.3.3, and is presented in Chapters 2 to 6 of this thesis. Chapter 2 describes the synthesis of poly(DEAEMA-co-PEGMA) hydrogels and their composition-dependent pH-sensitivity. In Chapter 3, synthesis of pH-sensitive core-shell nanoparticles by emulsion polymerization is discussed. The chemical characterization of the nanoparticles on their pH-sensitivity and proton buffering capacity is performed and presented. Biological characterization of the nanoparticles on their capability to disrupt endolysosomes and deliver the small molecule calcein to the cell cytosol is described in

Chapter 4. In this Chapter, the cytotoxicity of the core-shell nanoparticles is also examined by the metabolism and growth/proliferation of cells. We then applied nanoparticles as an intracellular drug delivery system to several drug molecules such as antigen protein OVA, influenza A, and siRNA. The delivery efficiency and potential utility in treating disease are investigated in Chapter 5. The design of a biodegradable system based on the pH-sensitive core-shell nanoparticles with a cleavable crosslinker is discussed in Chapter 6. The preliminary results to evaluate the degradation and calcein delivery are presented as well. The thesis closes with a summary of conclusions gathered in this work and a discussion of important future directions.

2 Synthesis and Characterization of pH-Sensitive Hydrogels

Environmental-responsive hydrogels could be potentially used as drug delivery system since they provide sudden dramatic changes in the degree of swelling upon the small changes in the environmental conditions.[70] The natural pH changes in the intracellular pathway (as described in Section 1.1) make it possible to take advantage of a pH-sensitive hydrogel for disrupting endolysosomes efficiently at low pH (4-6) and release drug molecules into the cell cytosol. In addition, acidic conditions (5-6.5) may exist naturally (*e.g.* in solid tumors[74-76]) or be induced artificially (*e.g.* acid byproducts by degradable polymers with enzymatic reaction[72, 73]). Acid-sensitive hydrogels could be of interest for selective drug release in response to these environments other than intracellular endolysosomes. Therefore, we will first discuss the synthesis and characterization of pH-sensitive bulk hydrogels to obtain a detailed understanding on their swelling behavior. We aimed to identify a series of chemical compositions that could provide us sharp transition in hydrogel swelling ability around endolysosomal pH (4-6). Fabricating the pH-sensitive core-shell nanoparticles through surfactant-free emulsion polymerization for intracellular drug delivery will then be introduced in the subsequent chapters.

Diethyl aminoethyl methacrylate (DEAEMA) has been reported as a monomer to form an pH-responsive hydrogel system.[71] However, hydrophobicity of the monomer limits its miscibility in an aqueous solvent.[77] The possible conditions to form a

homogeneous hydrogel system are identified by a phase diagram. Using PEGMA as a co-monomer, the formed hydrogels provide pK_b value ~ 6.7.[72] This system could provide an idea sharp transition responding to endolysosomal pH. PEGMA could increase the biocompatibility of the system by making a hydrophilic, steric 'hairy' layer at the gel surfaces to reduce electrostatic interactions of potential drug molecules with the gels. Thus in our study, the compositions of poly(DEAEMA-co-PEGMA) are studied.

2.1 Materials and Methods

2.1.1 Materials

All reagents were used as received without further purification. 2-diethylamino ethyl methacrylate (DEAEMA), tetraethylene glycol dimethacrylate (TEGDMA), 2-aminoethyl methacrylate hydrochloride (AEMA, 90%), and ammonium peroxodisulfate (APS) were purchased from Sigma-Aldrich Chemical Co. Poly (ethylene glycol) monomethacrylate (PEGMA, MW_{PEO}=200, 400, or 1000 g/mol), and poly fluor™ 570 methacryloxyethyl thiocarbamoyl rhodamine B were purchased from Polysciences Inc. Polydimethylsiloxane (PDMS) were made from Sylgard® 184 Silicone Elastomer Kit (Dow Corning Corporation).

2.1.2 Mapping Ternary Phase Diagram of DEAEMA/Water/Ethanol System

Clear, transparent formulations are indicative of a stable homogenous phase as the

sizes of the any microemulsion domains are much smaller than the wavelength of light.[78] To quantify the optical clarity of gel precursor solutions, varying amounts of DEAEMA and EtOH were micropipetted into a glass, flat-bottomed, 96-well microplate (500-µl well capacity, Alltech Associates, Inc.) and mixed thoroughly. The appropriate amount of aqueous solution was then added with mixing to obtain a total volume of 350 µl. Each ternary composition was run in triplicate. Absorbance values were collected at a wavelength of 450 nm using a microplate spectrophotometer system (SPECTRAmaxTM 250, Molecular Devices Corp.) to quantify turbidity. Absorbance data were plotted on a contour diagram using JMP 3.0 software (JMP, SAS Institute Inc.).

2.1.3 Polymerization of pH-sensitive Hydrogels

Crosslinked poly(DEAEMA-co-PEGMA) hydrogels were prepared by premixing the comonomers DEAEMA, PEGMA, and the crosslinking reagent TEGDMA. Using results from the ternary phase diagram measurements as the guidance, EtOH and water were added to reach the desired solvent concentration while maintaining a homogeneous system. APS was used as a free radical initiator. In a typical polymerization process, 103µL DEAEMA (0.5mM), 155µL PEGMA 200 (0.5mM), and 1.5µL TEGDMA (0.5 % mol crosslinker/mol comonomers) were mixed in 269 µL 25 v% EtOH, giving a final solution containing 50 wt% comonomers. For fluorescent labeling of gels, 10µL poly fluor^{TM} 570 methacryloxyethyl thiocarbamoyl rhodamine B stock solution (50 mg/mL in 25% EtOH) was added as needed. The initiator APS (20 µL of 200mg/mL APS in water, freshly made) was added, and the mixture (~500µL) was transferred to a PDMS ring mold (H=5mm, R=2.5 mm, cut by a revolving punch, Small Parts Inc.) adhered to an

oxygen plasma-treated glass slide. A disc-shaped poly(DEAEMA-co-PEGMA) hydrogel was polymerized by placing the gel precursor/initiator solution in an oven at 60°C for 30 min under atmospheric pressure.

The resulting gels were immersed in excess water for 3 days on a shaker to remove residual monomer/initiator. The cleaned gels were stored in water at 4 °C until use.

2.1.4 Swelling Study of pH-Sensitive Hydrogels

Poly(DEAEMA-co-PEGMA) hydrogel discs were transferred to a 6-well plate, and equilibrated in phosphate buffer of varying pH (100 mM ionic strength, 3mL) with mild shaking in a Jitterbug shaker (Boekel Scientific, Model 130000). The wet mass of each sample was measured at each condition to determine the mass swelling ratio (Q), defined as mass of gel at swelling status over the mass of deswollen gel at pH 9. To assess equilibrium swelling, the gels were allowed to equilibrate for up to 24 hrs. The mass of the gels was assessed at different time points (swelling over 2 hrs, 4hrs, 8hrs, and 24hrs) to confirm that swelling had reached equilibrium. To assess the temperature sensitivity of gel swelling, the swelling ratio was measured at 25 °C and 37 °C. To assess swelling kinetics, the hydrogel discs were first equilibrated in a pH 7.48 buffer. For the swelling phase, gels were transferred to a pH 5.66 buffer, and the masses of gels was measured every 10 min for the first hour, every 20 min for the second hour, and every 30 min until it reached equilibrium. For the deswelling phase, gels were then transferred back to a fresh pH 7.48 buffer, and the masses of gels were measured every 10 min for 1 hour, and then measured at 8 hours. To assess reversibility of swelling, gels were equilibrated in pH7.48 buffer for 2 days, and then were equilibrated in pH 5.88 buffer and pH 7.48

buffer alternately. For each condition, the swelling ratio was determined after the gels had reached equilibrium swelling.

2.2 Synthesis and Characterization of pH-Sensitive Hydrogels

In this chapter, we aimed to synthesize a pH-sensitive hydrogels with $pK_b \sim 7$, which can thus respond to endolysosomal pH. The pH responsiveness of the polymers were expected to provide enough swelling, which could be used to release drugs at a control rate, or be applied to disrupt endolysosomes at acidic environments. As mentioned in Chapter 1, Peppas and coworkers have used DEAEMA and PEGMA as comonomer for pH-sensitive controlled release,[72] we suggested similar monomers of the hydrogel (Figure 2.1) which could provide pK_b around 6.5.

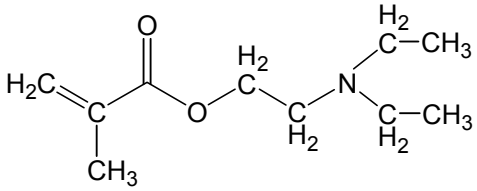

Diethyl amino ethyl methacrylate

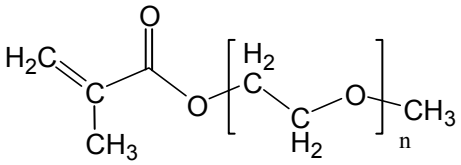

Poly (ethylene glycol) monomethacrylate

Figure 2.1 Chemical structures of monomers for poly(DEAEMA-co-PEGMA) hydrogels.

2.2.1 Phase Diagram of DEAEMA/Water/Ethanol System

The hydrophobicity of DEAEMA monomer severely limits its solubility in water. Prior studies by the group of Peppas have introduced ethanol (EtOH) as a useful

co-solvent for DEAEMA.[79] To form homogeneous bulk hydrogels for characterization of the swelling properties of polyDEAEMA gels, we first mapped out a ternary phase diagram of DEAEMA in a water/ethanol co-solvent system, in order to identify monomer/solvent compositions that would allow homogeneous polymerization of hydrogels. For this purpose, optical densities in the visible range were used to quantify turbidity in solutions reflecting phase separation. A ternary diagram of OD vs. monomer/solvent composition (Figure 2.2) showed that DEAEMA had minimal solubility in water. As increasing amounts of EtOH present, the ternary phase progresses from a turbid multi-phase region to a homogeneous single phase. This ternary diagram provided a starting point for choosing suitable single-phase solution conditions. Addition of the liquid comonomer PEGMA (*e.g.* MW_{PEO}=200, 400 g/mol) increased the solubility of DEAEMA in water/ethanol solutions. In the case of wax-like PEGMA (MW_{PEO}=1000 g/mol, T_g = 40 °C), elevated temperature (~ 40 °C) was needed to dissolve the macromonomer and form homogeneous solutions.

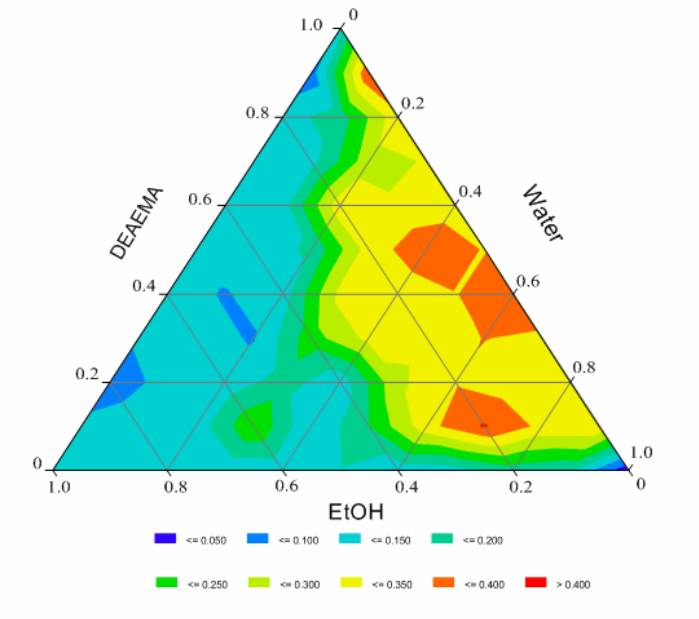

Figure 2.2 Pseudo-ternary phase diagram for the water, EtOH and DEAEMA system.

Absorbance (at 450 nm) was recorded for solutions of the indicated ternary compositions; values less than 0.25 indicated a clear, single-phase precursor solution; values above 0.25 indicated phase separation. Each data point was the average of duplicate samples, and the standard deviation between the duplicates was less than 0.05 for all the cases.

2.2.2 Equilibrium Swelling of pH-Sensitive Poly(DEAEMA-co-PEGMA) Hydrogels

All of the compositional variables and many aspects of synthesis conditions can impact the pH-sensitivity, equilibrium swelling, and swelling kinetics of polyelectrolyte hydrogels.[70] Parameters such as the molecular weight of comonomer PEGMA, the ratio of each monomer in the comonomer mixture, the ratio of crosslinker to monomers, the solvent concentration, the starting pH of monomers mixture, and the ionic strength of buffer could potentially affect the transition point and swelling ability of hydrogels. To determine how these compositional parameters of poly(DEAEMA-co-PEGMA) hydrogels control gel swelling behavior, we synthesized a series of different hydrogels as listed in Table 2.1, using the DEAEMA/water/EtOH conditions identified from the phase diagram described above. Disk-shaped gel samples were polymerized at 60°C using APS as a free radical initiator and washed in water extensively.

The mole ratio of DEAEMA to PEGMA was fixed at 1:1, but the total comonomer concentration was varied from 20-60 wt%. In addition, gels were prepared using PEGMA with different molecular weights (MW_{PEO}=200, 400, 1000) to determine the role of the PEG side chain length in gel swelling responses. Finally, two crosslinker ratios (0.5 or 1 mol% of comonomer moles) were compared.

Table 2.1 Compositional Parameters of pH-Sensitive Hydrogels

Sample	DEAEMA (mg)	PEGMA (mg)	DEAEMA: PEGMA (wt:wt)	Solvent* (mg)
PEG200_50%**	95.4	154.6	3:5	250.0
PEG400_20%	27.0	73.0	2:5	400.0
PEG400_30%	40.5	109.5	2.5	350.0
PEG400_40%	54.0	146.0	2:5	300.0
PEG400_50%	67.5	182.5	2:5	250.0
PEG400_60%	79.1	219.0	2:5	200.0
PEG1000_50%	36.0	214.0	1:5	250.0

*25 v% EtOH was used as solvent.

** 50% represents the wt% of the comonomer in the precursor solution.

Swelling of the gels was quantified using the mass swelling ratio, defined as:

$$mass\ swelling\ ratio\ (Q) = \frac{mass\ of\ swelling\ gel\ at\ different\ pH\ (W_s)}{mass\ of\ deswollen\ gel\ at\ pH\ 9\ (W_d)}$$

We first examined the effect of comonomer concentration on the swelling ratio. As shown in figure 2.3, the swelling ratio of hydrogels synthesized with DEAEMA and PEGMA400 (2:5 wt:wt) at different comonomer concentration (20-60 wt%) revealed that gels prepared with a higher comonomer concentration (from 40 to 60 wt%) during synthesis exhibited greater swelling. We chose 50 wt% of comonomer, which proved a reasonable swelling ratio as well as great mechanical property of hydrogels, for our further study.

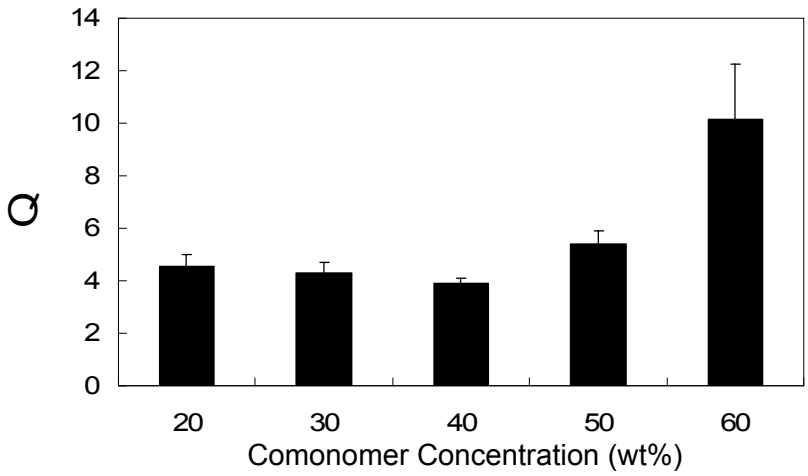

Figure 2.3 Mass swelling ratio (Q) of hydrogels with different comonomer concentrations at 37 °C. DEAEMA and PEGMA400 were used at 2:5 (wt:wt) ratio with 1 mol% of crosslinker TEGDMA. The total mass was kept 500 mg. Hydrogels were swelling in phosphate buffer of physiological ionic strength (100 mM) at pH 4.79. Shown are average ± standard deviation (S. D.) of triplicate samples.

The equilibrium swelling as a function of pH was next characterized for gels where the molecular weight of the poly(ethylene glycol) chains of PEGMA was varied. As shown in Figure 2.4, gels made with PEGMA200 or PEGMA400 could respond to reducing pH, and gave gel pK_b around pH 7.4. However, gels made with PEGMA1000 did not show much transition in the given pH range. In addition, lower molecular weight of PEGMA led to much larger swelling capacity as the highest swelling ratio at pH 4.79 were 3.2, 1.9 and 1.1 respectively for gels made with PEGMA200, 400, and 1000. These results showed that the higher molecular weight (MW) PEGMA provided more non-pH-sensitive hydrophilic chains into the system, which essentially affected the gel swelling capacity but not the gel transition point. Comparison of the swelling data

in Figure 2.4 (Q ~ 2 at 25 °C for PEGMA400 gels at pH 4.79) with that of Figure 2.3 (Q ~ 5 at 37 °C for PEGMA400 gels prepared with 50 wt% comonomers at pH 4.79) also reveals a substantial temperature dependence of poly(DEAEMA-co-PEGMA) gel swelling, which are discussed further below.

The effect of the crosslink density in the hydrogels was also tested for two different crosslinker concentrations, 0.5 or 1 mol% relative to comonomers (Figure 2.5). This two-fold change in crosslinker concentration had a minor effect on gel swelling and did not alter the pH where swelling onset was detected.

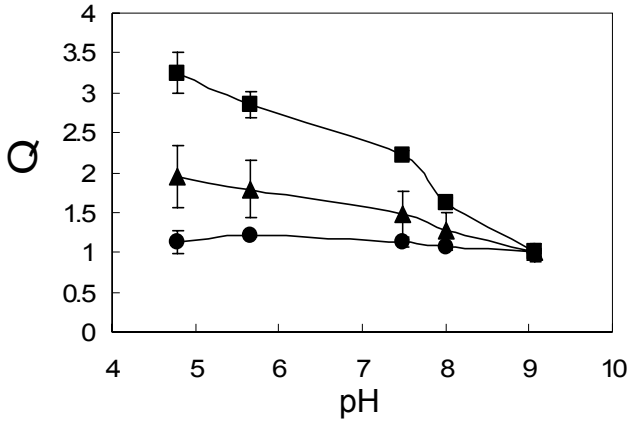

Figure 2.4 Mass swelling ratio (Q) of hydrogels with different PEGMA molecular weight at 25 °C. Gels (500 mg total mass as-synthesized) were prepared with DEAEMA and PEGMA (MW_{PEO}=200 (■), 400 (▲), or 1000 (●) g/mol) at 1:1 (mole:mole) and 50 wt% total comonomer concentration. The average ± S.D. of triplicate samples are shown.

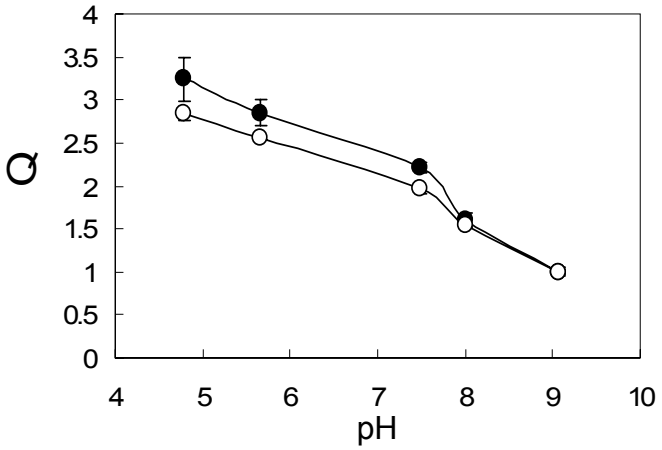

Figure 2.5 Mass swelling ratio (Q) of hydrogels with different crosslinker ratio at 25 °C. Gels were made with DEAEMA and PEGMA200 with 0.5 (●) or 1 (○) mol% of comonomer (1:1 mole: mole between DEAEMA and PEGMA, 50 wt% of total weight of 500 mg). The average ± S.D. of triplicate samples are shown.

In summary, DEAEMA was the major monomer to provide pH sensitivity. The molecular weight of PEGMA would not affect the gel pK_b, but the swelling ability was reduced by the long PEG chain. The crosslinker ratio only affected the swelling capacity not the pK_b as well. Because gels composed of a 1:1 ratio of DEAEMA:PEGMA200 with 0.5 mol% crosslinker ratio and 50 wt% of comonomers concentration exhibited the most dramatic swelling changes in response to pH, this composition was used for the further studies. In Figure 2.6, a picture showed gels made with this composition at freshly made, swelling, and deswelling status.

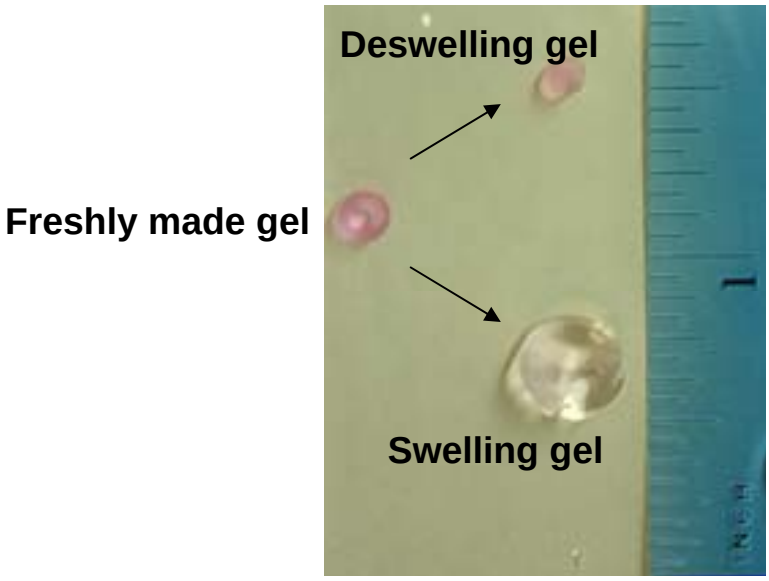

Figure 2.6 Picture of hydrogels at freshly formed, swelling, and deswelling status. Gels were made with DEAEMA and PEGMA200 comonomer (1:1 mole:mole between DEAEMA and PEGMA, 50 wt% of total weight of 500 mg) with 0.5 mol% TEGDMA. Gels were swelling at pH 4.79 buffer and collapsing at pH 9 phosphate buffer with 100 mM ionic strength.

2.2.3 Dynamic Swelling

It is necessary to define and calculate the responsive characteristic time of gels as this will be a significant parameter controlling drug loading and release profiles from gels used for drug delivery. To this end, changes in the swelling ratio as a function of time were measured following transfer of gels equilibrated at extracellular pH/ionic strength conditions to acidic pH conditions and *vice versa*. As indicated in Figure 2.7, hydrogels were able to respond to the environmental pH change immediately. Within 90 min, the gels could reach their equilibrium swelling when located in pH 5.66 buffer (Figure 2.7A).

The response curve was nonlinear, as gels swelled rapidly in the first 30 min, and the swelling speed decreased as it reached equilibrium. Swelling of these polyelectrolyte gels was reversible, as hydrogels were able to shrink to the original size when put back in pH 7.48 buffer. As in Figure 2.7B, deswelling of the gels reached 95% of equilibrium within 60 min. The deswelling curve was in a linear pattern. The difference between the swelling curve and deswelling curve might indicate that the two processes were controlled by a different mechanism. This aspect would be potentially used for rapid first-order drug release as the gel's deswelling process could eject the drug loaded to the environment in a controllable manner. Note that swelling kinetics are typically dominated by diffusion times for the ions in the solution.[80] Thus, we would expect very different swelling/deswelling kinetics for nanoparticles, where ions need only diffuse much shorter distances (nanoparticles vs. bulk gels). These measurements provide a first-order idea of how fast the gels may respond, and we expect particles to respond much more quickly. Here, we tested overall reversibility, which at least for one cycle, could be relevant in cells.

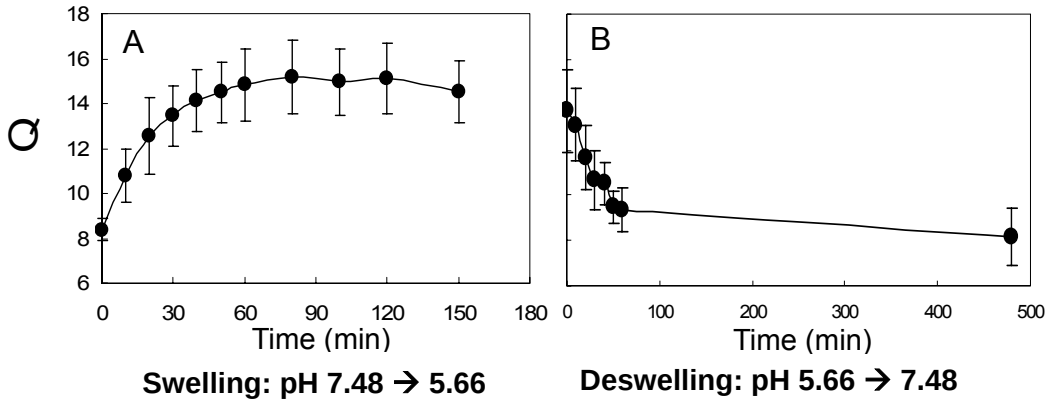

Figure 2.7 Dynamic swelling of hydrogels at 37 °C. Hydrogels (PEG200_50% with 0.5mol% crosslinker) were equilibrated in pH 7.48. (A) Swelling ratio in pH 5.66 buffer.

Hydrogels were transferred to pH 5.66 phosphate buffer with 100 mM ionic strength, and weighed every 10 min for an hour, every 20 min for another hour, and every 30 min before reaching equilibrium. (B) Deswelling of the same gels from (A) when transferred back to a pH 7.48 buffer at 100 mM ionic strength. Hydrogels were weighed every 10 min for the first hours, and then at 8 hours. The average ± S.D. of triplicate samples are shown.

For some applications, cyclic gel swelling/deswelling may be of interest for pulsatile drug delivery.[72] To determine whether DEAEMA gels were able to repeat their swelling cycle, gels were equilibrated in buffers of alternative near-neutral and acidic pH (Figure 2.8). These experiments confirmed that the swelling/deswelling repsonsiveness of poly(DEAEMA-co-PEGMA) hydrogels was reversible. Gels were able to cycle multiple times between a swollen or collapsed state with limited hysteresis in the endpoint responding to each of the two pHs tested.

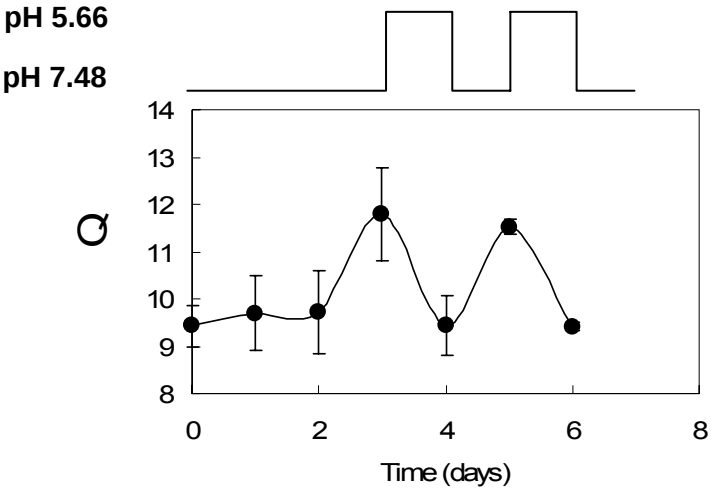

Figure 2.8 Reversible swelling of gels at endolysosomal and physiological pH at 37 °C. Hydrogels (PEG200_50% with 0.5mol% crosslinker) were equilibrated at pH 7.48 for

two days. On day 3, gels were transferred to a pH 5.66 buffer, and the swelling ratio was examined after 12 hrs when gels reached the equilibrium swelling. On the subsequent days, gels were exposed to fresh physiological pH (pH 7.48) and endolysosomal pH (pH 5.66) alternately, and the swelling ratio was determined by the average of two individual samples. Error bars are S.D. of duplicate samples.

2.2.4 Temperature Sensitivity of Poly(DEAEMA-co-PEGMA) Hydrogel pH-Responsive Swelling

As mentioned above, we noticed different swelling ratios for measurements made on the same gel compositions at different temperatures (Figure 2.3 and Figure 2.4). To further analyze the temperature sensitivity of the gels, we did a swelling study at 25 °C and 37 °C with different gel compositions. Interestingly, for all of the gel compositions studied (in Figure 2.9) higher temperature at 37 °C led to a larger swelling ratio and sharper swelling transition compared to room temperature (25 °C). This comparison confirmed that poly(DEAEMA-co-PEGMA) responded to temperature change as well. We could potentially use this character to guide the design of a drug loading and releasing profile at both different temperature and pH.

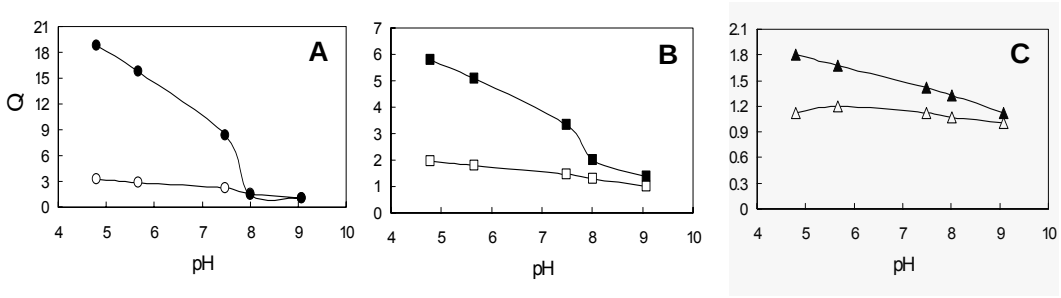

Figure 2.9 Mass swelling ratio (Q) at 25 °C and 37 °C with different hydrogel

compositions. The swelling ratios of hydrogels synthesized with DEAEMA and PEGMA200 (A), PEGMA400 (B), or PEGMA1000 (C) were studied at 25 °C (open symbols) and 37 °C (filled symbols).

In this chapter, we synthesized and characterized pH-sensitive poly(DEAEMA-co-PEGMA) hydrogel. The ternary phase diagram suggested us compositions forming homogeneous hydrogel system. The characterizations of equilibrium swelling, dynamic swelling, and reversible swelling of gels with different chemical compositions gained us knowledge of the effect of a variety of parameters on the transition pH and swelling capability of the bulk hydrogels.

3 Synthesis and Characterization of pH-Sensitive Core-Shell Nanoparticles

The study of p(DEAEMA-co-PEGMA) hydrogels confirmed that DEAEMA was potentially a good candidate as an acid-sensitive responsive drug delivery system. Bulk gels could be utilized as injectable implants to release drugs in an environment-sensitive manner or to respond to artificially-induced mild local pH changes in a tissue (as mentioned in Chap 2). However, we also hypothesized that translation of the bulk gel swelling properties to nanoparticles might allow the gel swelling in response to reducing pH to be used for endolysosomal disruption and efficient cytosolic drug delivery. We now needed to design a process to fabricate hydrogel nanoparticles, whose size is in the cellular uptake range. In general, particles less than ~5-10 μm can be engulfed by microphage through phagocytosis, while nanoparticles less than 250 nm can be internalized by many cell lines through endocytosis or macropinocytosis.[24] We were therefore particularly interested in synthesis of pH-responsive particles smaller than 250 nm.

In this chapter, we fabricated pH-sensitive nanoparticles through surfactant-free emulsion polymerization by the hydrophobicity of DEAEMA. Instead of using a comonomer system with PEGMA, we applied only DEAEMA to achieve better pH-sensitivity as the bulk gel studies from last chapter suggested that the presence of PEG chains reduced the pH responsiveness of the gels. Unlike pursuing a homogenous single phase of precursor solution for the synthesis of bulk hydrogel, an emulsion suspension is favored for emulsion polymerization process. PEGMA comonomer would

render the resulting polymer chains more hydrophilic, and could destabilize the emulsion polymerization. Therefore, to introduce hydrophilicity to the nanoparticles, we proposed a core-shell structure with the hydrophilic components favored by the cells to the outside shell. This structure could physically segregate the drug or cell binding function on the shell and the endolysosomal-disrupting capability in the core. On the other hand, current intracellular drug delivery systems which could perform well for endolysosomal escape (*e.g.*, PEI) often show noticeable cytotoxicity mainly due to the exposure of endosomal-disrupting components to the cells as well as inefficient unpacking of the drug molecules in cell cytosol.[24, 42] This hydrophilic 'protective' shell could prevent the hydrophobic and endolysosomal-disrupting components from contacting the cells, resulting in minimum cytotoxicity. The investigation of the core-shell nanoparticles for endolysosomal escaping and toxicity reducing in the biological system will be addressed in the subsequent chapters.

3.1 Materials and Methods

3.1.1 Materials

All reagents were used as received without further purification. 2-diethylamino ethyl methacrylate (DEAEMA, 99%), methyl methacrylate (MMA, 99%), 2-aminoethyl methacrylate hydrochloride (AEMA, 90%), ammonium peroxodisulfate (APS) and glutathione (GSH, reduced form) were purchased from Sigma-Aldrich Chemical Co. Poly(ethylene glycol) dimethacrylate (PEGDMA, MW_{PEO}=200 g/mol) was purchased from Polysciences Inc. Cy5 mono-NHS ester was purchased from GE Healthcare UK

Limited. The Limulus Amebocyte Lysate (LAL) QCL-1000® Kit and LAL water were purchased from Lonza Walkersville, Inc.

3.1.2 Synthesis of pH-Sensitive Core-Shell Nanoparticles

Emulsion polymerization

DEAEMA (1 mL, 4.97 mmol) or MMA (528 μL, 4.97 mmol) premixed with PEGDMA 200 (10 μL, 0.03 mmol) were dispersed in water (9 mL) with stirring and equilibrated at 70 °C for 15 min before adding APS (50 μL of 200 mg/mL freshly made solution) as the initiator. The emulsion polymerization was allowed to proceed at 70 °C for 3 hours to grow the particle core, followed by injection of AEMA (50 μL of 800 mg/mL freshly made solution, 0.24 mmol) to grow the particle shells for an additional 1.5 hours. The nanoparticles were purified by dialysis (10,000 MWCO Slide-A-Lyzer® Dialysis Cassettes, Pierce Chemical Co.) in deionized water for three days followed by ultrafiltration (10,000 MWCO PLGC Ultrafiltration Membrane, Millipore Co.) three times and centrifugation three times with PBS (pH 7.4) at 15,000 x*g*. Purified particles were stored in PBS at 4 °C.

Morphology of pH-Sensitive Core-Shell Nanoparticles

The primary amine-containing shells of nanoparticles were fluorescently labeled by incubating Cy5 mono-NHS ester (5 μL of 1 mg/mL solution in DMSO) with nanoparticles (~ 5 mg) in PBS (395 μL) overnight with moderate shaking at 4 °C. Unconjugated dye was removed by centrifugation (three times in 1mL PBS, at 15,000 x*g* for 10 min each). The labeled particles were visualized using a Zeiss LSM 510

Confocal Laser Scanning Microscope (CLSM) using a 100X oil objective.

Transmission electron microscopy (TEM) was used to characterize the morphology of the nanoparticles. Condensed particles (10 μL, ~ 0.5 mg) were dehydrated through graded concentrations of ethanol (50%, 70%, 90%, 100%), and air-dried overnight on TEM grids. Samples were examined using a JEOL JEM 1200 EX II at 60 KV or a Phillips EM410 at 80 KV.

CryoEM was performed to measure the size of the nanoparticles in water. A nanoparticle suspension in water (3 μL) was placed on a 2/4 Quantifoil holey carbon film after glow-discharging the grid. Excess liquid was blotted by filter paper, and then the grid was plunged into liquid ethane using a Leica EM-CPC rapid freezing device, vitrifying the aqueous suspension. The grid was directly loaded into a JEOL 2200FS TEM using a Gatan 626 cryo-specimen holder at liquid nitrogen temperature, and imaged at a low dose condition using 200kV accelerating voltage and 30 eV energy slit. TEM images were recorded at a magnification of 50,000X on a slow-scan CCD camera (Gatan Inc.).

3.1.3 pH Sensitivity and Buffering Capacity of Core-Shell Nanoparticles

To characterize the pH sensitivity of the core-shell nanoparticles, the hydrodynamic diameters, determined by dynamic light scattering (DLS, Brookhaven 90Plus instrument), were measured for particles equilibrated in physiological ionic strength phosphate buffers (100 mM) with pH ranging from 4.9 to 9.5 at 25 °C or 37 °C. Particles (~ 0.1 mg) were suspended in 1 mL buffer solution. The particle size was detected at different time points (5 min, 10 min, and 30 min) repeatedly to examine the swelling/deswelling

equilibrium.

The mass swelling ratio of polyDEAEMA core-shell nanoparticles was compared to that of PMMA core-shell nanoparticles to further validate the pH sensitivity and swelling behavior in this system. The same amount of nanoparticles (~ 0.25 mg) was suspended in different pH buffer as described above overnight to reach equilibrium swelling. Centrifugation (15,000x*g*, 15 min) was then performed to pellet the particles in each buffer solution. The weight of particles was determined after removing the supernatant.

To determine the buffering capacity of nanoparticle suspensions, we examined the protonation of tertiary amine group on the nanoparticles by pH titration. Nanoparticles (0.05 mmol repeat units of DEAEMA or MMA, 9.26 mg or 5.01 mg particles, respectively) were suspended in 0.1 M NaCl (20 mL) with 500 μL of 0.1 M NaOH. The pH of the solution was recorded as HCl (0.1 M) was added stepwise to each suspension using a pH meter (Φ 350 pH/Temp/mV Meter, Beckman Coulter, Inc.).

3.1.4 Endotoxin Evaluation by LAL Assay

To evaluate potential LPS/endotoxin contamination of nanoparticles, the Limulus Amebocyte Lysate (LAL) QCL-1000® Kit was used to test the concentration of endotoxin in the nanoparticles according to the manufacturer's instructions. Nanoparticles (25 μg/mL) or endotoxin standard (at different concentration) were suspended in LAL water. 50 μL of the nanoparticles suspension or standard were dispensed in a 96-well plate, which was pre-warmed to 37 °C. At time zero, 50 μL of the lysate solution (LAL) was added to each sample. Ten minutes later, 100 μL of the substrate solution (prewarmed to 37 °C) was added to detect the endotoxin chromogenically. Stop

solution (50 μL) made from sodium dodecylsulfate (SDS) was used at total time of 16 minutes to stop the color reaction and to prevent the saturation of the color express. The endotoxin concentration was then determined by the absorbance at 405 nm using a microplate spectrophotometer system (SPECTRAmax^{TM} 250, Molecular Devices Corp.)

3.1.5 Zeta Potential

50 μL of PDEAEMA nanoparticles (without or with AEMA shell) were suspended in different NaCl solutions (5 mM) with pH ranging from 4 to 10 adjusted by 0.1 M HCl or NaOH. The value of the zeta potential was read from a Particle Size Analyzer 90Plus (Brookhaven Instruments Corporation).

3.2 Synthesis and Characterization of pH-Sensitive Core-Shell Nanoparticles

3.2.1 Emulsion Polymerization

Emulsion polymerization is commonly used to form micro- or nano-sized polymer particles, and we adopted this method here to form our polyDEAEMA hydrogel nanoparticles. A common type of emulsion polymerization is an oil-in-water emulsion, in which droplets of monomer (the oil) are emulsified (with surfactants) in a continuous phase of water. Macroscopic monomer droplets are in equilibrium with monomer dissolved in micelles of surfactant dispersed throughout the aqueous phase. Polymerization takes place in these micelles, which become latex particles that form

spontaneously in the first few minutes of the process; these latex particles are comprised of many individual polymer chains. Particle coagulation is prevented because each particle is surrounded by the surfactant; the charge on the surfactant repels other particles electrostatically. When water-soluble polymers are used as stabilizers instead of surfactant (Figure 3.1), the repulsion between particles arises because these water-soluble polymers form a steric barrier, a "hairy layer" around a particle that repels the others. This repulsion helps to keep particles separate, thus ultimately providing a monodisperse particle suspension.

As DEAEMA is basic and hydrophobic when unprotonated, it can form unstable micelles[77] or phase separate from water solutions, as discussed in Chapter 2. However, this character serves as an advantage and enables this monomer to be used for surfactant-free emulsion polymerization in water, as DEAEMA itself can form micelles in water, without further need for surfactants to form monomer-laden micelles in the initial stage.

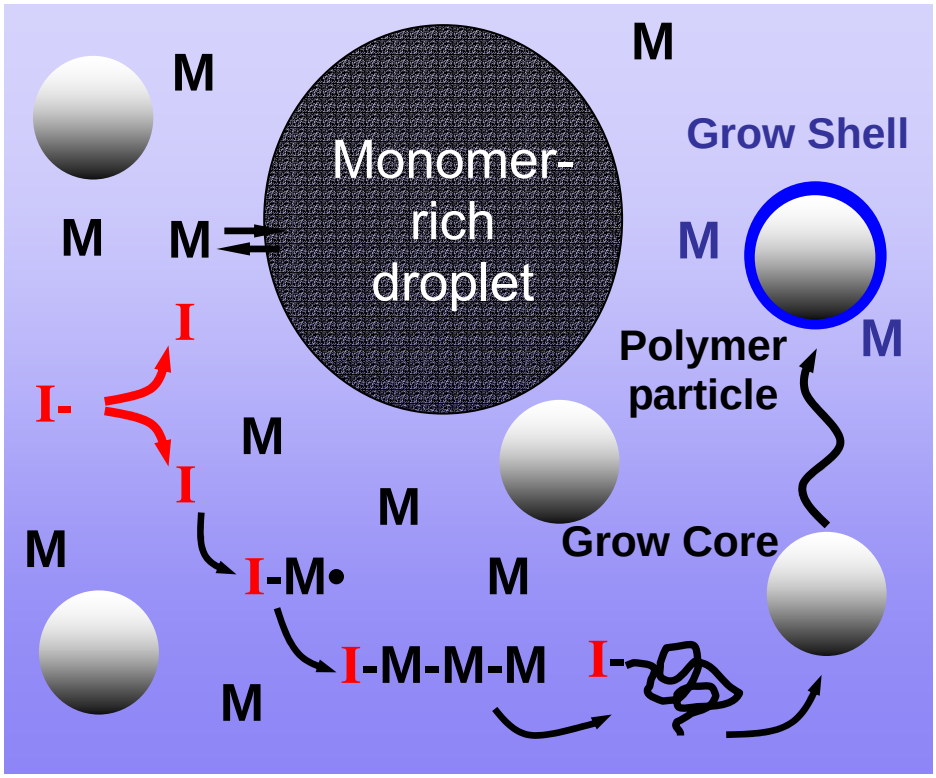

Figure 3.1 Schematic of surfactant-free emulsion polymerization. A small amount of hydrophobic monomer is dissolved in the aqueous phase, and in equilibrium with large droplets of monomer in the starting emulsion. As initiators break down and create free radicals, they encounter the dissolved monomer and initiate chain growth. As the chains grow, they precipitate, and form a nascent polymer particle, which is stabilized in the suspension due to electrostatic charge of the initiator fragments as well as the monomer units themselves. To grow a 'shell' structure, a second monomer is injected after an initial 'core' polymerization stage is carried out.

As shown in Figure 3.1, the particles were synthesized by a two-stage surfactant-free emulsion polymerization in water. In the first stage, DEAEMA, which possesses a tertiary amine with a pK_b of 7.0-7.3,[72, 73, 77, 81] was polymerized for 3 hours with

poly(ethylene glycol) dimethacrylate (PEGDMA, MW_{PEO} = 200 g/mol) as a crosslinker to form the pH-sensitive core of the particles (Figure 3.2). Control particles lacking pH-sensitivity were synthesized by replacing DEAEMA with the non-ionizable monomer methyl methacrylate (MMA). In the second stage, AEMA was injected to the stirring latex suspension to polymerize a pH-insensitive hydrophilic shell layer rich in primary amines (Figure 3.2). The polymerization was stopped after another 1.5 hours and the particles were purified by extensive dialysis and centrifugation/washing. To enable tracking of the nanoparticles by fluorescence microscopy, the fluorochrome Cy5 succinimidyl ester was covalently conjugated to the primary amines available in the particle shells.

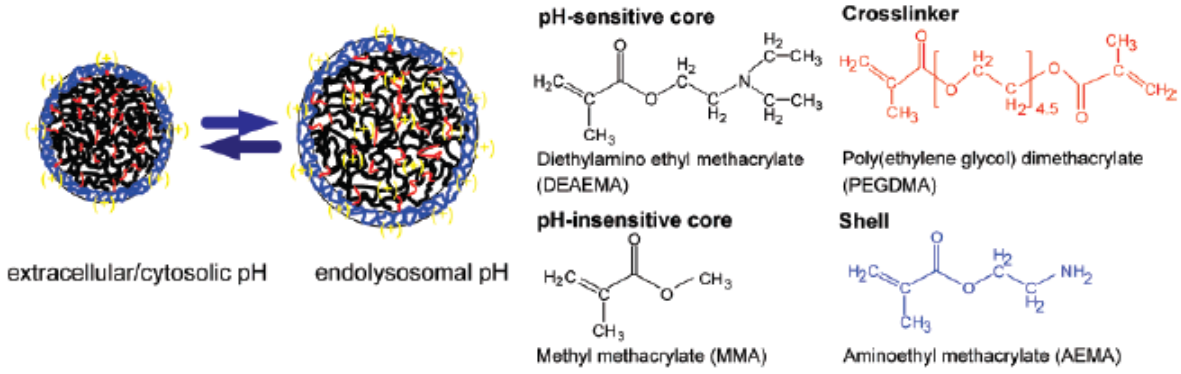

Figure 3.2 Schematic structure and chemical composition of pH-responsive core-shell nanoparticles. At extracellular/cytosolic pH, tertiary amines of DEAEMA repeat units in the particle cores are largely uncharged, and the particles are collapsed; at endolysosomal pH, the core tertiary amines ionize, and the particles swell. Surfactant-free polymerization of DEAEMA or MMA formed the core structure of hydrogel nanoparticles, crosslinked by PEGDMA; AEMA was polymerized in a second stage to form a thin shell structure rich in primary amines.

The surfactant-free emulsion polymerization is a very simple synthesis process. As mentioned above, it enables control over the size of the nanoparticles, which should be highly monodisperse. In addition, we did not have to use surfactant to stabilize the micelle, which made the formed nanoparticles very easy to be cleaned, as surfactant can remain in the polymer and can be difficult to remove. Overall, this process is an excellent system to generate pure synthetic particles for biological applications.

3.2.2 Morphology of Nanoparticles

TEM and CryoEM were performed to verify the monodispersity, and to examine the size of the as-synthesized nanoparticles. As expected, the emulsion polymerization yielded highly monodisperse particles as revealed by both TEM and CryoEM (Figure 3.3). During the preparation of TEM samples, the particles needed to be dehydrated. This process could affect the particle size, so CryoEM was further used to analyze particle morphology and size in hydrated conditions. The particles used in our cell culture studies were 205 ± 5 nm in diameter as observed in CryoEM (Figure 3.3B), which was in good agreement with the diameter of 208 ± 4 nm determined by DLS at 37 °C in aqueous phosphate buffer at pH 7.4 and physiological ionic strength (Figure 3.4A).

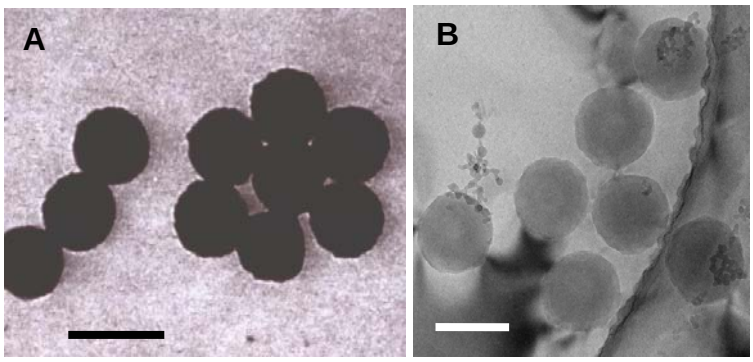

Figure 3.3 TEM and CryoEM images of nanoparticles. Scale bars 500nm for TEM (A), 200nm for CyroEM (B).

3.2.3 pH Sensitivity and Buffering Capacity of Core-Shell Nanoparticles

Compared to our bulk hydrogel system described in Chapter 2, we used only DEAEMA as the monomer, instead of a comonomer system with PEGMA, as the bulk gels studies suggested that the presence of long PEG chains reduces the pH-sensitivity of DEAEMA gels. In addition, PEGMA comonomer would render the resulting polymer chains more hydrophilic, and could destabilize the emulsion polymerization. However, DEAEMA is the major monomer to provide pH-sensitivity, and the group of Armes has shown that PDEAEMA-containing latex particles exhibit sharp swelling transitions near neutral pH,[82, 83] analogous to bulk hydrogels composed of weak polybase network chains.[84]

To characterize the pH sensitivity of our core-shell nanoparticles, the hydrodynamic diameters were measured by DLS for particles equilibrated in phosphate buffers at physiological ionic strength with pH ranging from 4.9 to 9.5 at 25 °C or 37 °C (Figure 3.4). Particle swelling/deswelling equilibrated within 10 min, and was reversible in

response to changes in buffer pH. As shown in Figure 3.4 A, PDEAEMA core-shell nanoparticles were largely deswollen at elevated pH, but swelled abruptly between pH 7.0 and 6.8 at 37°C. The particles exhibited a 2.8-fold change in diameter (by DLS) on moving from the extracellular/cytosolic pH of 7.4 to an endolysosomal pH of 5, corresponding to a ~ 22-fold volume change. Similar swelling trends were observed by measuring the swelling ratio (hydrated mass/dry mass, Figure 3.4B). Note that the primary amines of the AEMA groups (pK_b ~ 11) in the particle shells should remain highly ionized across this entire pH range; only the tertiary amines of the particle cores will respond to the changes in pH. The swelling response of DEAEMA-containing nanoparticles showed modest temperature sensitivity: at 25 °C, the swelling transition was detected at pH ~ 7.4, while at 37 °C, the swelling transition moved to pH ~ 7.0. Control nanoparticles with pH-insensitive PMMA cores and PAEMA shells (diameter of 284 ± 11 nm as determined by DLS at pH 7.4) exhibited no size/swelling change in aqueous phosphate buffers having pH 4.5 to 9.5 (Figure 3.4B).

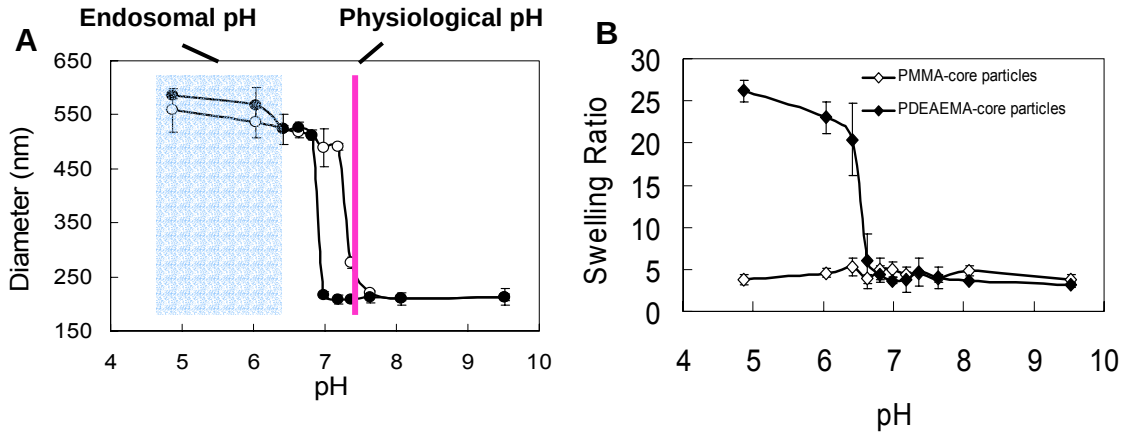

Figure 3.4 pH-responsive swelling of core-shell nanoparticles. (A) Hydrodynamic diameters of the nanoparticles equilibrated in 100 mM phosphate buffers of different pHs, determined by DLS at (○) 25°C or (●) 37°C. (B) Mass swelling ratio of core-shell nanoparticles at 37°C. (◇) PMMA core-shell nanoparticles and (◆) PDEAEMA

core-shell nanoparticles. Shown are average ± S. D. of triplicate samples.

The morphology of PDEAEMA-core nanoparticles with fluorophore-labeled shells was also directly observed at extracellular/cytosolic and endolysosomal pH using confocal laser scanning microscopy (CLSM). At pH 7.5 in the deswollen state (Figure 3.5A), the shell-labeled particles appeared as punctuate spheres, while particles incubated in pH 4.8 phosphate buffer swelled, with the fluorescent shell of the swollen nanoparticles clearly resolved (Figure 3.5B).

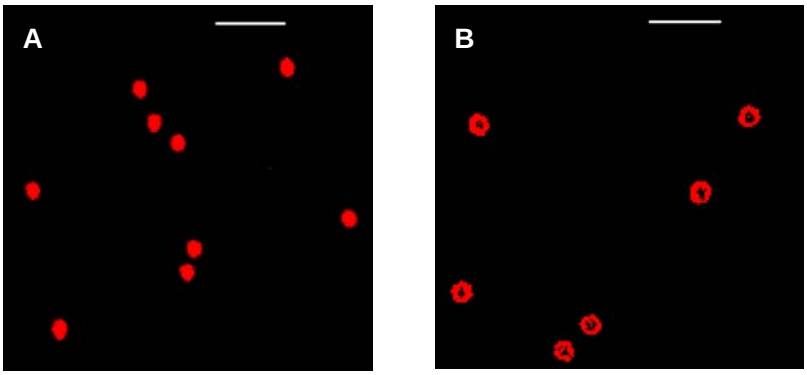

Figure 3.5 Morphology and pH-responsive swelling of core-shell nanoparticles. CLSM fluorescence images of PDEAEMA core-shell nanoparticles with Cy5 fluorophore conjugated to the PAEMA shell of the nanoparticles at pH 7.5 (A) or pH 4.8 (B) in 100 mM phosphate buffer at 25 °C. Scale bars 5 μm.

The swelling measurements indicated a sharp onset of particle core ionization at endosomal pH, but the proton sponge mechanism of endosomal escape relies on the buffering capacity of polymers undergoing ionization.[85] Titration of initially basic aqueous particle suspensions with HCl revealed that the PDEAEMA-core particles had a substantial buffering capacity near neutral pH (Figure 3.6). At 25 °C, the PDEAEMA

cores of nanoparticles bound up to 0.46 moles H^+ per mole of DEAEMA units, buffering acidified solution near a pH ~7.1. This buffering capacity was not affected by the PAEMA shell structure. PMMA core nanoparticles, on the other hand, showed no pH buffering activity once the primary amines of the PAEMA shell were protonated. This titration experiment further proved that the pH-responsiveness of the particles derives from the absorption of protons by tertiary amines of DEAEMA at the swelling transition pH. The osmotic pressure, generated when water entering the gels to dilute the counterions which were associated with charged groups on the polymer chains, provided the hydrogel swelling ability. This proton absorption character met our proposed requirements for endolysosomal disruption via the 'proton sponge effect'.

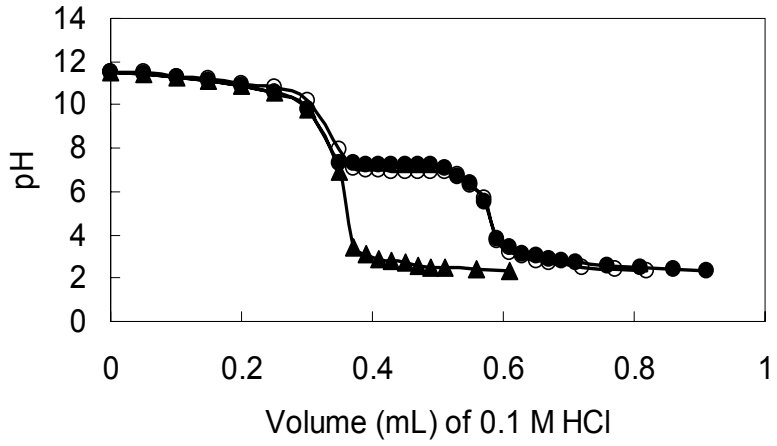

Figure 3.6 Titration measurement of core-shell nanoparticle buffering capacity at 25 °C. (●) PDEAEMA-core/PAEMA-shell nanoparticles, (○) PDEAEMA-core/no-shell nanoparticles, and (▲) PMMA-core/PAEMA-shell nanoparticles.

3.2.4 Analysis of Endotoxin Contamination

Some cells such as dendritic cells (DCs) are highly sensitive to the presence of lipopolysaccharide (LPS, also known as endotoxin), which can trigger activation of these cells through Toll-like receptor-4. Nanoparticles were thus prepared using endotoxin-free water or buffers. We detected the LPS concentration was 0.0027 EU/μg nanoparticles, or 0.0685 ± 0.001 EU/mL (S.D. from triplicate samples) at the concentrations of 25 μg/mL nanoparticles used in our cell experiments. This result confirmed that the endotoxin contamination in these particles was below levels reported to stimulate DCs or to trigger substantial changes in DC function.[86-88]

3.2.5 Stability of Core-Shell Nanoparticles

Stability in Intracellular Conditions

As expected based on the incorporation of chemically stable PEGDMA crosslinks, we found that the particles were stable at least one week in neutral saline; the particles swelled slightly over a week but retained a narrow size distribution (Figure 3.7). The dry weight of the particles was essentially unchanged after one week in PBS (1.5 ± 0.7% weight loss, based on triplicate samples). In addition, the particles exhibited a nearly identical size distribution in pH 7.4 serum-free medium containing 10 mM glutathione (GSH) to mimic the reducing environment of the cytosol (Figure 3.7).

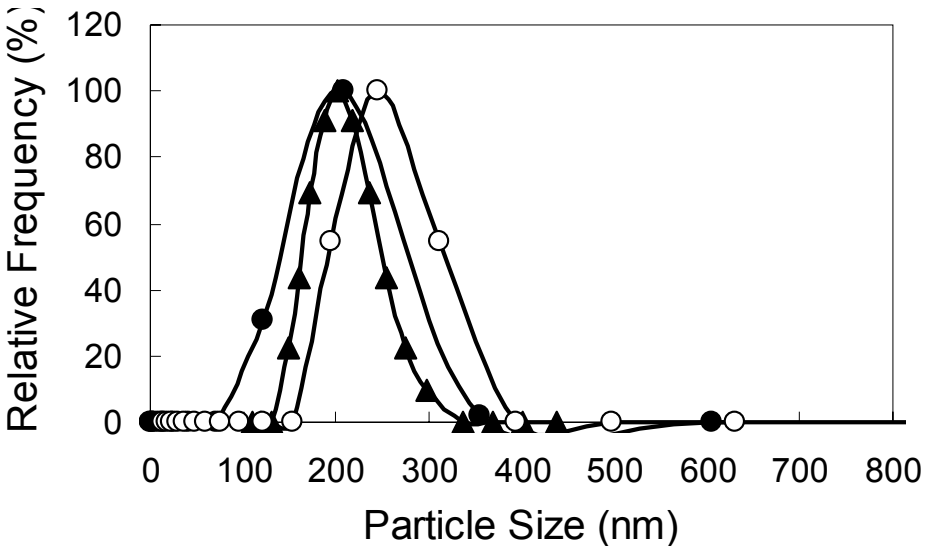

Figure 3.7 Size distributions of PDEAEMA core-shell nanoparticles assessed in different media over time. Nanoparticles (270 μg/mL) were incubated in PBS (pH 7.4) or 10 mM GSH (in serum free medium, pH 7.4) at 37 °C. The size distributions of the nanoparticles were measured after different incubation times: (●) 2 days in PBS, (▲) 2 days in GSH, and (○) 7 days in PBS.

Zeta-Potential of Nanoparticles at Different pH

We detected the zeta potential of the nanoparticles in different pH buffers to understand the stability and the surface charge of the nanoparticles. The zeta potential is the electric potential in the interfacial double layer (DL) at the location of the slipping plane, versus a point in the bulk fluid away from the interface. In other words, the zeta potential is the potential difference between the dispersion medium and the stationary layer of fluid attached to the dispersed particle. Its value can be related to the stability of colloidal dispersions. Colloids with high zeta potential are electrically stabilized, while colloids with low zeta potentials tend to coagulate or flocculate unless sterically

stabilized (*e.g.*, by water-soluble surface-anchored polymer chains). In Figure 3.8, the zeta potential of PDEAEMA nanoparticles with or without AEMA shells were examined in the NaCl solutions (5 mM) with different pHs. The values of the zeta potential started decreasing at pH 7.0 for both core-shell and core-only nanoparticles. In the case of core-only nanoparticles, it reached a much lower level (~ 27 mV) than that of core-shell nanoparticles (~ 44 mV) at pH 7.4. This result confirms that the AEMA shell rich in primary amine provides a positive charge at near-neutral pH, facilitating drug binding and cell binding. The non-shell particles would not bind negatively charged drugs (such as DNA or some proteins) very efficiently. In addition, it was not favored by the slightly negatively charged cell membrane. However, the IEP isoelectric points (IEPs) were around pH 9 for both core-shell and non-shell nanoparticles. Ultimately, we were unable to explain the similarity of the IEPs despite the shell structure, and the difference between the IEPs and the polymer pK_a of AEMA or pK_b DEAEMA.

The particles were prepared with APS as initiator. Therefore the surface of the particles is rich in sulfate, which means they are zwitterionic instead of highly positively charged. Armes reported similar findings in their APS-initiated latex particles.[82] This hypothesis could be further evaluated by NMR on the particles in the collapsed state (*e.g.*, pH 7.4 buffered D_2O) to determine the ratio of amino to persulfate groups in the shell.

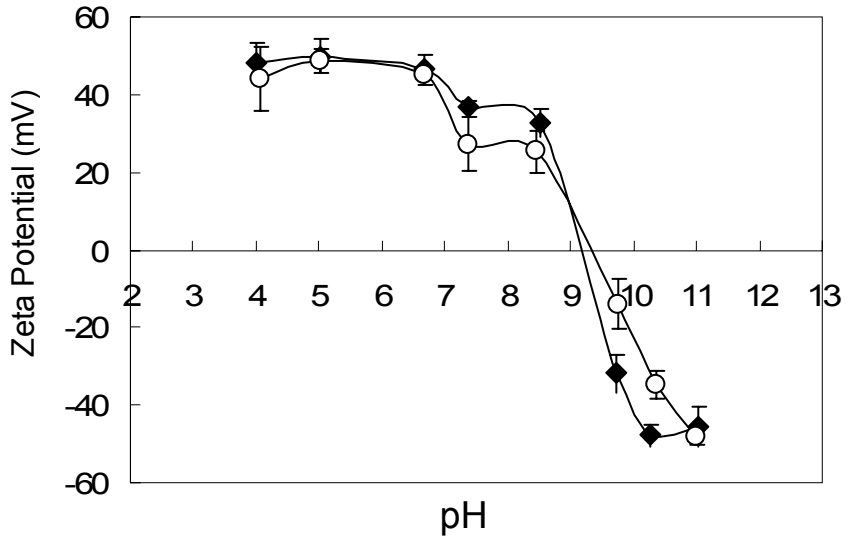

Figure 3.8 Zeta potential of PDEAEMA nanoparticles in the sodium chloride solutions at different pHs. Particles with AEMA shells (filled circles) or without AEMA shells (open circles) were examined in the NaCl solutions (5 mM) with different pHs. Shown are mean ± S.D. of three individual measurements.

In this chapter, we fabricated hydrogel nanoparticles by surfactant-free emulsion polymerization. The formed core-shell nanoparticles were highly monodisperse, with size of ~ 200 nm shown by EM. We proved that those PDEAEMA-core/PAEMA-shell nanoparticles were able to swell to a 2.8-fold change in diameter (by DLS) on moving from the extracellular/cytosolic pH of 7.4 to an endolysosomal pH of 5, which was caused by the absorption of protons by the tertiary amine groups at reducing pH lower than DEAEMA's pK_b. This 'proton sponge' effect could be applied for endolysosomal escape as we designed. The characterization and application of these nanoparticles to the biological system will be discussed in the following chapter.

4 Endolysosomal Escape of pH-Sensitive Core-Shell Nanoparticles

We successfully synthesized core-shell nanoparticles that can respond to endolysosomal pH and reversibly swell and buffer pH. We hypothesized that the pH sensitivity of these core-shell nanoparticles would facilitate endosome/phagosome disruption, while preventing cytotoxicity via sequestration of the hydrophobic pH-sensitive component under the more hydrophilic shell of the particles. Buffering polymers are thought to disrupt acidifying endolysosomes via an osmotic pressure buildup associated with chloride accumulation (the proton sponge effect).[89, 90] In addition, membrane disruption might further be aided by swelling of the particles *in situ*.

In this chapter, we tested this hypothesis first in an immortal cell line (DC2.4), using a small molecule calcein to examine the delivery efficiency, delivery mechanism, and cytotoxicity. Application of this system to cytosolic delivery of macromolecules to primary dendritic cells will be discussed in the following chapter.

4.1 Materials and Methods

4.1.1 Materials

All reagents were used as received without further purification. RPMI 1640, DMEM (with 4.5 g/L glucose), and Trypsin/EDTA (0.25% trypsin/2.21 mM EDTA in HBSS without sodium bicarbonate, calcium, and magnesium) were purchased from

Mediatech Inc. Fetal bovine serum (FBS) was purchased from Hyclone. MTT Cell Proliferation Assay Kit was purchased from American Type Culture Collection (ATCC). LysoTracker® Red DND-99, Fura-2AM, and CyQUANT® NF Cell Proliferation Assay Kit were purchased from Invitrogen. Bafilomycin A1 and Calcein were purchased from Sigma-Aldrich Chemical Co. Trypan blue (0.04%) was purchased from VWR.

4.1.2 Cell Culture and Calcein Delivery

DC2.4 cells, a dendritic cell clone originally derived by Shen *et al.*,[91] were a gift from Professor Kenneth Rock. These cells were cultured and passaged in complete RPMI 1640 medium containing 10% FBS, 50 μM 2-mercaptoethanol, 5 mM L-glutamine, 10 mM HEPES, and penicillin/streptomycin. Murine embryonic fibroblasts (MEFs) were obtained from ATCC, and cultured and passaged in complete DMEM medium containing 10% FBS, 50 μM 2-mercaptoethanol, 4 mM L-glutamine, 10 mM HEPES, and penicillin/streptomycin.

To test delivery efficiency of small molecules by the core-shell nanoparticles, DC2.4 cells ($1.2x10^5$ cells/well) were plated in Lab-Tek™ chambers and cultured overnight (~ 18 hours). Calcein was added to the cells (150 μg/mL, 0.24 mM) with or without 25 μg/mL PDEAEMA core-shell or PMMA core-shell nanoparticles in complete medium (RPMI 1640 with 10% fetal bovine serum (FBS)) for 1 hour at 37 °C. After three washes with medium to remove extracellular calcein/particles, the cells were imaged live by CLSM at 37 °C. The modified delivery process for LysoTracker®, bafilomycin A1, or Fura 2AM are described in the related sections.

4.1.3 TEM Imaging of Nanoparticles in Dendritic Cells

DC2.4 cells were plated in Petri dishes (6-well plates, $1.2x10^6$ cells/well) and cultured in complete medium for 18 hours. Cells were treated with or without 25 μg/mL PDEAEMA or PMMA core-shell nanoparticles for 1 hour at 37 °C. After washing three times with complete medium, the cells were fixed in 2.5% glutaraldehyde, 3% paraformaldehyde, 5% sucrose in 0.1 M sodium cacodylate buffer (pH 7.4), following by post fixation in 1% osmium tetroxide in veronal-acetate buffer (pH 7.0). The cells were stained in block overnight with 0.5% uranyl acetate in veronal-acetate buffer. After water rinsing, cells were then dehydrated through graded concentrations of ethanol (50%, 70%, 90%, and 100%) and embedded in Spurrs resin. Sections were cut on a Reichert Ultracut E microtome with a Diatome diamond knife at a thickness setting of 50 nm and stained with 2.0% uranyl acetate followed by 0.1% lead citrate. Samples were examined using a JEOL JEM 1200 EX II at 60 KV or a Phillips EM410 at 80 KV.

4.1.4 Cytotoxicity

MTT Assay for Cell Metabolic Rate

DC2.4 cells were plated in 96-well plates at a density of $5x10^4$ cells/well. After incubation at 37 °C for 18 hours in complete medium, cells were incubated with 25 μg/mL (or different concentration) PMMA core-shell, PDEAEMA core-shell, PDEAEMA-core/no-shell nanoparticles, or blank medium for 1 hour at 37 °C. After washing three times with complete medium, cells were treated with MTT reagent immediately or after an additional 24 hours culture in complete medium post-particle

treatment, followed by adding MTT detergent after an additional 4 hours. The cell density was then determined by the absorbance at 570 nm wavelength using a microplate spectrophotometer system (SPECTRAmax^{TM} 250, Molecular Devices Corp.)

Cell-Growth Assays of Cell Viability

For cell-growth assays, cells were harvested after nanoparticle treatment as above, washed, and replated in 96-well plates at a density of $2.5x10^4$ cells/well. The replated cells were then cultured for an additional 3 days, and the number of cells grown out in these cultures was determined by the CyQUANT® NF Cell Proliferation Assay Kit at 488 nm/530 nm using a fluorescence microplate reader (SPECTRAmax^{TM} GEMINI, Molecular Devices Corp.)

4.2 Calcein Delivery

4.2.1 Cytosolic Calcein Delivery with Nanoparticles

Because of our interest in delivering membrane-impermeable molecules into dendritic cells for vaccines and antiviral drug delivery, we investigated the uptake of the nanoparticles by a dendritic cell clone,[91] DC2.4. Calcein, a membrane-impermeable fluorophore, was used as a model drug molecule and tracer to monitor the stability of endosomes/phagosomes following particle uptake.[43] Calcein delivery with PDEAEMA (pH-sensitive) and PMMA (pH-insensitive) core-shell nanoparticles was carried out as described in Section 4.1.2. Briefly, DC2.4 cells ($1.2x10^5$ cells/well) were plated in Lab-Tek^{TM} chambers for 18 hours, and then calcein (150 μg/mL, 0.24 mM) was added to

the cells with or without nanoparticles (25 μg/mL) in complete medium for 1 hour at 37 °C. After three washes with medium to remove extracellular calcein and particles, the cells were imaged live by confocal laser scanning microscopy (CLSM) at 37 °C. As shown in Figures 4.1 A/D/G, cells treated with calcein alone showed a punctuate distribution of fluorescence indicative of endolysosomal compartmentalization of the dye. In contrast, cells co-incubated with calcein and PDEAEMA-core/PAEMA-shell nanoparticles exhibited calcein fluorescence throughout the cytosol and nucleus (Figures 4.1 B/E/H). Calcein entry into the cytosol triggered by the presence of nanoparticles required the pH-sensitive core, as calcein remained in an endosomal distribution in cells co-incubated with calcein and PMMA-core/PAEMA-shell nanoparticles (Figures 4.1 C/F/I).

Figure 4.2 summarizes the frequency of cells observed by CLSM exhibiting endosomal *vs.* cytosolic/nuclear calcein distributions after 1 hour incubation under the three experimental conditions. Fewer than 5% of cells incubated with calcein alone or calcein together with PMMA core-shell nanoparticles exhibited a cytosolic/nuclear calcein distribution, while ~ 90% of cells incubated with PDEAEMA core-shell nanoparticles had calcein distributed throughout the cytosol. Particles prepared with PDEAEMA cores but lacking the PAEMA shell also triggered cytosolic entry of calcein (Figure 4.3) suggesting that the non-pH-responsive cationic amine groups in the shells are not required for the calcein distribution seen in Figures 4E and H.

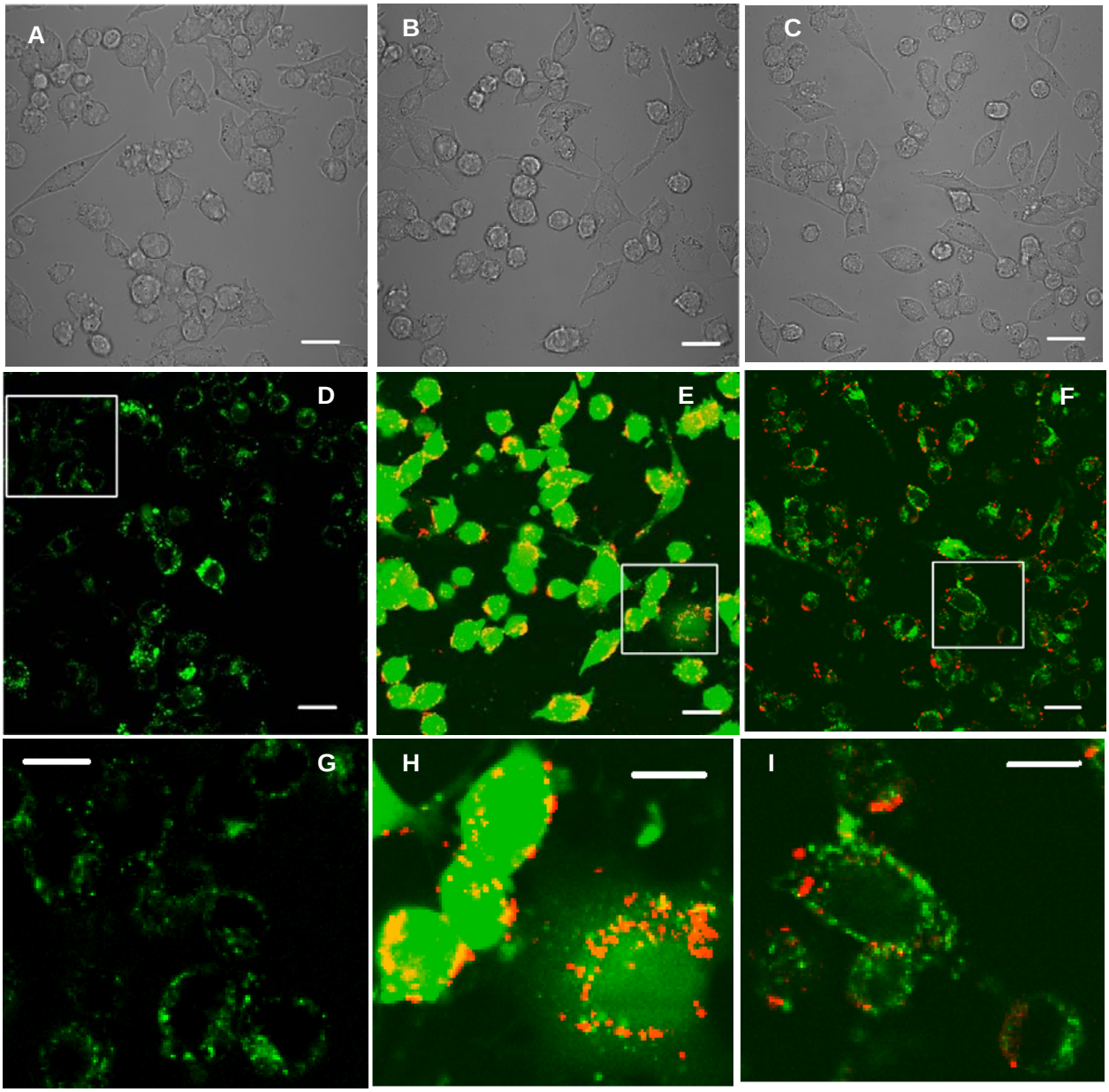

Figure 4.1 pH-responsive core-shell nanoparticles chaperone the delivery of the membrane-impermeable dye molecule calcein into the cytosol of dendritic cells. (A-I) CLSM images at 40X. (A-C) Brightfield images. (D-I) Fluorescence overlays (red, nanoparticles; green, calcein). (A, D, G) Cells were treated with calcein alone. (B, E, H) Cells were co-incubated with calcein and PDEAEMA-core/PAEMA-shell

nanoparticles. (C, F, I) Cells were co-incubated with calcein and PMMA-core/PAEMA-shell nanoparticles. Scale bars (A-F) 20 µm; (G-I) 10 µm.

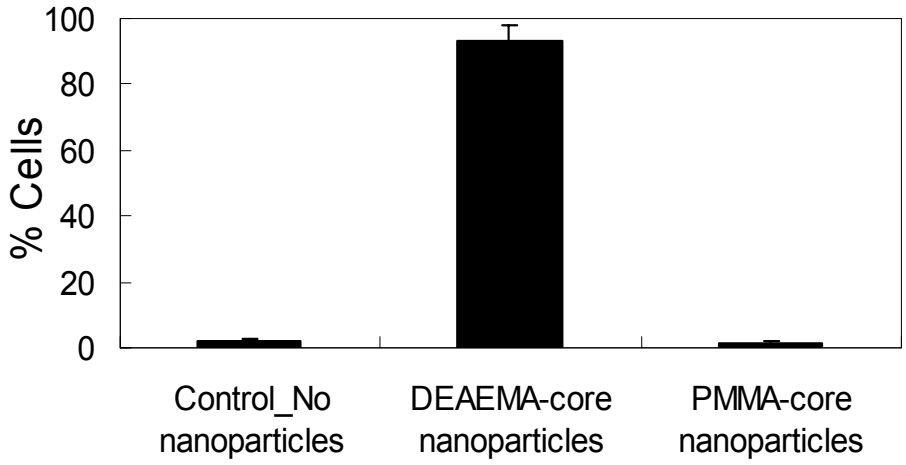

Figure 4.2 Cytosolic delivery efficiency of calcein in DC2.4. Average percentage of cells observed by CLSM exhibiting cytosolic/nuclear calcein distributions after 1 hour incubation from three independent experiments: calcein alone (no particles), calcein with PDEAEMA core-shell particles, or calcein with PMMA core-shell particles (*n*=350-700 cells scored per condition in each experiment; shown are means ± S.D.).

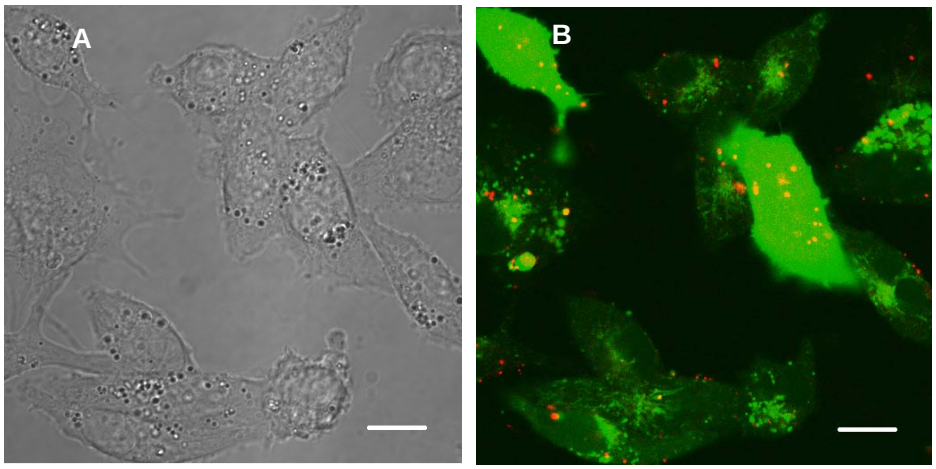

Figure 4.3 Crosslinked PDEAEMA nanoparticles lacking a PAEMA shell also trigger calcein delivery to the cytosol. Confocal images of live DC2.4 cells following 1 hour

incubation with 25 μg/mL PDEAEMA-core/no-shell nanoparticles and 0.24 mM calcein were collected at 100X. (A) Brightfield image. (B) Overlay of nanoparticle (red) and calcein (green) fluorescence. Scale bars 10 μm.

Experiments performed with different incubation times showed that the cytosolic delivery of calcein occurred within 45 min, and was observed for more than 95% cells incubated with calcein and PDEAEMA core-shell nanoparticles by 90 min. DCs treated with nanoparticles for 1 hour, washed, and then cultured for an additional 24 hours showed that most or all of the nanoparticles remain within the cells for at least 1 day (Figure 4.4). Note that DC2.4 proliferation occurred over this time period, which led to some dilution of the density of nanoparticles in any given cell after prolonged incubation.

Cytosolic delivery of calcein triggered by core-shell nanoparticles was not limited to dendritic cells, as we observed similar results in murine embryonic fibroblasts (Figure 4.5).

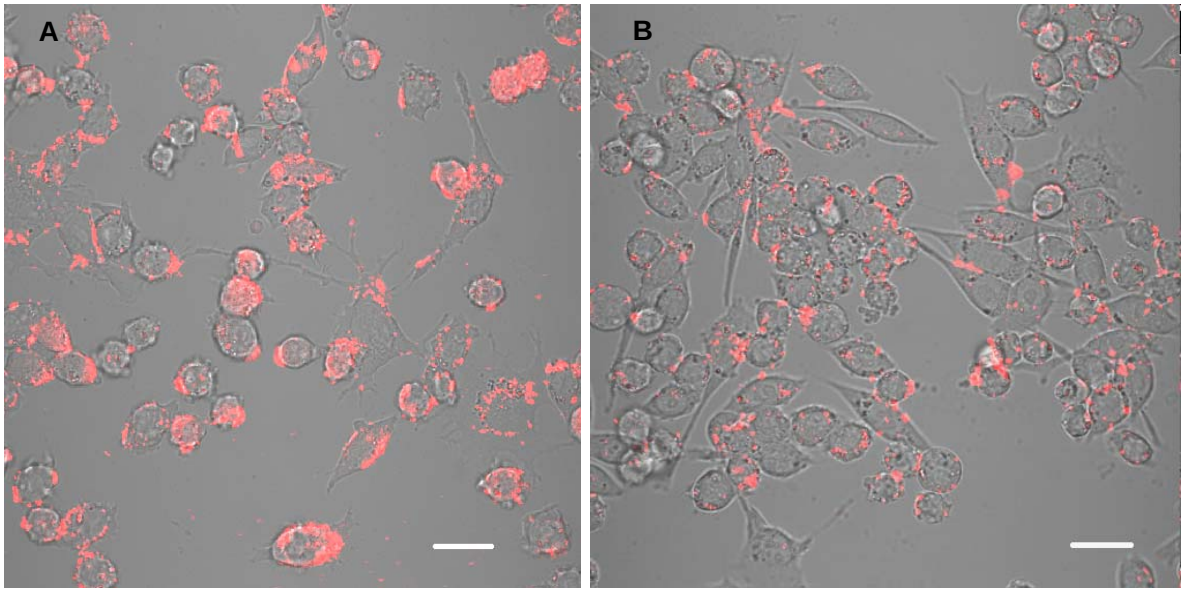

Figure 4.4 PDEAEMA core-shell nanoparticles stably retained in cells for at least 24 hours. DC2.4 cells were incubated with 25 μg/mL PDEAEMA core-shell nanoparticles for 1 hour, washed, and then imaged live by confocal microscopy at 40X (A). The cells were then cultured an additional 24 hours and imaged again to determine whether nanoparticles remain associated with the cells (B). Shown are overlays of nanoparticle fluorescence (red) and cells (brightfield). Scale bars 20 μm.

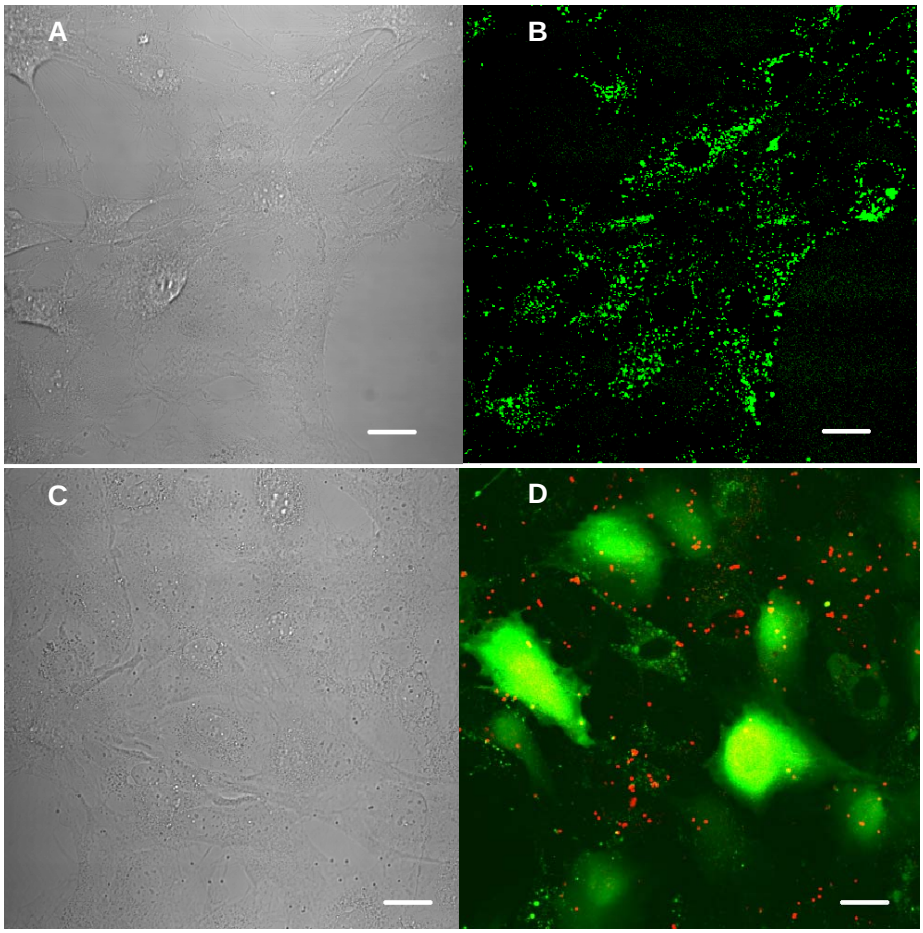

Figure 4.5 Core-shell nanoparticles deliver calcein to the cytosol of fibroblasts. Murine embryonic fibroblasts were incubated for 1 hour with 0.24 mM calcein (A, B) or calcein and 25 μg/mL pH sensitive PDEAEMA-core/PAEMA-shell nanoparticles (C, D), and then imaged live at 37 °C by CLSM at 40X. Shown are brightfield (A, C) and fluorescence overlays (red, nanoparticles; green, calcein fluorescence; B, D). Scale bars 20 μm.

4.2.2 Tracking Endosomal Disruption Triggered by Core-Shell Nanoparticles in Live Cells

As shown above, DEAEMA-core pH-sensitive nanoparticles were able to delivery calcein to the cell cytosol of DC2.4 efficiently. We next designed experiments to further

understand the mechanism underlying this process. The cellular uptake, localization of nanoparticles, necessity for co-internalization of drug molecules with the nanoparticles, and requirement for acidification of the endolysosomal environment were examined, and are discussed in detail below.

Cellular Uptake of Calcein and Nanoparticles

Particle size[24] usually plays an important role for endocytosis; substantial uptake of nanoparticles by cells in a short time period may be desirable to ensure adequate drug delivery to individual cells. To quantify relative uptake of core-shell nanoparticles of different compositions, we performed flow cytometry. As described in Chapter 3, particles were labeled with Cy5 dye on the shell, enabling fluorescence analysis.

Although CLSM images had proved the fluorescent label was on the particles (Figure 3.5), we used flow cytometry to further test the fluorescent labeling efficiency of the nanoparticles. Only particle samples were run through flow cytometer, and 99% of labeled particles showed a strong fluorescent marker (in Figure 4.6A). Similar results were obtained for PMMA core-shell nanoparticles (data not shown). We then analyzed the relative cellular uptake of these particles following the same incubation conditions used for calcein delivery studies as described in Figure 4.1. Cells were incubated with fluorescence-labeled nanoparticles for 1 hour at 37 °C and washed three times, and flow cytometry was then performed to identify the Cy5 positive cells. As shown in Figure 4.6 B, the majority of cells internalized nanoparticles irrespective of the core composition following this incubation treatment; 80% of cells were Cy5 positive for PDEAEMA core-shell nanoparticles, while 60% of cells were Cy5 positive for PMMA core-shell nanoparticles. Thus, cells are capable of internalizing the particles efficiently after 1

hour of incubation with nanoparticle suspensions.

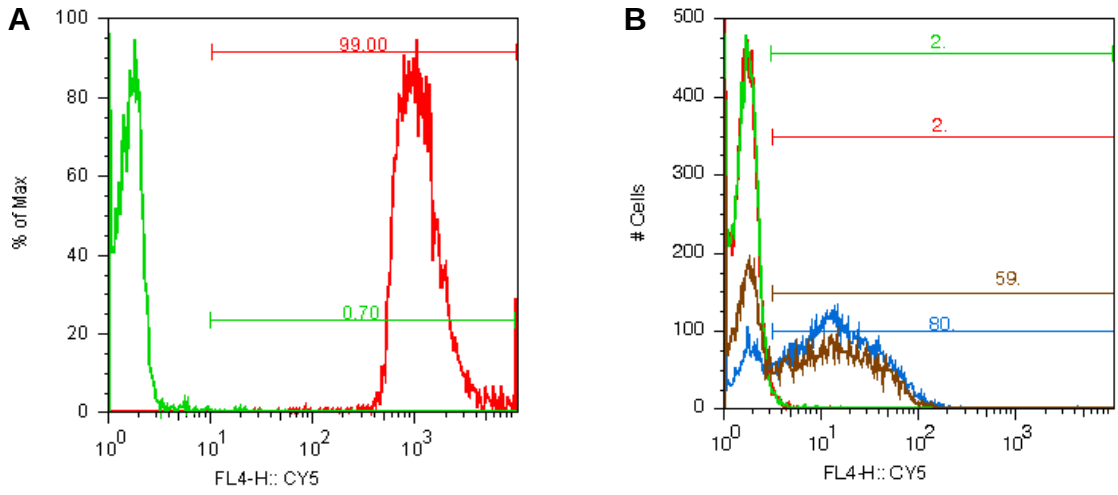

Figure 4.6 Quantification of relative uptake of nanoparticles by DC2.4 cells. (A) Fluorescent labeling efficiency of nanoparticles. Flow cytometric analysis of (cell-free) nanoparticle suspensions showed 99% labeled (red) PDEAEMA core-shell nanoparticles were Cy5 positive compared to non-labeled control (green) nanoparticles. (B) Percentage of cells that showed Cy5 positive without (red) or with treatment of calcein alone (green), PDEAEMA core-shell nanoparticles (blue), and PMMA nanoparticles (brown).

Particle Localization

The data shown in Figures 4.1-4.5 do not clarify the precise sub-cellular localization of the nanoparticles following binding/internalization by cells. As shown in the confocal images (Figures 4.1 E, F, H, and I), both PDEAEMA and PMMA core-shell nanoparticles were taken up by the phagocytic DC2.4 cells, and treatment of cells with 0.04% (wt/vol) trypan blue to quench extracellular fluorescence[91, 92] following particle incubation confirmed that particles associated with cells were in fact internalized (data

not shown). Optical sectioning of cells treated with PDEAEMA-core/PAEMA-shell nanoparticles also provided further evidence that particles in cells exhibiting cytosolic calcein fluorescence were localized within the cells, rather than being simply bound to the plasma membrane (Figure 4.7).

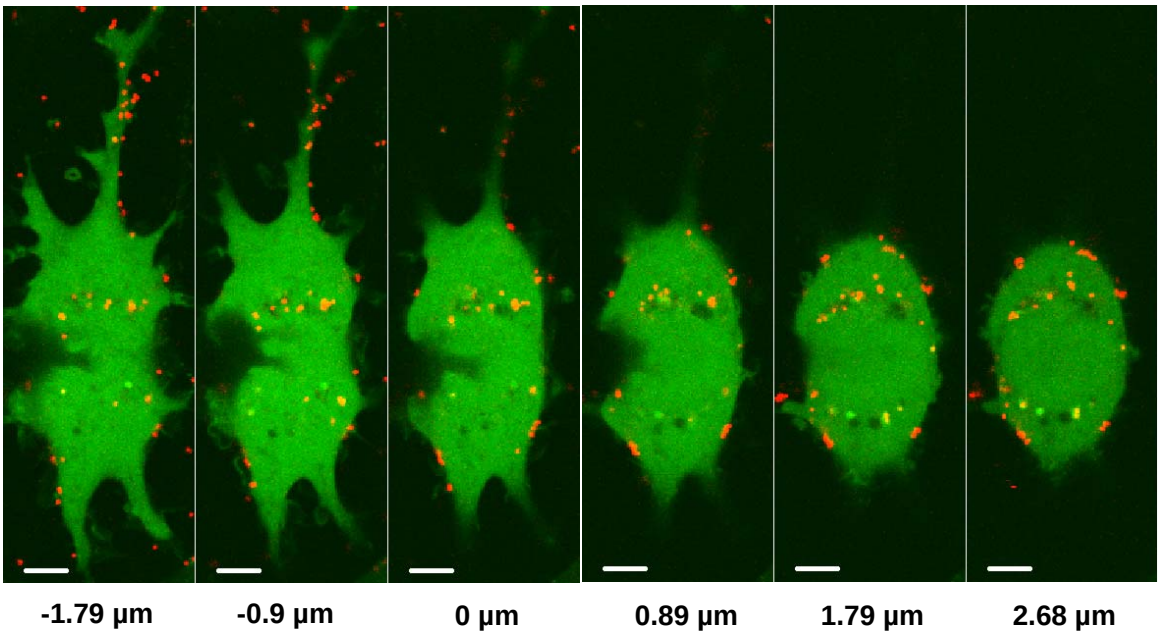

Figure 4.7 Optical sectioning of calcein- and nanoparticle-loaded dendritic cells. Serial confocal optical z-sections at 100X of nanoparticle (red) and calcein (green) fluorescence, illustrating the intracellular localization of nanoparticles in a calcein-flooded DC. Scale bars 5 µm. The number under each image gives the z-distance/interval of each image relative to the approximate vertical center of the cell.

The internalized nanoparticles could be localized in endolysosomes following endocytosis/macropinocytosis. To obtain more direct evidence for escape of the core-shell nanoparticles from endolysosomes into the cytosol, we performed confocal fluorescence imaging of cells incubated with nanoparticles in the presence of a

fluorescent marker of endolysosomal compartments, as well as transmission electron microscopy (TEM) on fixed thin sections of cells incubated with nanoparticles. The pH-sensitive fluorescent indicator LysoTracker® Red DND-99 (1 μM, Invitrogen) was added together with 0.24 mM calcein and 25 μg/mL core-shell nanoparticles to DC2.4 cells for 1 hour at 37 °C in order to label endolysosomal compartments during calcein uptake. After washing, cells were imaged by CLSM at 37 °C. The CLSM images (Figure 4.8 A, B, and C) revealed that a significant fraction of the internalized PDEAEMA core-shell nanoparticles (blue) failed to co-localize with endolysosomal vesicles (red) while delivering calcein (green) to the cytosol. In contrast, cells co-incubated with calcein and PMMA core-shell nanoparticles exhibited strong co-localization of nanoparticles (blue), endolysosomal vesicles (red), and calcein (green), which had a punctuate vesicular distribution (Figure 4.8 D, E and F). To more directly interrogate the location of internalized nanoparticles, TEM images were taken of thin sections (50 nm) from fixed and stained cells following 1 hour incubation of DC2.4 cells with nanoparticles. Core-shell nanoparticles with a pH-insensitive PMMA core were localized within membrane-bounded endosomes/phagosomes (Figure 4.8 G). However, PDEAEMA core-shell nanoparticles were observed both within membrane-bounded vesicles (Figure 4.8 H) and within the cytosol (Figure 4.8 I). These trends were consistently observed in imaging 55 particles from three individual experiments (8 PMMA particles, and 47 PDEAEMA particles, of which 10 were in endosomes and 37 were in the cytosol). Together, these data support the conclusion that the pH-sensitive PDEAEMA core-shell nanoparticles do not remain trapped in acidic intracellular compartments, but instead escape to the cytosol following internalization.

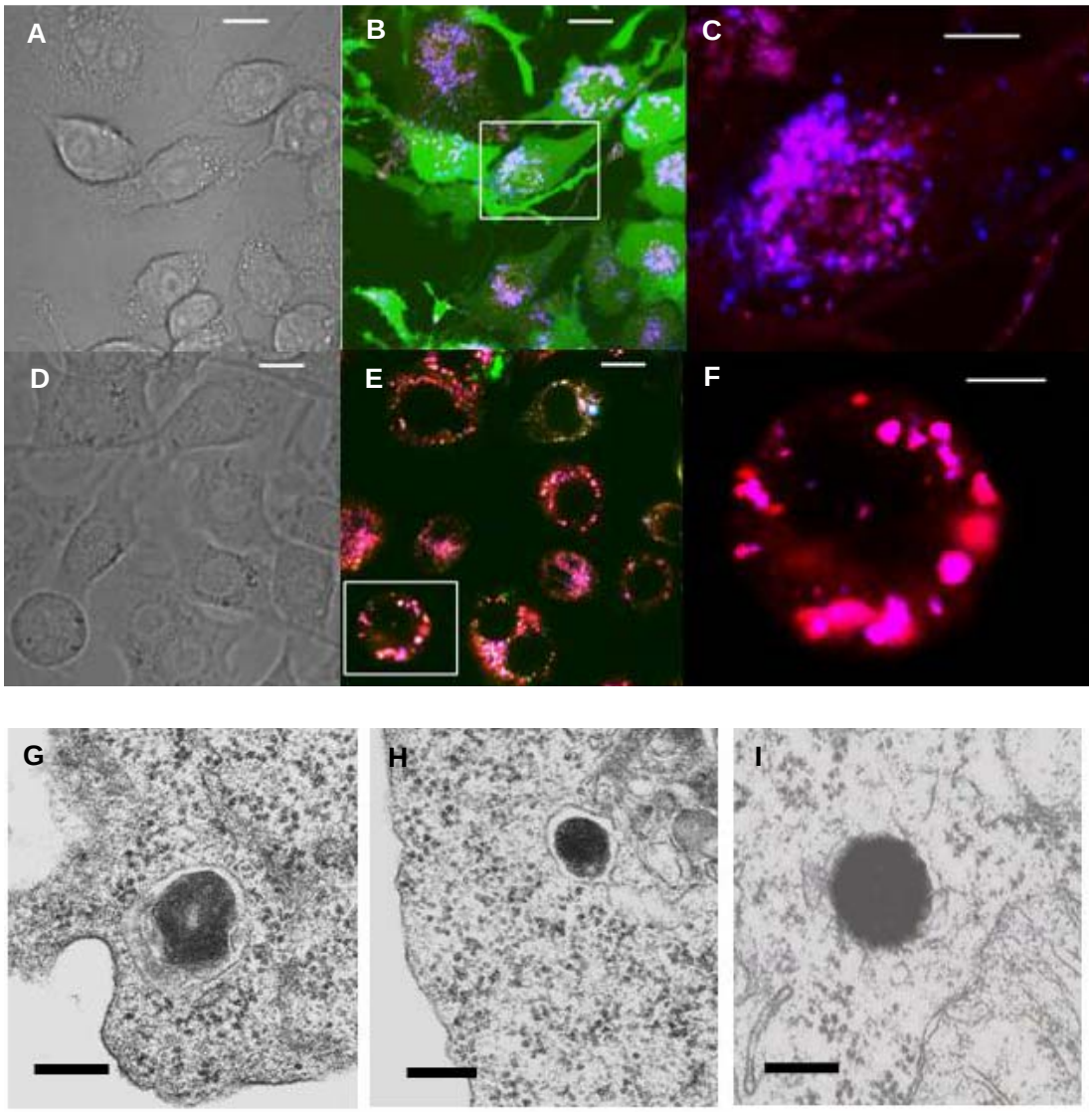

Figure 4.8 Endosomal escape of pH-responsive core-shell nanoparticles. (A-F) DC2.4 cells were co-incubated with LysoTracker® Red DND-99 (to label endolysosomes), calcein, and either PDEAEMA-core/PAEMA-shell (A-C) or PMMA-core/PAEMA-shell nanoparticles (D-F). Confocal images were taken at 100X, collecting brightfield images (A, D) as well as fluorescence (B, C, E, F) from calcein (green), LysoTracker® Red (red), and Cy5-labeled nanoparticles (blue). Scale bars 10μm (A, B, D, E) and 5 μm (C, F, zoomed views of boxed areas in B, E showing overlaid LysoTracker® Red and nanoparticles fluorescence). (G-I) TEM images of nanoparticle localization within

DC2.4 cells: (G) Cell sections with PMMA-core/PAEMA-shell particles revealed the particles internalized in membrane-bound compartments. (H-I) Cell sections with PDEAEMA-core/PAEMA-shell particles showed particles internalized either in membrane-bound compartments (H) or in the cell cytosol without a clear binding membrane structure (I). Scale bars 500 nm.

Endocytosis and Acidification Requirement for Efficient Cytosolic Calcein Delivery

The intracellular distribution of calcein observed in the presence of PDEAEMA-core/PAEMA-shell nanoparticles could arise either due to the particles causing disruption of endosomes that contain calcein, or via nanoparticles permeating the cell surface plasma membrane (note that calcein that reaches the cytosol is also able to freely enter the nucleus by diffusion[93]). Though proton-absorbing polymers and lipids have been proposed to cause escape of molecules into the cytosol following endocytosis and endosome acidification via the proton sponge effect,[89] it has also been shown that polycations such as polyethylenimine (PEI) and poly-L-lysine (PLL) have the ability to directly interact with the plasma membrane (the exterior cell surface), generating nanoscale transient pores that allow leakage of molecules into and out of the cytoplasm.[94] To examine the mechanism of cytosolic delivery of calcein by the core-shell nanoparticles, we tested calcein uptake by DC2.4 cells under additional conditions.

First, to confirm that active internalization of the nanoparticles/calcein was required for calcein delivery to the cytosol, DCs were equilibrated at 4 °C for 30 min to block endocytosis/macropinocytosis, and then calcein alone, or calcein and PDEAEMA core-shell nanoparticles, were added to the cells (using the same calcein and nanoparticle concentrations as described in Figure 4.1). Neither calcein nor nanoparticles were

internalized by cells following incubations up to 3 hours at 4 °C, although some particles bound to the plasma membrane of cells (Figure 4.9), suggesting that calcein/nanoparticle uptake and calcein entry into the cytosol of DCs required an active internalization process such as endocytosis or macropinocytosis.

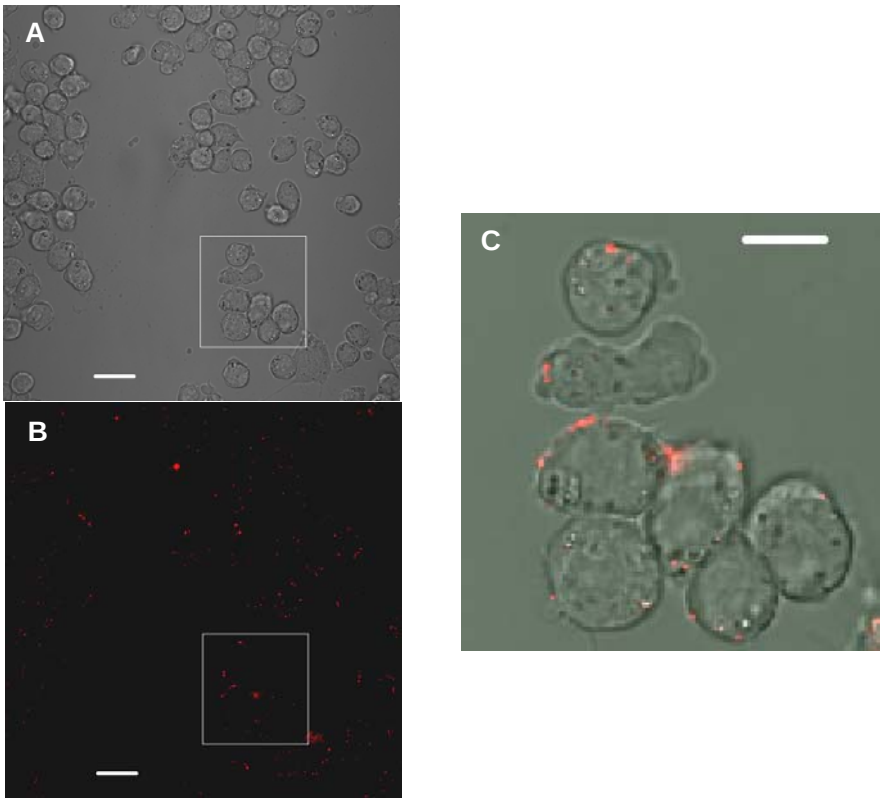

Figure 4.9 Calcein and nanoparticle internalization require active internalization in DC2.4 cells. CLSM images (40X) of live DC2.4 cells following incubation with calcein (green) and 25 μg/mL PDEAEMA core-shell nanoparticles (red) at 4 °C for 3 hours. (A, B) Cells with calcein and PDEAEMA core-shell nanoparticles: (A) Brightfield image and (B) overlay of fluorescent images. Scale bars 20 μm. (C) Overlay of boxed area from A and B. Scale bar 10 μm.

If the core-shell nanoparticle promoted calcein escape to the cytosol via a transient osmotic pressure which was generated only under the acidic conditions in endolysosomes, calcein and nanoparticles were requested to localize in the same endolysosomal compartment. Nanoparticles internalized into discrete vesicles from calcein should be unable to promote calcein access to the cytosol. To test this hypothesis, we designed a simple experiment to deliver calcein and nanoparticles separately. Calcein alone was incubated with DC2.4 for 1 hour at 37 °C (same calcein concentration as described in Figure 4.1). After washing off the extra calcein carefully, samples were treated with PDEAEMA core-shell nanoparticles (25 μg/mL) only, or with nanoparticles and calcein for one more hour at 37 °C. As shown in Figure 4.10 A, cells treated first with calcein only showed endolysosomal compartmentalization of the calcein dye. As we expected, samples treated with calcein first then with nanoparticles showed the similar distribution of calcein dye inside the cells (Figure 4.10B). Note that although the cellular uptake of nanoparticles was obvious, they were hardly co-localized with the calcein. However, control cells where co-internalization of calcein and nanoparticles was shown efficient cytosolic delivery of calcein (Figure 4.10C). These results confirmed that to facilitate the cytosolic delivery of calcein, nanoparticles had to be co-internalized by cells and present in the same endolysosomes with calcein. This conclusion directed us later in the design of drug loading/binding for the intracellular delivery system for macromolecules.

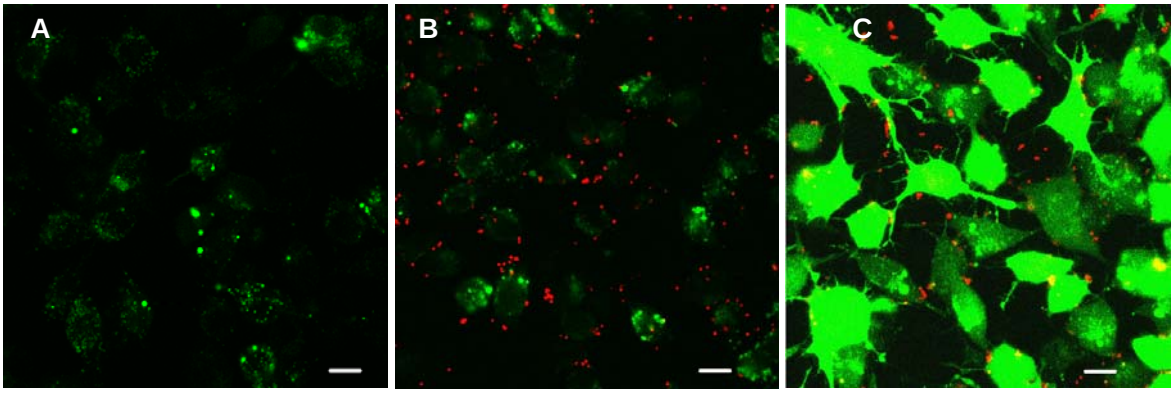

Figure 4.10 Calcein internalized in separate endosomal compartments from nanoparticles not delivered to the cytosol. DC2.4 cells were incubated with calcein for 1 hour at 37 °C. After 3 washes with warm medium, cells were incubated with complete medium (A), PDEAEMA core-shell nanoparticles only (B), or calcein and PDEAEMA core-shell nanoparticles (C). Confocal images were taken at 63X, collecting fluorescence from calcein (green), Cy5-labeled nanoparticles (red). Scale bars 10μm.

To test whether acidification of endolysosomes is necessary for the pH-sensitive nanoparticles to facilitate calcein delivery to the cytosol, we incubated DCs with the H^+-ATPase inhibitor bafilomycin A1 (80 nM)[89, 95] for an hour at 37 °C before calcein and pH-sensitive nanoparticles treatment (one more hour at 37 °C). Consistent with the proton sponge mechanism, bafilomycin A1 inhibition of endolysosomal acidification blocked nanoparticle-mediated calcein delivery to the cytosol (data not shown).

Next, as a test of plasma membrane integrity during the incubation of DCs with core-shell nanoparticles at 37 °C,[96] we loaded DCs with the fluorescent dye fura-2AM (Invitrogen) according to the manufacturer's instructions. Fura-2AM enters cells as a membrane-permeable acetomethoxy ester, but is cleaved by intracellular esterases following loading into the cell, to form a membrane-impermeable product that is trapped

in the cytosol. We incubated fura-loaded DCs with core-shell nanoparticles, and imaged the fluorescence from fura over 3 hours at 37 °C by videomicroscopy in 1-min intervals to determine if fura escaped to the surrounding medium. Fura fluorescence photobleached uniformly in cells over time, equally in the fura-only control (Figure 4.11 A and C, red line in E) and fura/nanoparticle co-incubation experiments (Figure 4.11 B and D, black line in E), no sign of fura loss driven by the nanoparticles was detected.

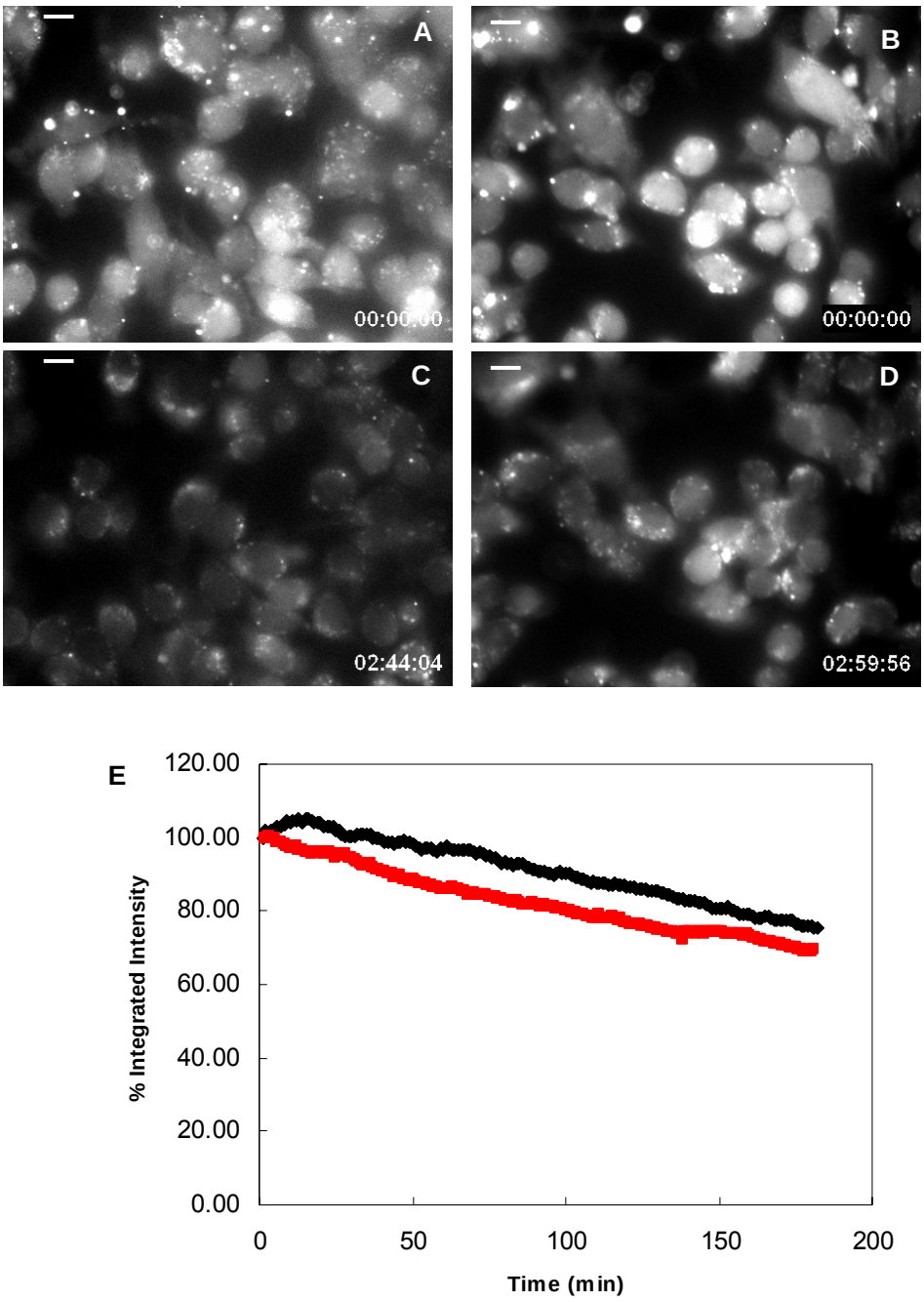

Figure 4.11 Fura fluorescence in cells incubated with or without PDEAEMA core-shell nanoparticles. (A-D) Images shown were the fura fluorescence at time 0 before adding nanoparticles (A, B) and after 3 hours without (C) or with (D) treatment of PDEAEMA core-shell nanoparticles. Scale bars 10 μm. (E) Integrated intensity changes over the

time for fura-loaded cells treated without (red line) or with (black line) PDEAEMA core-shell nanoparticles.

Based on these experiments, we conclude that the nanoparticles deliver calcein to the cytosol of cells by co-endocytosis of calcein and particles, followed by particle disruption of endolysosomes and escape of the dye into the cytosol/nucleus. This process appears to occur without disruption of plasma membrane integrity.

4.3 Cytotoxicity

4.3.1 Core-Shell Structure of Nanoparticles

A concern for the design of any intracellular delivery system is the cytotoxicity of the delivery material. As discussed in Chapter 1, some polymeric materials such as PEI, which have promising intracellular delivery efficiency for plasmid DNA, show noticeable toxicity and side effects on the metabolic activity of cells.[41, 97] Achieving efficient cytosolic delivery without concomitant cytotoxicity remains an ongoing challenge for synthetic delivery materials. Although poly dimethyl aminoethyl methacrylate (PDMAEMA, a water-soluble polymer)[90, 98-100] and PDEAEMA based co polymers (such as poly (DEAEMA-co-PLL)[101] have been used to bind and condense DNA for gene delivery, however, its hydrophobicity and potential toxicity is of concern.[90, 102, 103] To overcome potential toxicity due to interactions of the hydrophobic, polycationic PDEAEMA core of our nanoparticles, we enveloped this pH-sensitive component with a hydrophilic amino ethyl methacrylate (AEMA) shell: effectively sequestering the proton

sponge component of the system from any direct interactions with the external or internal cell membranes. In addition, the core-shell structure can be used to segregate the drug/cell binding and pH sensitivity functions of the particle carrier. We have tested the pH-sensitivity and endolysosomal disruption by the core in the previous section; now we turn to a discussion of the function of the shell structure in preventing toxicity of this nanoparticle carrier.

4.3.2 Effects of Nanoparticle Treatment on Cell Metabolism and Growth/Proliferation

To assess the cytotoxicity of the core-shell nanoparticles, a dimethylthiazolyl diphenyltetrazolium bromide (MTT) assay was used to determine the metabolic rate of cells exposed to nanoparticles *vs.* untreated controls. Here, $5x10^4$ DC2.4 cells were plated in triplicate in 96-well plates, and incubated with or without 25 μg/mL nanoparticles for 1 hour at 37 °C. The cells were then washed three times with warm complete medium. The metabolic rate (expressed as a percentage relative to controls that were not exposed to nanoparticles) was measured either immediately by the standard MTT assay (details in Section 4.1.4) to detect the acute effects of nanoparticles on the cells, or after an additional 24 hours of culture to measure the latent effects of nanoparticle treatment on cell metabolism (Figure 4.12). Core-shell particles with a pH-insensitive PMMA core had negligible cytotoxicity up to 24 hours post particle incubation. Likewise, core-shell nanoparticles with the pH-responsive PDEAEMA core also had very low toxicity: at nanoparticle concentration of 25 μg/mL that provided efficient intracellular delivery of calcein shown in Figure 4.1, cells had ~ 95% of the

metabolic activity of controls at either tested time point. Notably, nanoparticles lacking a PAEMA-rich shell (PDEAEMA core only) exhibited much greater cytotoxicity than core-shell particles. This may reflect the combined impact of cationic charge and hydrophobicity in crosslinked PDEAEMA, which is exposed in the 'core-only' particles but sequestered in the core-shell structures under the more hydrophilic PAEMA surface layer; the combination of cationic charge and hydrophobicity is a common feature of highly membrane-interactive polymers.[99, 100] Similar cell viability trends were obtained from a cell-growth assay, in which cells were treated with nanoparticles (or left untreated), and then replated and allowed to grow for three days, followed by measurement of total cell numbers (Figure 4.13).

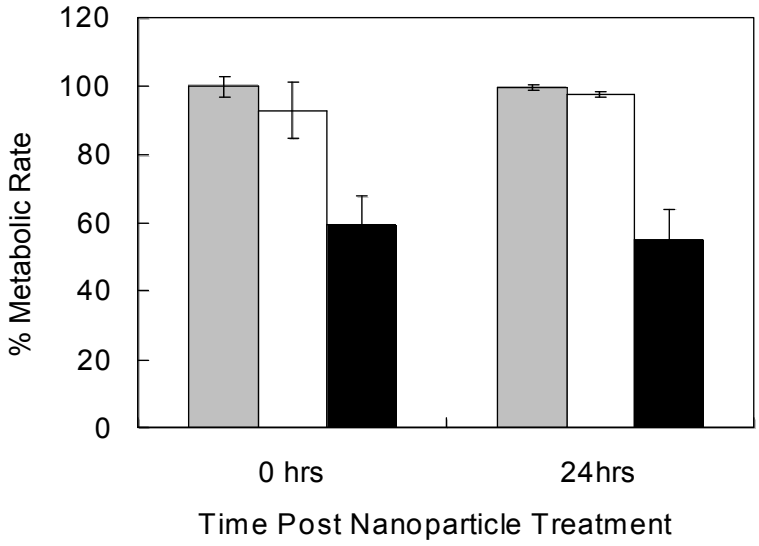

Figure 4.12 Metabolic rates of nanoparticle-treated cells relative to untreated controls. DC2.4 were incubated with PMMA-core/PAEMA-shell nanoparticles (stripe), PDEAEMA-core/PAEMA-shell particles (white), or PDEAEMA-core/no-shell nanoparticles (black) for 1 hour at 37 °C, washed, and then acute (0 hr) and latent (24 hrs)

effects on cell metabolism were measured by MTT assay. Error bars represent S.D. of triplicate samples.

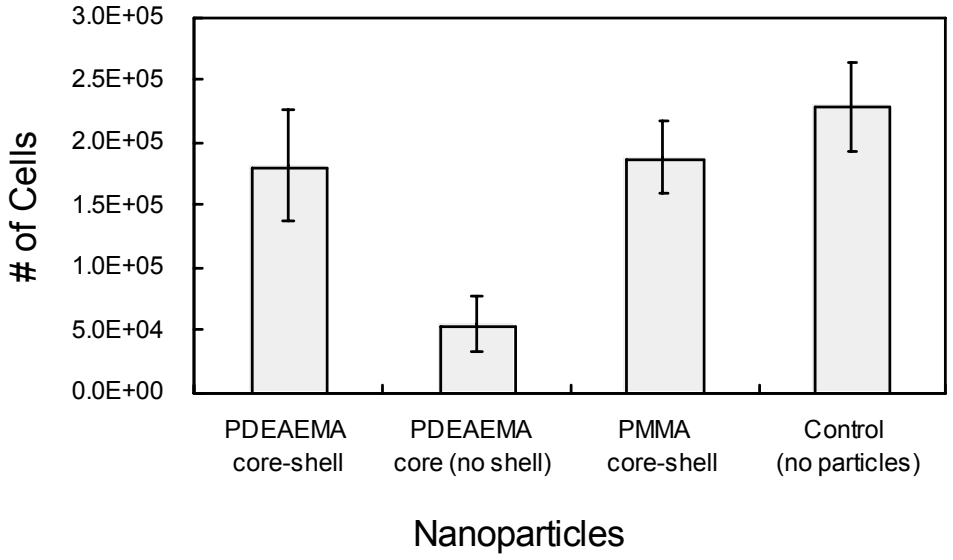

Figure 4.13 Cell-growth assay for cell viability. DC2.4 cells were incubated with 25 μg/mL nanoparticles or untreated for 1 hour, washed three times, then replated at $2.5x10^4$ cells/well and allowed to grow 3 days; the number of cells grown out for each condition was then quantified.

4.3.3 Dose Dependence of Nanoparticles on Cell Metabolism

The cytotoxicity assays performed above analyzed a single dose of particles (25 μg/mL) that provided near-100% calcein delivery in endosome-disruption studies. We also assessed the dose dependence of nanoparticle treatment on cell metabolism via the MTT assay, summarized in Figure 4.14. For the PDEAEMA core-shell

nanoparticles, cells did not show much metabolic rate change with up to 100 μg/mL of the particle treatment. This compares well to polyethyleneimine (PEI) polymers, which have often been reported to reduce metabolic rates to 50% of untreated cells at doses of 20-35 μg/mL.[42] However, as shown above for the single-dose studies, PDEAEMA-core/no-shell particles, even at a 25 μg/mL particle concentration, killed more than 40% of the cells. Thus, the core-shell structure provides a substantial protection from cytotoxic effects of the insoluble components of PDEAEMA chains exposing to the cell. (Note however that we cannot rule out access of soluble cellular proteins to the core of the core-shell particles, given that the shell is itself a hydrogel with nanoscale pores that may permit protein diffusion.)

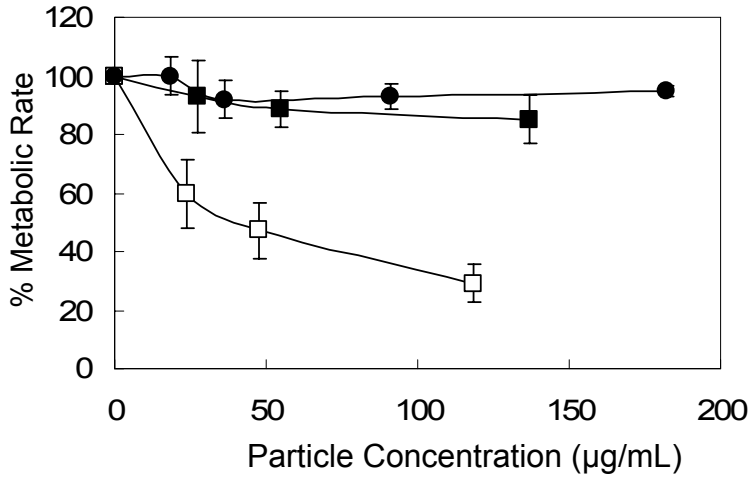

Figure 4.14 Effect of particle dosage on the metabolic rate. DC2.4 were incubated with PMMA core-shell nanoparticles (●), PDEAEMA core-shell nanoparticles (■), PDEAEMA-core/no-shell nanoparticles (□) for 1 hour at 37 °C, washed, and then acute (0 hr) effects on cell metabolism were measured by MTT assay. Error bars represent S.D. of triplicate samples.

In this chapter, we evaluated the pH-sensitivity of core-shell nanoparticles in a biological system, DC2.4 cells. The efficient cytosolic delivery of calcein by co-incubation with the nanoparticles suggested their capability of endolysosomal disrupting by the nanoparticles' pH-sensitive core via proton sponge effect. This process was carried out after the cellular uptake of calcein and nanoparticles via co-endocytosis without any cell membrane integrity. We further tested the effect of the presence of the 'protective' shell on cytotoxicity of the particles. This chemical modification of the nanoparticles highly reduced the cytotoxicity as expected, due to minimum exposure of the cells to PDEAEMA. In a broader view, this core-shell structure could be of significant use in designing any drug delivery systems with reduced cytotoxicity by preventing the cells from contacting the hydrophobic and insoluble components. Further application of core-shell nanoparticles for intracellular drug delivery will be discussed in next chapter.

5 Applications of pH-Sensitive Core-Shell Nanoparticles for Intracellular Drug Delivery

We have characterized our pH-sensitive core-shell nanoparticles in a biological system, DC2.4, and shown that: 1) these nanoparticles deliver calcein efficiently to the cell cytosol in a manner mechanistically consistent with the 'proton sponge effect'; and 2) cytotoxicity of these particles is minimized by encapsulating the endosome-disrupting polymer core within a hydrophilic shell. In this chapter, we consider several further applications of our nanoparticles for the intracellular delivery of macromolecules. After discussing the function of the shell structure for drug binding, we test the delivery of a model protein antigen, ovalbumin (OVA) to murine primary dendritic cells, the delivery of Influenza A virus to human monocyte-derived dendritic cells (MDDCs), and the delivery of siRNA into epithelial cells.

The promising cytosolic delivery efficiency of macromolecules motivated us to convert our nanoparticles into a biodegradable system. Strategies for biodegradable nanoparticles that could potentially provide a drug releasing mechanism and lead us to *in vivo* studies will be discussed in the next chapter.

5.1 Materials and Methods

5.1.1 Materials

All reagents were used as received without further purification. RPMI 1640,

DMEM (with 4.5 g/L glucose), and Trypsin/EDTA (0.25% trypsin/2.21 mM EDTA in HBSS without sodium bicarbonate, calcium and magnesium) were purchased from Mediatech Inc. Fetal bovine serum (FBS) was purchased from Hyclone. Ovalbumin (OVA) Alexa Fluor® 488 conjugate was purchased from Invitrogen. Recombinant murine granulocyte macrophage colony stimulating factor (GM-CSF) was from Peprotech, Inc. Influenza A Antigen Strain Texas from embryonated chicken eggs (strain: Texas 1/77 (H3N2)) was purchased from Meridian Life Science, Inc. Sodium bicarbonate (pH 9.0, 1.0 M), Alexa Fluor-488 succinimidyl ester, and dimethyl sulfoxide (DMSO) were purchased from Molecular Probes. Ficoll-Paque® was purchased from GE Healthcare Ltd. Recombinant human Interleukin 4 (rhIL-4), and recombinant human granulocyte macrophage colony stimulating factor (rhGM-CSF) were purchased from R&D Systems, Inc. siGLO Cyclophilin B Control siRNA (Human/Mouse/Rat), fluorescence labeled antiGFP siRNA, DNA primers, and Dharma*FECT*® transfection reagent were purchased from Dharmacon (Thermo Fisher Scientific, Inc.), and provided by Dr. James J. Liu. TaqMan® Universal PCR Master Mix, TagMan® probes, and primers were from Applied Biosystems.

5.1.2 Binding Efficiency of Core-Shell Nanoparticles

Binding Efficiency of OVA to Core-Shell Nanoparticles

Alexa Fluor® 488 conjugated OVA (0.1, 1, 10, 100, 250 μg/mL) was premixed

with 25 μg/mL PMMA or PDEAEMA core-shell nanoparticles for 5 minutes in 200 μL of serum free RPMI medium to allow electrostatic binding of OVA to nanoparticles. Free OVA was removed by centrifugation at 15,000x*g* for 15 min and the supernatant (~ 190 μL) was transferred to a 96-well plates. The OVA-decorated particles were resuspended in complete medium by sonicating for 15 min. The wash-off OVA was removed again by centrifugation at the same condition described above, and the supernatant (~ 190 μL) was saved in 96-well plates. The concentration of the free OVA in the supernatant was then determined by the fluorescence intensity of the solution at 488 nm/530 nm using a fluorescence microplate reader (SPECTRAmax™ GEMINI, Molecular Devices Corp.). The OVA bound to the nanoparticles was determined by subtracting OVA in the supernatant from the OVA added.

Binding Efficiency of Influenza A to Core-Shell Nanoparticles

To label Influenza A with fluorescent dye,[104] 50 μL of 1.0 M sodium bicarbonate (pH 9.0) was added to 500 μL (~ 2 x10^4 HA units) virus. Alexa Fluor-488 succinimidyl (0.005 μg/HA unit) was dissolved in 2 μL of DMSO, and added to the virus solution. After stirring for 1 hour at room temperature in the dark, the labeled Influenza A was dialyzed (Slide-A-Lyzer® Mini Dialysis Units 3500 MWCO, Pierce) in PBS (1.0 M, pH7.4) at 4 °C overnight in the dark. The volume change was recorded to calculate the final HA units of the labeled virus.

Alexa Fluor® 488 conjugated Influenza A (1000, 2000, 5000 HA unit/mL) was

premixed with 25 μg/mL PDEAEMA core-shell nanoparticles for 5 min in 200 μL of serum-free RPMI medium to allow electrostatic binding of the virus to the nanoparticles. Free Influenza A was removed by centrifugation at 15,000x*g* for 15 min and the supernatant (~ 190 μL) was transferred to a 96-well plates. The Influenza A-decorated particles were resuspended in complete medium by sonicating for 15 min. The concentration of the Influenza A in the supernatant was then determined by the fluorescence intensity of the solution at 488 nm/530 nm using a fluorescence microplate reader (SPECTRAmax^{TM} GEMINI, Molecular Devices Corp.). The Influenza A bound to the nanoparticles was determined by subtracting flu in the supernatant from the flu added

5.1.3 OVA Delivery and OT I Assay

Bone Marrow-Derived Dendritic Cells and Naïve T Cells Isolation and Cell Culture

Animals were cared for following institute, state, and federal guidelines under an IUCAC-approved protocol. Bone marrow-derived dendritic cells (BMDCs) were prepared following a procedure modified from Inaba *et al.*[105] Bone marrow progenitors were harvested from the femur and tibia of C57BL/6J female mice (The Jackson Laboratory). These cells were cultured ($1x10^6$ cells/mL/well in 24-well plate) in complete RPMI 1640 medium (10% FBS, 50 μM 2-mercaptoethanol, 5 mM L-glutamine, 10 mM HEPES, and penicillin/streptomycin) containing GM-CSF

(10 ng/mL). 80% of the medium was replaced with fresh complete medium containing GM-CSF (10 ng/mL) on day 2, 4, and 6 to obtain BMDCs. BMDCs were used on day 6-7.

Naïve $CD8^+$ OVA-specific T cells were harvested from the spleens of OT-I TCR transgenic mice[92, 106] (The Jackson Laboratory) using magnetic assistant cell sorting (MACS) beads ($CD8^+$ T cell negative selection kit, Miltenyi Biotec, Inc.) according to the manufacturer's instructions, and used immediately in OT-1 T cell priming assays.

Cytosolic Delivery of OVA by Fluorescence Microscopy

DC2.4 cells or day 6 BMDCs were plated in Lab-Tek™ chambers (Nunc 8-well chambered coverglasses, $1.2x10^5$ cells/well) and cultured in complete RPMI 1640 medium for 18 hours. OVA (200 μg/mL for DC2.4, or 100 μg/mL for BMDCs) was premixed with 25 μg/mL PMMA or PDEAEMA core-shell nanoparticles for 5 min to allow electrostatic binding of OVA to nanoparticles. Free OVA was removed by centrifugation at 15,000x*g* for 15 min. The OVA-decorated particles were resuspended in complete medium by sonicating for 15 min and added to cells for 1 hour at 37 °C. After three washes with complete medium to remove extracellular OVA and nanoparticles, the cells were imaged live by CLSM at 37°C.

OT-I T Cell Priming Assay

BMDCs were counted and plated in 24-well plates ($1x10^6$ cells/well) on day 6 and cultured in complete medium for 2 hours to allow the cells settle to the bottom.

Freshly dissolved OVA (0.1, 10, or 100 μg/mL) was premixed with 25 μg/mL PMMA or PDEAEMA core-shell nanoparticles for 5 min to allow electrostatic binding of OVA to nanoparticles. Residual free OVA was removed by centrifugation at 15,000x*g* for 15 min followed by aspiration of the supernatant. The OVA-decorated particles were then resuspended in complete medium by sonicating for 15 min. Soluble OVA (0.1, 10 or 100 μg/mL) or OVA-coated nanoparticles were added to cells for 1 hour at 37 °C. The cells were collected and washed with complete medium by centrifugation. After the resuspension, OVA-pulsed BMDCs were replated in 96-well plates in triplicate ($1x10^5$ cells/well/100 μL) for 3 hrs. OT-I $CD8^+$ T cells were added to each well ($5x10^5$ cells/well/100 μL), and co-incubated with BMDCs for 3 days. Interferon gamma (IFN-γ) in the supernatants of these cultures was then quantified using an ELISA kit (murine Interferon gamma (IFN-γ) Duoset ELISA Development Kit, R&D Systems) according to the manufacturer's instructions. The DCs stimulation and T cells co-culture were carried out in complete medium. A round-bottom 96-well plate was used to promote cell crawling and contacting.

5.1.4 Cytosolic Delivery of Influenza A

Isolation of Monocytes from Human Blood and Differentiation of Human Monocytes-Derived Dendritic Cells

Buffy coat (not older than 8 hours) was ordered and delivered at room temperature. The blood was diluted with PBMC wash buffer (PBS with 0.1% BSA and 0.6% Sodium Citrate) with 1:2 ratio (30-35 mL buffy coat to 66 mL PBMC buffer). 15 mL of Ficoll-Paque® was added to a 50 mL conical centrifuge tube, and 35 mL of cell suspension was layered on top carefully without disturbing the interface. After centrifugation at 400x*g* for 25 min at room temperature in a swinging bucket rotor without brake, the blood sample was separated into four portions from top to bottom: plasma (thick layer), buffy coat (very thin layer), Ficoll-Paque® (thick layer), and blood cells (red pellet at the bottom). The buffy coat was taken out carefully using a pipette with a long sharp tip to avoid any disturbance to the interfaces, and transferred to a new 50 mL conical tube. The tube was filled with PBMC buffer, and centrifuged at 300x*g* for 10 min with brake. The supernatant was removed carefully without disturbing the cell pellet, which was then washed twice with 15 mL of cold PBMC buffer and centrifuged at 200x*g* for 8 min at 4 ºC. The supernatant was clear after removing all the platelets. The monocytes were isolated using magnetic assistant cell sorting (MACS) beads (CD14 monocytes-positive selection kit, Miltenyi Biotec, Inc.) according to the manufacturer's instructions.

The monocytes were suspended in the RPMI 1640 complete medium (10% FBS, 50 μM 2-mercaptoethanol, 5 mM L-glutamine, 10 mM HEPES, and penicillin/ streptomycin) containing rhIL-4 (1,000 U/ml, 2.9x 0^4 U/ug) and rhGM-CSF (1,000 U/ml, $1.5x10^4$ U/ug). Cells were then plated in 24-well plates at the density of $1x10^6$ cells/well/mL. On day 2 and day 4, 80% of the medium was replaced by fresh

medium containing rhIL-4 and rhGM-CSF to derive MDDCs. MDDCs were used on day 6-7.

Cytosolic Delivery of Influenza A by CLSM

On Day 6, MDDCs were plated in Lab-Tek™ chambers (Nunc 8-well chambered coverglasses, $1.2x10^5$ cells/well) and cultured in complete medium for 18 hours. Influenza A (1657 HA unit/mL) was premixed with 25 μg/mL PDEAEMA core-shell nanoparticles for 5 min to allow electrostatic binding of Influenza A to nanoparticles. Free Influenza A was removed by centrifugation at 15,000x*g* for 15 min. The Influenza A-decorated particles were resuspended in complete medium by sonicating for 15 min and added to cells for 1 hour at 37 °C. After three washes with complete medium to remove extracellular Influenza A and nanoparticles, the cells were imaged live by CLSM at 37 °C.

5.1.5 Intracellular Delivery of siRNA

Cytosolic Delivery of siRNA by Fluorescence Microscopy

DC2.4 cells or BSC-40 cells, a type of epithelial cells from monkey kidney (ATCC), were plated in Lab-Tek™ chambers (Nunc 8-well chambered coverglasses, $1.2x10^5$ cells/well) and cultured in DMEM medium containing 10% FBS, 50 μM 2-mercaptoethanol, 4 mM L-glutamine, 10 mM HEPES, and penicillin/streptomycin. Fluorescence-labeled siRNA (2.6 μg/mL) was premixed with 25 μg/mL PDEAEMA

core-shell nanoparticles for 5 min to allow electrostatic binding of siRNA to nanoparticles. The siRNA-decorated particles were resuspended in complete medium by sonicating for 15 min and added to the cells for 1 hour at 37 °C. After three washes with complete medium to remove extracellular siRNA and nanoparticles, the cells were imaged live by CLSM at 37 °C.

Transfection of Epithelial Cells by siRNA

BSC-40 cells were plated in 6-well plate ($2x10^5$ cells/well/mL) and cultured in DMEM complete medium for 18 hours. siGLO Cyclophilin B Control siRNA (2.6 μg/well, 100 nM) was premixed with 25 μg/mL PDEAEMA core-shell nanoparticles for 5 min to allow electrostatic binding of siRNA to nanoparticles. The siRNA-decorated particles were resuspended in complete medium (2 mL/well) by sonicating for 15 min. A positive control was prepared using Dharma*FECT*® transfection reagent (Dharmacon, Thermo Fisher Scientific, Inc.) as the delivery system for the same amount of siRNA. According to the manufacturer's instructions, siRNA (2.6 μg/well, 100 nM) and Dharma*FECT*® transfection reagent (5 μL/well) were diluted in 200 μL serum-free medium separately, and incubated for 5 min at room temperature. The two solutions were mixed gently by pipetting carefully up and down, and incubated for 20 min at room temperature. 1600 μL of antibiotic-free complete medium was added to the solution for the final desired volume of transfection medium (2 mL/well).

siRNA-coated nanoparticles or siRNA-mixed lipid were added to cells for 1 hour

(for siRNA/nanoparticles) or 4 hours (for siRNA/lipid) at 37 °C. The cells were washed with warm PBS three times, and cultured in DMEM complete medium for 24 hours (recorded from the start of the incubation). Cells were collected by trypsinization and centrifugation at 400x*g* for 5 min. Cellular RNA was isolated by a RNeasy Mini Kit (QIAGEN) according to the manufacturer's instructions.

Detection of mRNA Level by RT-PCR

To prepare a reverse transcription-polymerase chain reaction (RT-PCR) for testing the remaining targeted mRNA, the concentration of total RNA of each sample was measured and diluted to make sure there was sufficient and similar amount RNA for each sample. Cyclophilin B was the house keeping gene here and actin was chosen as the control or calibrator gene. 5 μL of each sample (~ 400 ng of RNA, to provide ~ 10-20 ng cDNA for amplification) was mixed with 10 μL of TaqMan® Universal PCR Master Mix (combines AmpliTaq Gold® DNA Polymerase, AmpErase® UNG, dNTPs with dUTP, Passive Reference I for signal normalization, and optimized buffer components in an easy-to-use premix; Applied Biosystems), TagMan® probes, and primers of Cyclophilin B and actin genes in RNase-free water to make a final volume of 20 μL. The one-step real time RCR was carried out in a MicroAmpTM optical 96-well reaction plate (with Barcode, Applied Biosystems) with the following thermal cycle conditions: 1 cycle of three sequential incubations (50 °C for 2 min, 60 °C for 30 min, and 95 °C for 5 min), followed by 50 cycles of amplification (95 °C for 5 s and 62 °C for 30 s) in a 7700 prism sequence detection system (Perkin-Elmer Applied

Biosystems). The target mRNA concentration was evaluated by the comparative Ct method.

5.2 Drug Binding Efficiency

It is necessary for a drug delivery system to have an efficient mechanism to load and release it's drug molecules. As we mentioned in Chapter 1, many of the polycationic systems that could efficiently aid transport of macromolecules into the cytosol are formulated by physical complexation of the polycationic molecules and drug (*e.g.*, polyplexes or lipoplexes of cationic polymers/lipids with DNA or RNA). These strategies usually result in complexes lack of control over carriers/drug particle size and stability,[24, 54, 55] which is a critical determinant of cellular uptake *in vitro* and biodistribution and toxicity *in vivo*.[24] In addition, the loading efficiency directly determines the dose of drug that can be delivered, which is a significant parameter for the design of a drug delivery system.

In this project, we designed a core-shell structure to segregate the function of cell/drug binding from the function of endolysosomal disruption by pH-sensitivity. This approach allows independent tuning of the chemistry used to bind the drug molecules and the pH-sensitive component, which we proved to enable highly efficient endolysosomal disruption in Chapter 4. In this study (shown in Figure 5.1), we incorporated 2-aminoethyl methacrylate (AEMA) groups into the shell, providing primary amines capable of electrostatically binding negatively charged drugs (*e.g.*

proteins, siRNA, or DNA). The binding efficiency of the core-shell nanoparticles to some model drug cargos tested for intracellular delivery, such as OVA and influenza A, are discussed in this section.

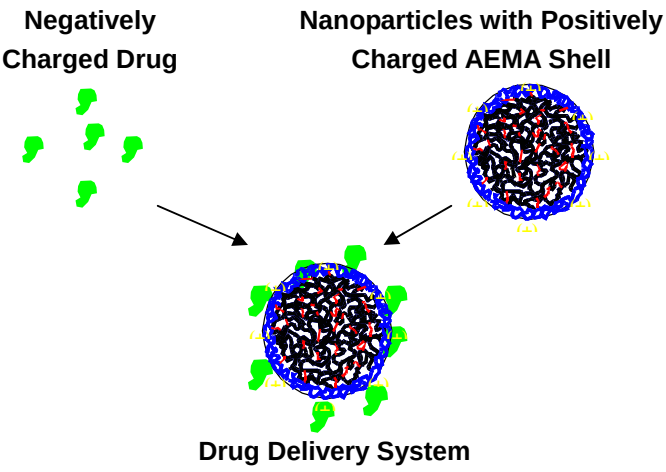

Figure 5.1 Schematic of drug delivery system formation. Negative charged drug molecules, such as proteins, siRNA, or DNA, adsorbed to the positively charged AEMA shell of nanoparticles electrostatically.

5.2.1 Binding Efficiency of OVA to Core-Shell Nanoparticles

OVA Binding at Different Concentration

To test the ability of core-shell nanoparticles to deliver a model protein vaccine antigen (OVA) into dendritic cells, we first assessed electrostatic binding of OVA to the nanoparticles as a function of OVA concentration. The loading efficiency of OVA to the AEMA shell of the nanoparticles is shown in Figure 5.2. In this experiment, OVA at different concentrations were mixed with 25 μg/mL PDEAEMA

or PMMA core-shell nanoparticles. After a 5 min incubation period, the unbound OVA was removed by centrifugation and measured. The OVA loading efficiency (solid symbols with solid lines) was 100% for both types of nanoparticles at low concentration of OVA (0.1, or 1 μg/mL). When the OVA concentration was increased, the binding was more efficient for PDEAEMA nanoparticles than for PMMA nanoparticles: at OVA concentrations of 10, 100, and 250 μg/mL, the binding efficiency for PDEAEMA nanoparticles was 100%, 58%, and 52% respectively, while the binding efficiency for PMMA nanoparticles was 70%, 35%, and 28% respectively. The bound OVA amount increased proportionally as the OVA in the solution increased (*e.g.* 10, 58, 130 μg/mL of OVA bound to PDEAEMA nanoparticles when the OVA concentration was 10, 100, 250 μg/mL respectively).

As expected, after OVA-coated nanoparticles were washed with complete medium, which was rich in serum and promoted competitive binding between the serum protein and the OVA to the nanoparticles, we saw a dramatic decrease of the binding efficiency for both types of nanoparticles (empty symbols with dashed lines), while the difference of binding efficiency between two types of nanoparticles still remained. These binding curves allowed drug delivery systems to be prepared with known quantities of OVA to the amount of core-shell nanoparticles used (25 μg/mL).

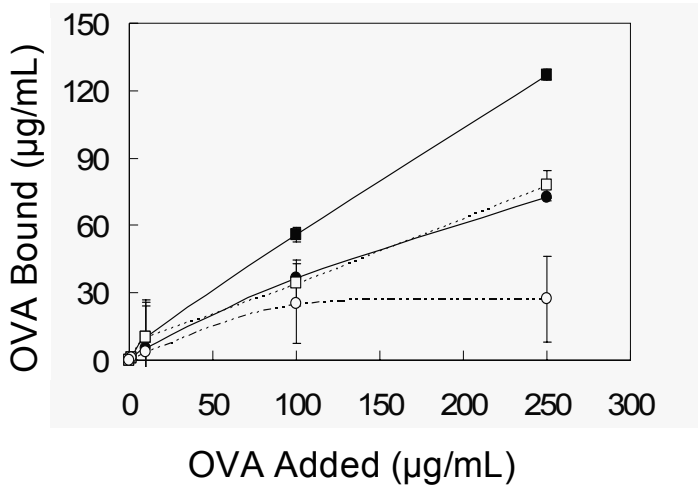

Figure 5.2 OVA binding to core-shell nanoparticles at pH 7.4. Soluble OVA (0.1, 1, 10, 100 or 250 µg/mL) was premixed with 25 µg/mL PDEAEMA core-shell nanoparticles (square) or PMMA core-shell nanoparticles (circle) for 5 min in 200 µL of serum-free RPMI medium to allow electrostatic binding of OVA to nanoparticles. The OVA-decorated particles were resuspended in complete medium by sonicating for 15 min and washed by centrifugation. The OVA bound (solid symbols with solid lines) to the nanoparticles and the remaining OVA after washing (open symbols with dashed lines) were determined. Shown are the mean ± S.D. from triplicates.

Effect of pH on OVA Loading Efficiency

The primary amine group on AEMA shell has a pK_b of appximately 11. Thus, the pH range from endolysosomal to physiological pH should not have an effect on the charge density of the AEMA shell. However, the DEAEMA would be affected dramatically, as the tertiary amine group would be highly charged when the pH is lowered below pH 7. As we hypothesized that not only the shell but the core would have some effects on protein binding efficiency, we expected more binding with

PDEAEMA nanoparticles at reduced pH. As shown in Figure 5.3, OVA binding efficiency (100%) was similar at a range of pHs when the OVA concentration was low (10 μg/mL). However, the binding efficiency was much higher at endolysosomal pH (~5-6) than that of physiological pH at higher OVA solution concentrations (100, and 250 μg/mL). This result explained that more positive charge was present as the tertiary amine groups in the core were protonated and the PDEAEMA nanoparticles were swelling. In addition, the size change of the nanoparticles (swelling to much larger size) could potentially provide more surface area and binding sites on the shell, and thus cause the higher binding efficiency.

After we washed OVA-bound nanoparticles in complete medium (pH 7.4), the binding efficiency was reduced to the level similar as that shown in Figure 5.2 (empty square with dashed line). This result further tested our hypothesis above, and provided us information that in the endolysosomal disrupting process when nanoparticles were swelling, the drug should be stably bound to the nanoparticles. However, we could lose OVA (drug molecules) if the delivery system could not be endocytosed efficiently, as binding competition between other proteins or positively charged molecules in the cell culture could decrease the bound OVA on the nanoparticles. A method to encapsulate the drug in the nanoparticles could be a future direction for drug loading and protection.

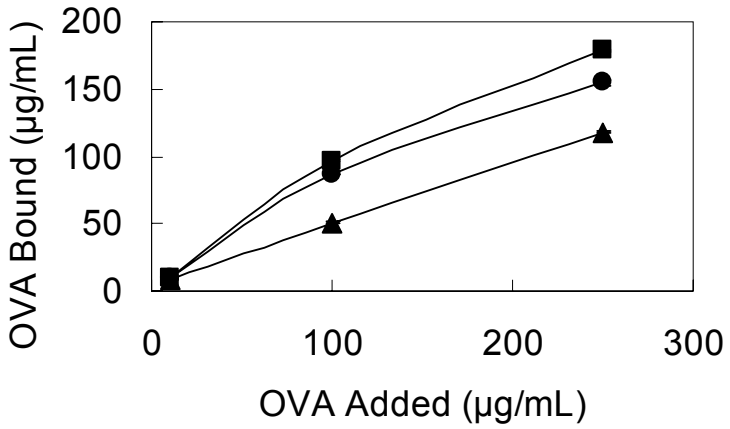

Figure 5.3 OVA Binding efficiency at different pH overnight. Soluble OVA (10, 100, and 250 μg/mL) was premixed with 25 μg/mL PDEAEMA core-shell nanoparticles overnight with moderate shaking in 200 μL phosphate buffer (100 mM) with pH 4.98 (●), 6.03 (■), and 7.48 (▲) to allow electrostatic binding of OVA to nanoparticles. The OVA conjugated to the nanoparticles was determined. Shown are the mean ± S.D. from triplicate samples.

In addition, we found that long incubation times of nanoparticles with OVA (~ 18 hours in Figure 5.3) did not improve the protein binding efficiency compared to the very brief incubations (5 min, in Figure 5.2), as the binding efficiency at pH7.4 was similar in these two cases. This comparison suggested that the electrostatic binding process reached equilibrium quickly when the drug molecules met the nanoparticles in the solution.

5.2.2 Binding Efficiency of Influenza A to Core-Shell Nanoparticles

Similar to the OVA delivery experiments, we adsorbed fluorescently-labeled Influenza A to the shell of nanoparticles through electrostatic interactions. The particle binding efficiency for different concentrations of virus protein is shown in Figure 5.4. The pH-sensitive nanoparticles (25 μg/mL) had ~ 55-65% binding efficiency at the given virus protein concentration. Typically, a concentration of 1000 HA unit/mL[107] is used to elicit and recall T cell responses from human peripheral blood T cells stimulated with DCs *in vitro*. We thus mix 1657 HA unit/mL of virus protein with our nanoparticles to provide a 1000 HA unit/mL final overall concentration bound to nanoparticles.

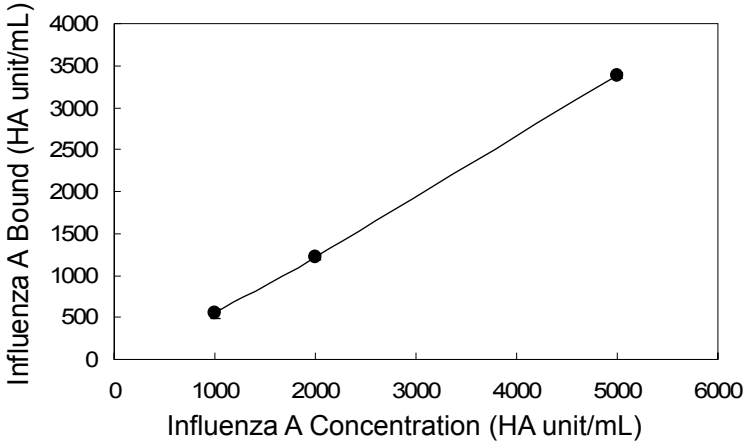

Figure 5.4 Binding efficiency of Influenza A to pH-sensitive nanoparticles at pH 7.4. Influenza A (1000, 2000, and 5000 HA unit/mL) was premixed with 25 μg/mL PDEAEMA core-shell nanoparticles for 5 min in 200 μL of serum-free RPMI medium to allow electrostatic binding of Influenza A to the nanoparticles. Influenza A bound to the nanoparticles was determined. Shown are the mean ± S.D. from triplicate samples.

For the case of siRNA, another model drug we used, fluorescent-labeled siRNA (2.6 μg/mL, 100 nM) showed 100% binding to the nanoparticles at the concentration (25 μg/mL) we examined for the cytosolic delivery. Binding efficiency at other siRNA concentrations was not evaluated due to the cost and the availability of siRNA sample.

5.3 Delivery of Protein Vaccine Antigens to Promote Class I MHC Presentation to $CD8^+$ T Cells

Having observed efficient cytosolic delivery of calcein and low cytotoxicity of DCs following treatment with the pH-sensitive core-shell nanoparticles, we now tested the ability of these particles to chaperone the cytosolic delivery of a protein and promote a functional response. As we discussed in Chapter 1, dendritic cells could bind peptides derived from pathogens to their MHC complexes at the cell surface for recognition by naïve T cells. This presentation of antigens to cytotoxic T cells is greatly amplified (up to 1000-fold) by delivery of antigens to the cytosol, where the DC intracellular machinery can load them efficiently onto class I MHC molecules for presentation to $CD8^+$ T cells.[60, 61] However, the cytosolic delivery to DCs were very inefficient.[64-66] Here, we applied ovalbumin (OVA) as the model antigen protein, and investigated the cytosolic delivery efficiency as well as the immune response from naïve T cells.

5.3.1 OVA Delivery in Dendritic Cells

For these experiments, we employed bone marrow-derived dendritic cells (BMDCs), to determine whether delivery in primary cells differed from results obtained using the DC2.4 cell line. We first tested delivery of the model protein antigen OVA (45 KDa). OVA is known to be internalized by cells into endosomal compartments and has also been commonly used as an endocytic tracer.[108, 109] Fluorescent OVA (200 μg/mL for DC2.4, and 100 μg/mL for BMDCs) was premixed with core-shell nanoparticles (25 μg/mL) for 5 min to allow electrostatic adsorption of the protein to the cationic surfaces of the core-shell particles. The majority of free OVA was removed by centrifugation and aspiration of supernatant. The OVA-adsorbed particles were then resuspended in complete medium and added to DC2.4 (Figure 5.5) or BMDCs (Figure 5.6) for 1 hour at 37 °C, followed by washing and confocal imaging. Similar to the prior results obtained for calcein, OVA fluorescence was observed throughout the cytosol and nucleus in DC2.4 (Figure 5.5 A, B) and BMDCs (Figure 5.6 A, B) co-incubated with OVA-coated PDEAEMA core-shell nanoparticles. The frequency of cells with cytosolic OVA was ~ 36% (n=150) for DC2.4 and ~ 43% for BMDCs (n=150). When DC2.4 or BMDCs were incubated with OVA-coated PMMA core-shell nanoparticles, the fluorescence was instead observed with a punctuate distribution in the endosomal compartments (Figure 5.5 C, D for DC2.4, and Figure 5.6 C, D for BMDCs). Notably, since OVA was tightly absorbed on the surface of the core-shell nanoparticles due to the positively charged amine groups in the AEMA shell, a mechanism for releasing OVA from the

nanoparticles may be necessary to further enhance the frequency of cells exhibiting cytosolically-distributed protein. Studies addressing this issue will be discussed in next chapter.

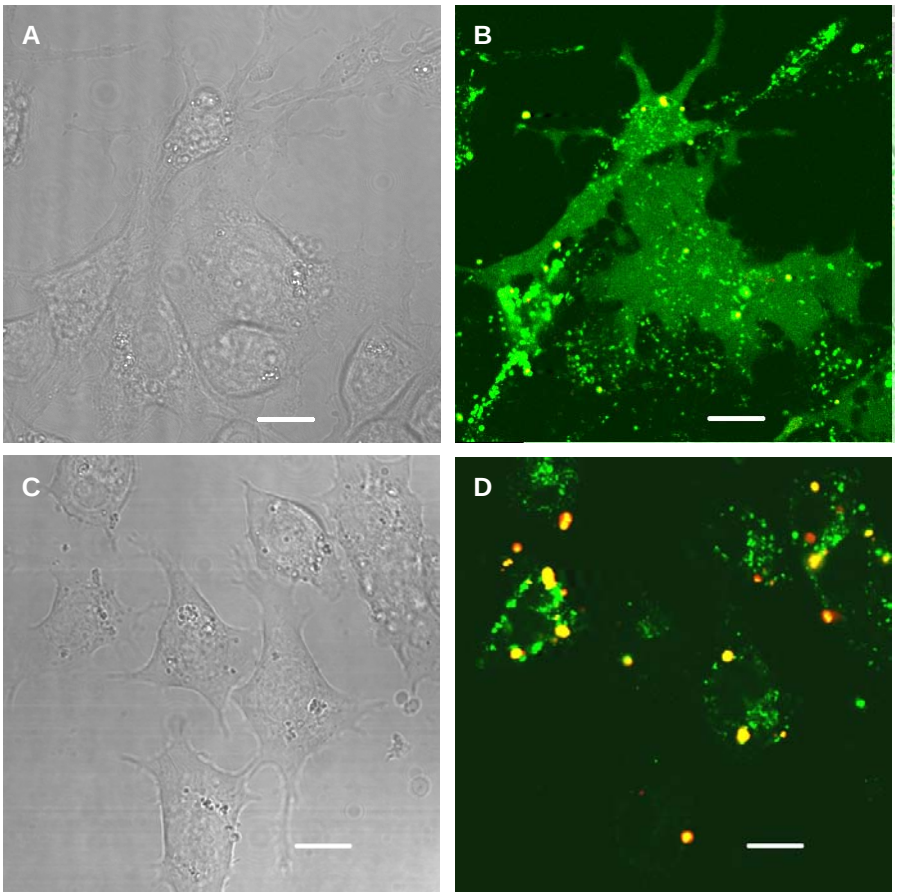

Figure 5.5 Cytosolic delivery of OVA by core-shell nanoparticles to DC2.4 cells. CLSM images at 100X: (A, C) Brightfield images; (B, D) Fluorescence overlays of OVA (green) and nanoparticles (red). (A, B) Cells incubated with OVA adsorbed to PDEAEMA core-shell nanoparticles. (C, D) Cells incubated with OVA adsorbed to PMMA core-shell nanoparticles. Scale bars 10μm.

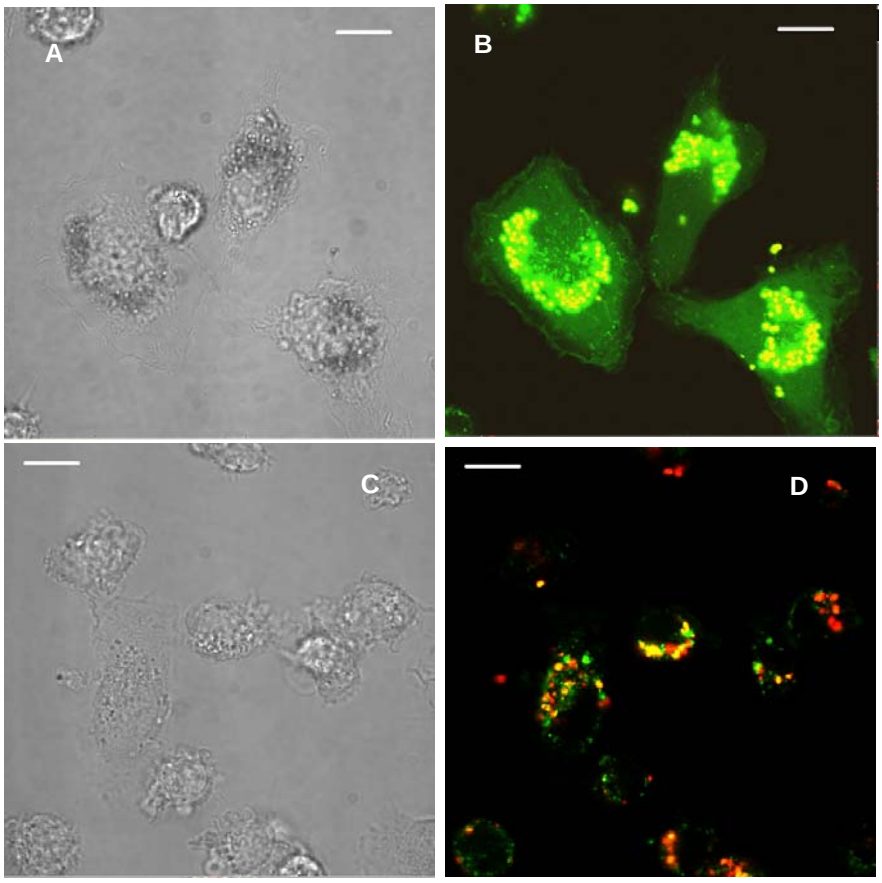

Figure 5.6 pH-sensitive core-shell nanoparticles deliver OVA to the cytosol of primary dendritic cells. (A-D) CLSM images at 100X: (A, C) Brightfield images; (B, D) Fluorescence overlays of OVA (green) and nanoparticles (red). (A, B) BMDCs incubated with OVA adsorbed to PDEAEMA core-shell nanoparticles. (C, D) Cells incubated with OVA adsorbed to PMMA core-shell nanoparticles. Scale bars 10μm.

5.3.2 Functional Test of Cytosolic OVA Delivery: Priming of OVA-Specific $CD8^+$ T Cells by Nanoparticle-treated DCs

OT I T Cell Priming

DCs can internalize protein antigens by endocytosis and break them down into peptides. When incubated with high concentrations of soluble antigens, dendritic cells have the ability to load peptides derived from a small fraction of such exogenously-derived antigen onto class I MHC molecules, a process known as cross presentation.[67] DCs displaying antigen bound to MHC I molecules on their surfaces can then activate $CD8^+$ T cells. However, direct delivery of protein antigens to the cytosol of DCs can substantially enhance the presentation of antigen on MHC I molecules. To determine whether nanoparticle-mediated transport of OVA to the cytosol could enhance priming of $CD8^+$ T cells by DCs, we treated BMDCs with different concentrations of soluble OVA or OVA (the same quantity) adsorbed to either PDEAEMA or PMMA core-shell nanoparticles for 1hour. Antigen/nanoparticle-loaded DCs were then mixed with naïve OT-1 $CD8^+$ T cells that specifically respond to a peptide derived from OVA.[106] Interferon gamma (IFN-γ) secreted by the T cells in response to antigen presentation by the DCs was measured by ELISA after 3 days. As shown in Figure 5.7, some IFN-γ secretion was triggered by DCs incubated with soluble OVA (10 or 100 μg/mL), consistent with prior data from our laboratory and others, showing that a small amount of spontaneous cross presentation can occur when DCs are incubated with high concentration of soluble antigen.[92] However, DCs loaded with OVA via pH-responsive nanoparticles elicited

much higher IFN-γ level (~ 4–5 fold) from T cells at the given concentrations (0.1, 10, and 100 g/mL). In contrast, DCs pulsed with OVA via pH-non-responsive nanoparticles elicited the similar level of IFN-γ as the soluble OVA control. Notably, to reach the same level of IFN-γ secretion (*e.g.* 2000 pg/mL as indicated by the blue dot line), a larger amount of OVA (100 μg/mL) was needed if it was delivered as a soluble protein or with pH-non-sensitive PMMA nanoparticles. However, only less than 1 μg/mL of OVA was needed if it was delivered with pH-sensitive PDEAEMA nanoparticles. This comparison indicated a more than 100-fold increase in functional antigen delivery by using our pH-sensitive nanoparticles. This result also indicated that our nanoparticles could not only be used as a type of drug delivery system, but might also be useful as a signal amplifier to enable *ex vivo* screening of T cell responses to immunization; studies related to this aspect will be addressed in Section 5.4.

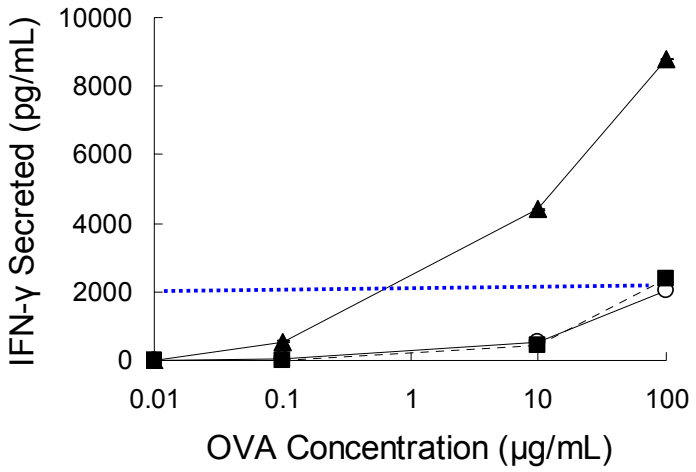

Figure 5.7 Cytosolic delivery of OVA for OT-I T cell priming. BMDCs were incubated with different concentrations of soluble OVA (○), OVA-coated PDEAEMA

core-shell nanoparticles (▲), or OVA-coated PMMA core-shell nanoparticles (■), before being washed and mixed with naïve OT-1 OVA-specific $CD8^+$ T cells. IFN-γ secreted by the T cells in response to antigen presentation by the DCs was measured by ELISA after 3 days. Shown are mean ± S.D. of triplicate samples.

Effect of OVA Loading Methods

As we discussed in Section 5.2.1, the binding efficiency of OVA to the nanoparticles varied when the binding conditions were changed. The actual OVA concentration that was bound to the nanoparticles and added to BMDCs is important, as it determines the eventual dosage and efficiency of the T cell priming. In this experiment, we tested different ways to deliver soluble or bound OVA to BMDCs (Figure 5.8). We used 10 μg/mL of OVA, which provided us 100% binding efficiency in pH 7.4 serum-free (SF) medium, and $2x10^5$ cells/well/100μL of BMDCs with $1x10^6$ cells/well/100μL of T cells. As we always washed off nanoparticles after one hour of incubation, we washed the cell samples with soluble OVA as well. This led to the possibility that the differences seen in OVA delivery to DCs in soluble *vs.* particle-bound form could be partially due to differences in the kinetics of OVA uptake for soluble *vs.* particle-bound protein. For instance, rapid particle internalization could lead to faster protein uptake when bound to particles. To determine if soluble OVA could be as effective as particle-delivered OVA given enough time, we carried out control stimulation condition where OVA protein was left in the medium with the DCs throughout the 3-day T cell stimulation period, to allow

additional antigen uptake. As shown in Figure 5.8, we observed slightly higher secretion of IFN-γ from the samples where we left soluble OVA in the medium for three days, when compared to the samples that we washed off OVA after one hour incubation. However, the degree of cross-presentation/T cell stimulation measured was still much lower than that of detected for particle-delivered OVA, demonstrating that the enhanced response to particle-bound OVA was not simply due to a kinetic difference in antigen uptake/processing.

In the studies of calcein delivery discussed in Chap 4, we demonstrated that co-endocytosis of calcein and nanoparticles in the same endolysosomal compartment could lead to efficient cytosolic delivery of calcein via endolysosomal escape of the nanoparticles co-localized. We tested here whether co-delivery of nanoparticles and OVA by simple mixing could achieve same effect as calcein delivery. BMDCs was incubated with OVA-mix nanoparticles (briefly mixing for 5 min without centrifugation) or OVA-bound nanoparticles (briefly mixing for min with centrifugation). Interestingly, we found that activation of the T cells (determined by the IFN-γ secretion level) in the samples of OVA-mix DEAEMA nanoparticles (~ 9000 pg/mL) was much less than that of the samples of OVA-bound DEAEMA nanoparticles (~ 15000 pg/mL), while the difference between the sample of OVA-mix PMMA nanoparticles and OVA-bound PMMA nanoparticles was negligible. These comparisons confirmed that the presence of pH-sensitive nanoparticles was the key to improve the cytosolic delivery efficiency of OVA, as the T cells response and cytokine secretion were low in the case of pH-insensitive nanoparticles. Since

PMMA core-shell nanoparticles possessed similar binding efficiency as PDEAEMA core-shell nanoparticles by the similar AEMA shells (data not shown), the low efficiency of OVA delivery proved that both OVA bound- or OVA-mix PMMA nanoparticles could only cause a small amount of spontaneous cross presentation as soluble OVA. We suspected that the cellular uptake of OVA was highly improved when OVA was bound to the nanoparticles using centrifugation, which suggested by the difference between OVA-mix and OVA-bound DEAEMA nanoparticles.

We know that serum free medium was used in a lot of protocols for drug delivery, as the presence of serum protein could lead to the instability of the drug delivery system that formed by the complexation of polymers and drug molecules.[24, 54, 55] However, incubation with serum free medium may not provide enough nutrients that are needed by cells. In addition, it limits the applications for *in vivo* studies, as proteins are always present in the physiological environment. Therefore, the stability and function of drug delivery systems in complete medium containing serum protein is important. As emphasized, the core-shell structured hydrogel nanoparticles were expected to provide predefined size, and stability in biological system which were suggested by the efficiently delivery of OVA and high level of IFN-γ secretion in the serum containing medium.

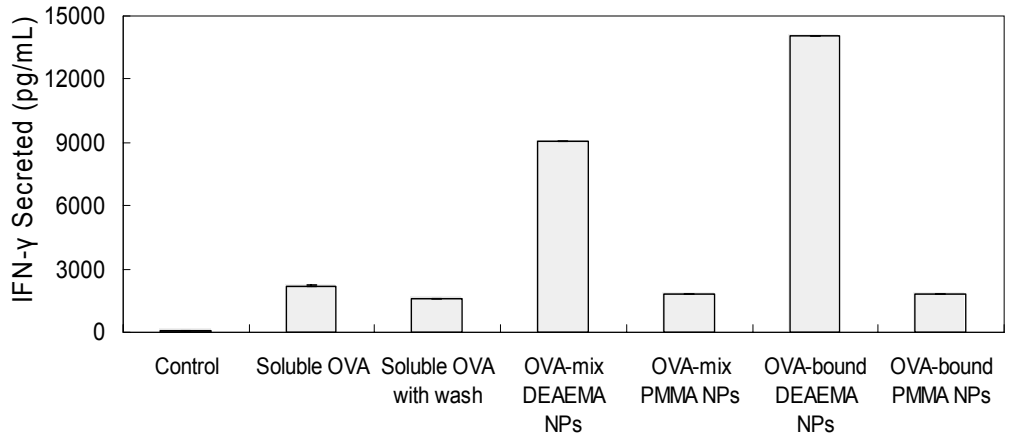

Figure 5.8 Cytosolic delivery of OVA for OT I T cell priming with different OVA loading methods. BMDCs were incubated with the same concentration of soluble OVA (10 μg/mL) (with or without wash-off after 1 hour of incubation), OVA mixed with PDEAEMA or PMMA core-shell nanoparticles (without centrifugation), OVA-bound PDEAEMA or PMMA core-shell nanoparticles (with centrifugation). IFN-γ secreted by the T cells in response to antigen presentation by the DCs was measured by ELISA after 3 days. Shown are mean ± S.D. of triplicate samples.

In conclusion, we demonstrated that pH-sensitive PDEAEMA core-shell nanoparticles were able to efficiently deliver the antigen protein OVA to the cytosol of dendritic cells. The delivered OVA could further promote the cross presentation of OVA-derived peptides on MHC I molecules and thus led to enhanced $CD8^+$ T cell priming compared to soluble protein delivery, as evidenced by high levels of IFN-γ secretion by OVA-specific T cells. Nanoparticle-mediated OVA delivery enhanced the efficiency of cross-presentation by a factor of ~100-fold based on the dose response of T cell priming by DCs treated with antigen-loaded core-shell particles.

This enhancement could be further explored for *ex vivo* human vaccine screening, which is discussed in next section.

5.4 Cytosolic Delivery of Influenza A

Vaccination studies in humans are hampered by the limited assays that can be used to measure the strength, breadth, and quality of immune responses elicited in human patients. For assessment of T cell responses, clinical trials are limited to analyzing the phenotype/function of T cells recovered from peripheral blood samples. In cases where the immune response involves a known peptide antigen and HLA combination, it is possible to directly identify antigen-specific T cells from blood samples using recombinant peptide-MHC tetramer technology.[110-112] However, for novel vaccines where the immunodominant antigens are poorly defined or unknown, the only recourse for *ex vivo* analysis of the immune response lies in restimulation of effector or memory T cells *in vitro* using patient-derived dendritic cells pulsed with the vaccine antigen.[107, 113, 114] For vaccines employing complex antigens (*e.g.*, whole tumor lysate vaccines), there is no guarantee that incubation of vaccine antigen with DCs *in vitro* will lead to sufficient cross-presentation of any given epitope to properly mimic the potential antigen display elicited *in vivo*. Thus, a hurdle facing analysis of vaccine trials is the possibility that the restimulation assays used to detect $CD8^+$ T cell responses *ex vivo* may be inadequate to detect immune responses *even if they were actually elicited* by the vaccine.

The ability of the core-shell nanoparticles developed here to promote cross-presentation by DCs for CD8 T cell priming opens the possibility that these particles could be used to facilitate *in vitro* restimulation assays on detection of effector or memory T cell responses during human vaccine clinical trials. As a first step in this direction, we explored the possibility of delivering a complex antigen (whole inactivated virus) for restimulation of memory T cells readily obtainable from human populations (influenza memory T cells).[107]

Influenza is an infectious disease of birds and mammals caused by viruses. Flu spreads around the world in seasonal epidemics, killing millions of people in pandemic years and hundreds of thousands in non-pandemic years. For instance, a deadly avian strain named H5N1 ('bird flu') has posed the greatest risk for a new influenza pandemic since it first killed humans in Asia in the 1990s. Vaccinations against influenza are usually given to people to prevent the virus infection. However, a vaccine formulated for one year may be ineffective in the following year, since the influenza virus changes rapidly over time and different strains become dominant. In this section, we investigated the possibility of our nanoparticles to deliver a type of flu virus into human dendritic cells and to promote an immune response. We used whole inactivated Influenza A (H3N2) as our test strain.

5.4.1 Influenza A Delivery by Fluorescence Microscopy

We employed human monocyte-derived dendritic cells (MDDCs), to determine whether the pH-sensitive nanoparticles could deliver Influenza A virus protein to the human dendritic cells efficiently. Fluorescent Influenza A (1000 HA unit/mL) was premixed with PDEAEMA core-shell nanoparticles (25 μg/mL) for 5 min to allow electrostatic adsorption of the protein to the cationic surfaces of the core-shell particles. The majority of free Influenza A was removed by centrifugation and aspiration of supernatant. The Inlfuenza A-adsorbed particles were then resuspended in complete medium and added to MDDCs for 1hour at 37 °C, followed by washing and confocal imaging. Similar to the prior results obtained for calcein and OVA delivery, Influenza A fluorescence was observed throughout the cytosol and nucleus in MDDCs (Figure 5.9 B, pointed by white arrows) co-incubated with Influenza A-coated PDEAEMA core-shell nanoparticles. Incubation of MDDCs with Influenza A also showed high amounts of virus uptake, likely through normal antigen capture/uptake mechanisms specifically evolved for efficient recognition of pathogens by DCs (Figure 5.9 D). Notably however, even for the high levels of free virus internalized by the cells, signatures of free cytosolic fluorescence extending into dendrites of the cells was lacking, suggesting that nanoparticles may be favoring cytosolic entry over the response to the free virus. A potential complication for this particular choice of antigen is the possibility that the inactivated whole virus preparation may have some residual intrinsic endosome-disruption activity from the native cellular entry proteins of the virus. Following on these preliminary

investigations, analyses of T cell responses to the delivery of Influenza A using flu-specific human T cells is ongoing with collaborators at the Dana Farber Cancer Institute/Harvard Medical School.

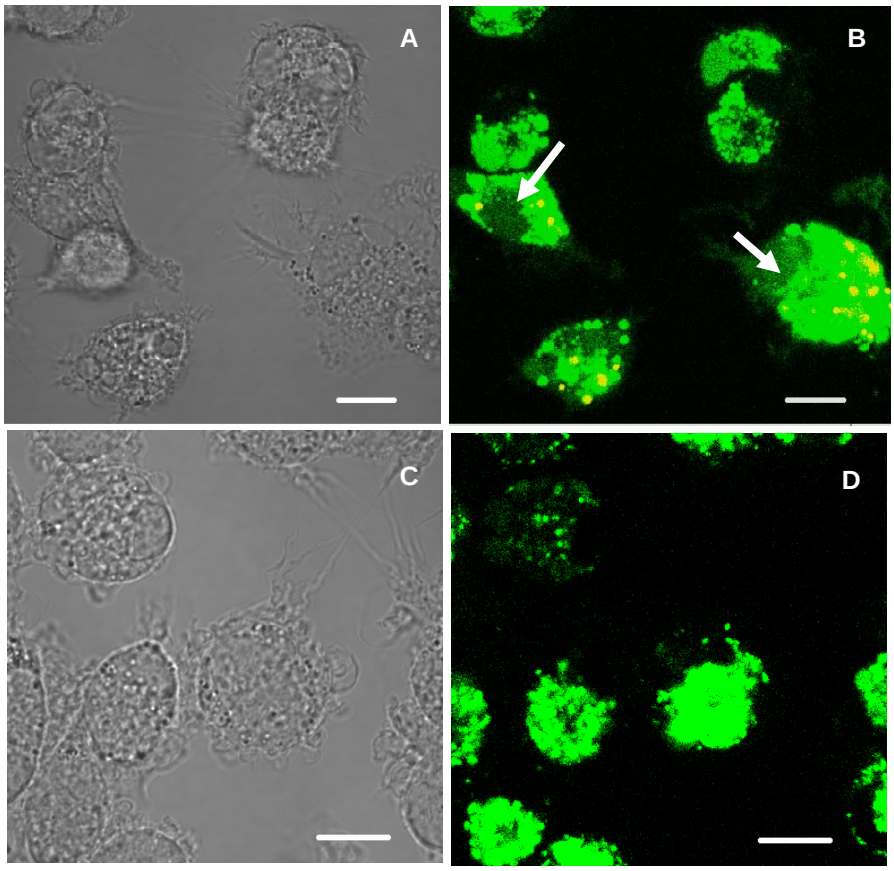

Figure 5.9 Cytosolic delivery of Influenza A to MDDCs. CLSM images at 100X: (A, C) Brightfield images; (B, D) Fluorescence overlays of Influenza A (green) and nanoparticles (red). (A, B) Cells incubated with Influenza A adsorbed to PDEAEMA core-shell nanoparticles. (C, D) Cells incubated with Influenza A alone. Scale bars 10µm. White arrows pointed the cells with cytosolic delivery of Influenza A protein.

5.5 Intracellular Delivery of siRNA

In addition to protein delivery, a final area of therapeutic delivery we have briefly examined with the core-shell nanoparticle system is the delivery of double-stranded RNA oligonucleotides for RNA interference (RNAi). RNAi is originally considered as a self-defense mechanism of cells to the infection by RNA. As mentioned in Chapter 1, in recent years, the potential use of siRNA as therapeutic agents has attracted great attention. For instance, treating severe and chronic diseases (*e.g.* cancer) could be done by silencing RNA and regulating protein levels with siRNA. However, the extremely low efficiency of intracellular delivery of siRNA and the relatively high dose of siRNA required for gene silencing limit its therapeutic applications. An ideal delivery system that would (1) be able to bind siRNA in a reversible manner to ensure subsequent release of the siRNA; (2) escape from endosomal compartment; and (3) be biocompatible. Our pH-sensitive core-shell nanoparticles could be a good candidate as a siRNA delivery system.

5.5.1 siRNA Delivery by Fluorescence Microscopy

We employed DC2.4 and an epithelial cell line from monkey kidneys, BSC-40, to determine whether the pH-sensitive nanoparticles could deliver siRNA to the cell cytosol efficiently. Cy5-labeled siRNA (100 nM) was premixed with PDEAEMA or PMMA core-shell nanoparticles (25 μg/mL) for 5 min to allow electrostatic adsorption of the siRNA to the cationic surfaces of the core-shell particles. The

siRNA-adsorbed particles were then resuspended in complete medium and added to DC2.4 cells for 1 hour at 37 °C, followed by washing and confocal imaging. Similar to the prior results obtained for calcein and OVA delivery, Cy5 fluorescence of siRNA was observed throughout the cytosol and nucleus in DC2.4 (Figure 5.10 B) co-incubated with siRNA-coated PDEAEMA core-shell nanoparticles. The cytosolic/nuclear delivery efficiency was $43.0 \pm 2.3\%$ (S.D. of three individual samples, n=150 cells were scored). When DC2.4 were incubated with siRNA-coated PMMA core-shell nanoparticles, the fluorescence was instead observed with a punctuate distribution in the endosomal compartments (Figure 5.10 D).

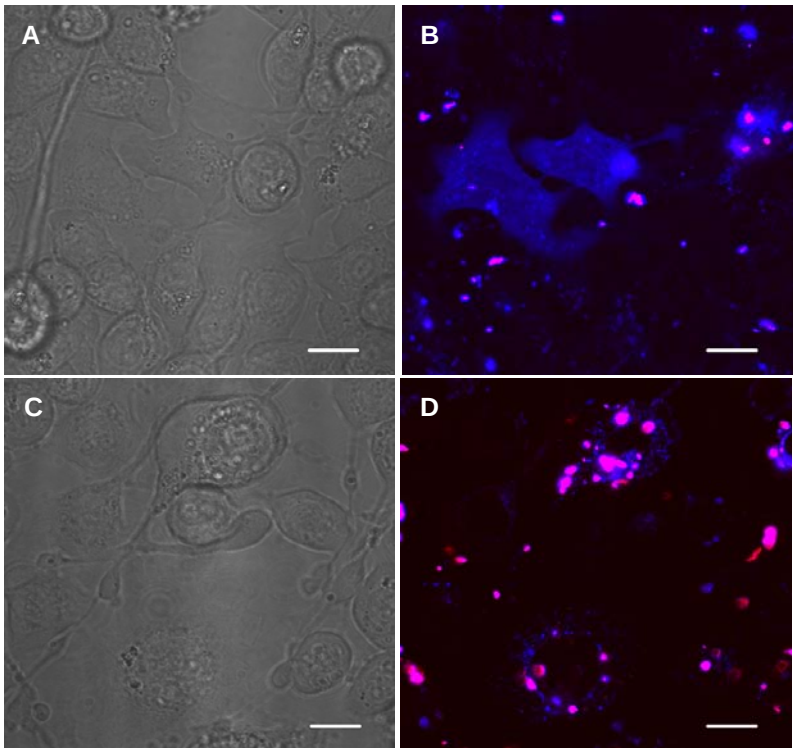

Figure 5.10 pH-sensitive core-shell nanoparticles deliver siRNA to the cytosol of DC2.4 cells. (A-D) CLSM images at 100X: (A, C) Brightfield images; (B, D) Fluorescence overlays of siRNA (blue) and nanoparticles (red). (A, B) DC2.4 incubated with siRNA adsorbed to PDEAEMA core-shell nanoparticles. (C, D) Cells

incubated with siRNA adsorbed to PMMA core-shell nanoparticles. Scale bars 10μm.

We tested the intracellular delivery of fluorescent siRNA to BSC-40 cells in a similar protocol. In this study, we tested an antiGFP siRNA, which has the sequence as listed in Table 5.1.

Table 5.1 Sequence of antiGFP siRNA

working strand	U.G.C.G.C.U.C.C.U.G.G.A.C.G.U.A.G.C.C.dT.dT.3'-Cy5
complementary strand	Cy3-G.G.C.U.A.C.G.U.C.C.A.G.G.A.G.C.G.C.A.dT.dT

Non-labeled core-shell nanoparticles were used in this study, as both of the strands for siRNA were labeled. In Figure 5.11 B, the Cy5 and Cy3 dye were co-localized and displayed a punctuate distribution in the cells. This result showed that with PMMA core-shell nanoparticles, siRNA was confined in endolysosomes. When BSC-40 cells were incubated with siRNA-coated PDEAEMA core-shell nanoparticles (Figure 5.11 D), the Cy3 and Cy5 fluorescence was observed throughout the whole cytosol, indicating the efficient intracellular delivery of siRNA. At the same time, the Cy5 fluorescence was shown as punctuate dots in certain locations inside the cells, besides flooding the cell cytosol together with Cy3 label. It could be the evidence that the working strands with Cy5 label were targeting specific mRNA sequences, after being released from the endolysosomes. This hypothesis needed to be further investigated by examining the mRNA level of the cells.

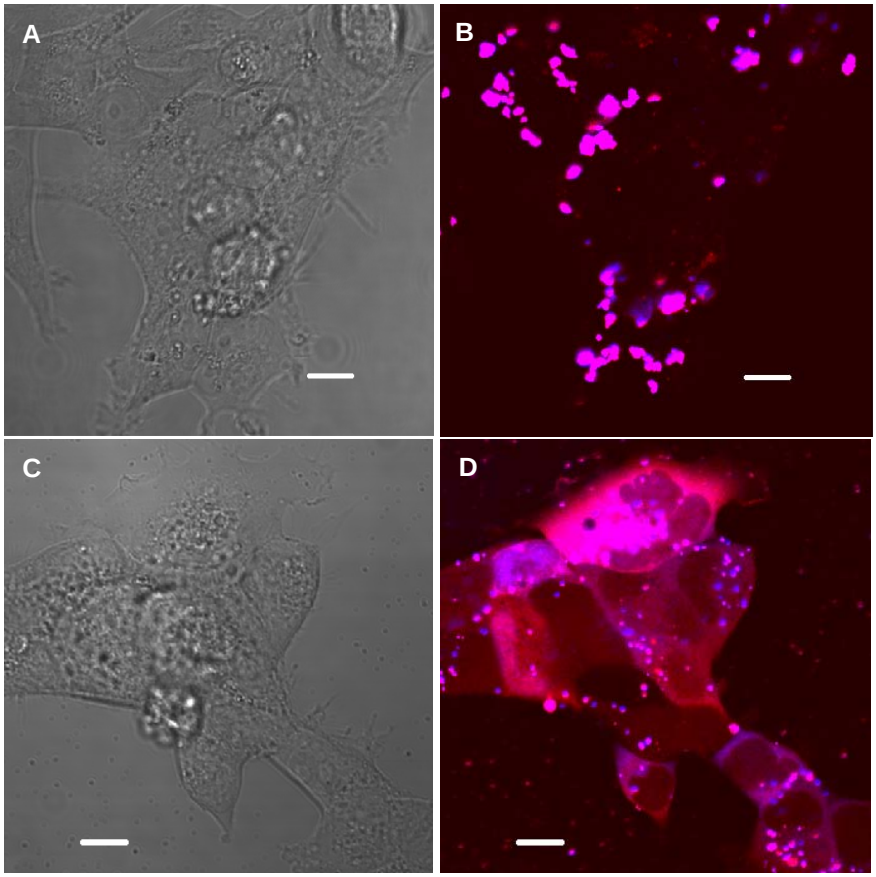

Figure 5.11 Intracellular delivery of siRNA to epithelial cells, BSC-40. (A-D) CLSM images at 40X: (A, C) Brightfield images; (B, D) Fluorescence overlays of different siRNA strands (blue, Cy5-labeled working strand; and red, Cy3-labled complementary strand). (A, B) DC2.4 incubated with siRNA adsorbed to PMMA core-shell nanoparticles. (C, D) Cells incubated with siRNA adsorbed to PDEAEMA core-shell nanoparticles. Scale bars 20 μm.

5.5.2 Gene Silencing Following Particle-Mediated siRNA Delivery

To evaluate the efficiency of siRNA delivery, we used reverse transcription RCR (PT-PCR) to detect the mRNA level of siRNA-transfected cells. RT-RCR is a

process in which single-stranded RNA is reverse transcribed into complementary DNA (cDNA) by using total cellular RNA together with a reverse transcriptase enzyme, a primer, dNTPs and an RNase inhibitor. The resulting cDNA can be used in a real time PCR reaction, which can make a large number of copies of the specific gene *ex vivo* in short periods. With the amplification of PCR, we can screen for the genetic information expected in cells by applying proper primers.

As described in section 5.1.5, we transfected BSC-40 cells with siGLO Cyclophilin B control siRNA (100 nM) coated PDEAEMA nanoparticles (25 μg/mL) for 1 hour or siRNA/Lipid (Dharma*FECT*® transfection reagent, 2.5 μL/mL) for 4 hours. After a 24 hour incubation period, the cellular RNA was isolated, measured, and diluted for RT PCR in a 7700 prism sequence detection system (Perkin-Elmer Applied Biosystems).

After real time PCR, C_t, the number of PCR cycles at which a significant exponential increase in TaqMan® fluorescence is detected. This threshold cycle is directly correlated with the number of copies of DNA template present in the reaction. A quantitative approach, the comparative C_t method, was used to determine the mRNA amount in the cytosol. In this method, the C_t values of the samples of interest were compared to a control or calibrator, such as a non-treated sample or RNA from normal tissue (actin gene in our case). The C_t values of both the calibrator and the samples of interest were normalized to an appropriate endogenous housekeeping gene (cyclophilinB).

$$\Delta\left(\delta C_{t,Sample}\right) = \delta C_{t,Sample} - \delta C_{t,Calibrator}$$

$$\delta C_{t,Sample} = C_{t,Sample} - C_{t,housekeeping}$$

$$\delta C_{t,Calibrator} = C_{t,Calibrator} - C_{t,housekeeping}$$

The mRNA amount was determined as

$$mRNA = 2^{\delta C_{t,Sample}}$$

In figure 5.12, the knockdown rate of mRNA, which is the remaining amount of target mRNA in the transfected cells compared to that of untreated control, was plotted for different samples. For the positive control, siRNA delivered by commercial lipid (Dharma*FECT*® transfection reagent) for longer time (4 hours), 6.3±1.2% (S.D of three individual samples) of targeted mRNA remained in the cells. When cells were transfected with siRNA-coated PDEAEMA core-shell nanoparticles for only 1 hour, the target mRNA was calculated as 23.3 ± 14.0 % (S.D of three individual samples) of untreated cells. This result demonstrated the efficiency of the cytosolic delivery of siRNA by our nanoparticles. Note that the mRNA level was measured with total cellular RNA of all the cells in the sample, as it was assumed that the transfection of siRNA was homogenous. The result shown in Figure 5.12 was the average of the whole cell population. However, from the CLSM, we knew that the cytosolic delivery efficiency was ~ 43%, and not all the cells were affected in the same way for the siRNA delivery. This result indicated that some of the cells were affected by the siRNA delivered to the cytosol, and the targeted mRNA level could be close to zero. However, there were some cells that might not be affected at all, and the targeted mRNA level was still high. The flow cytometry technique could be further applied to detect remaining level of protein translated from the targeted mRNA with certain

fluorescent indicators through the cell population.

This inefficiency in different cells could be caused by the lack of drug unpacking mechanism. This limitation of the present system will be further discussed in the next chapter examining future directions for this research.

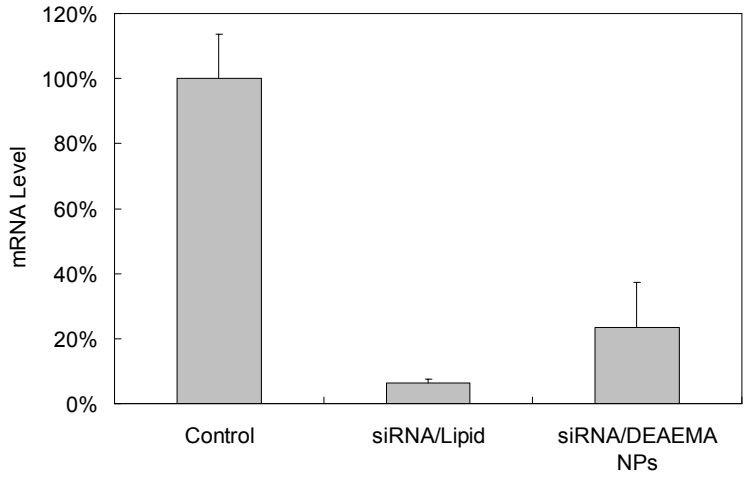

Figure 5.12 mRNA level of BSC-40 cells with the cytosolic delivery of siRNA. Cells were treated with no siRNA (control), siRNA with Dharma*FECT*® transfection reagent (siRNA/Lipid), or siRNA with pH-sensitive core-shell nanoparticles (siRNA/DEAEMA NPs), and cultured for 24 hours. For each condition, total cellular RNA of the whole cell population was isolated and detected by RT-PCR.

In this chapter, we applied the pH-sensitive PDEAEMA core-shell nanoparticles as an intracellular drug delivery system, and demonstrated that these particles are capable of efficient cytosolic delivery of membrane-impermeable macromolecules such as OVA protein, Influenza A, or siRNA to different cell types. By sequestering the hydrophobic, pH-buffering component of the polymer particles within the core by a more hydrophilic shell composition, these particles effectively disrupted endosomes

and delivered molecules to the cytosol of cells without overt cytotoxicity. These materials may be of utility for delivery of membrane-impermeable drug compounds or oligonucleotides to the cytosol of dendritic cells for immunotherapy, and other cell types for cytosolic drug therapy. In the next chapter, we will explore the extension of this concept to core-shell nanoparticles that quickly dissolve to non-toxic soluble components upon reaching the cytosol, to promote efficient unpacking of drugs carried to the cytosolic compartments.

6 Design of Biodegradable Nanoparticles

We have synthesized pH-sensitive core-shell nanoparticles and demonstrated their capability of delivering small molecules or macromolecules to the cell cytosol efficiently by endosome disruption. We would like to further test and apply our nanoparticles as a drug delivery system *in vivo*. However, lack of degradability is of great concern, as the biodistribution of nanoparticles in the blood stream and the accumulation of nanoparticles in the spleen and kidney might cause toxicity in long term.[115] Design of a biodegradable system that can dissolve and be excreted out of the body is necessary.

In addition, our studies with protein or siRNA delivery described in the last chapter suggested that the release of macromolecular drugs electrostatically bound to the particles is inefficient. This inefficient release is a barrier to an optimal function of the particles as a delivery system. A degradable particle could potentially facilitate drug 'unpacking' and address this issue.

6.1 Materials and Methods

6.1.1 Materials

Most reagents were obtained as described in Chapter 3. N, N-bis (acryloyl) cystamine (BAC), and glutathione (GSH, reduced form) were purchased from Sigma-Aldrich Chemical Co. Cy3 mono-NHS ester was purchased from GE

Healthcare UK Limited. Poly fluor™ 570 methacryloxyethyl thiocarbamoyl rhodamine B was purchased from Polysciences Inc.

6.1.2 Synthesis of Nanoparticles by Emulsion Polymerization

Similarly as described in Section 3.1.2, nanoparticles were synthesized with the biodegradable crosslinker BAC. Typically, BAC (16 mg, 0.5 mol%) was weighed and dissolved in EtOH (300 μL) at 70 °C. PEGMA1000 (220 mg, 20 wt%) was prewarmed at 70 °C, and added to the BAC solution. DEAEMA (960 μL, 80 wt%) was then mixed with PEGMA1000 and BAC solution, and dispersed in prewarmed water (9 mL) with stirring, and equilibrated at 70 °C for 20 min, before adding APS (50 μL of 200 mg/mL freshly made solution) as the initiator. The emulsion polymerization was allowed to proceed at 70 °C for 3 hours to grow the particle core, followed by injection of AEMA (50 μL of 800 mg/mL freshly made solution, 0.24 mmol) to grow the particle shells for an additional 1.5 hours. The nanoparticles were purified by dialysis (10,000 MWCO Slide-A-Lyzer® Dialysis Cassettes, Pierce Chemical Co.) in deionized water for three days followed by ultrafiltration (10,000 MWCO PLGC Ultrafiltration Membrane, Millipore Co.) three times and centrifugation three times with PBS (pH 7.4) at 15,000x*g*. Purified particles were stored in PBS at 4 °C. Fluorescent labeling the AEMA shell structure with Cy-3 mono-NHS ester was carried out as described in Section 3.1.2. The labeled particles could be visualized by Confocal Laser Scanning Microscope (CLSM). CryoEM was

performed to measure the size of the nanoparticles, as described in Section 3.1.2.

6.1.3 Degradation Study of BAC Crosslinked Nanoparticles

To mimic different physiological and cellular environments, GSH (10 mM) was dissolved in deionized water (pH 3), serum free PRMI 160 medium (pH 7.4), and complete PRMI 160 medium (pH 7.4). In addition, phosphate buffer at physiological ionic strength (100 mM) with different pH was used for certain conditions.

100 μL of purified nanoparticles (~ 0.5 mg) were suspended in 1 mL PBS (pH 7.4), GSH in water (pH 3), or GSH in SF medium (pH 7.4) with mild shaking in the Jitterbug at 37 °C. The degradation of the BAC nanoparticles was examined by quantifying the optical clarity of the suspension using UV/VIS Spectrum (Helios Gamma, Thermo Fisher Scientific Inc.) to collect absorbance values at a wavelength of 450 nm; or by evaluating the size distribution of the nanoparticles by DLS (Particle Size Analyzer 90Plus, Brookhaven Instruments Corporation).

6.1.4 Biological Characterization of BAC Crosslinked Nanoparticles

Calcein Delivery in DC2.4 Cells

The cytosolic delivery efficiency of BAC crosslinked nanoparticles was tested in DC2.4 cells with the small molecule calcein. DC2.4 cells were cultured according to

the conditions described in Section 4.1.2. DC2.4 cells ($1.2x10^5$ cells/well) were plated in Lab-Tek™ chambers and cultured overnight (~ 18 hours). Calcein was added to the cells (150 μg/mL, 0.24 mM) with or without 25 μg/mL BAC nanoparticles in complete medium (RPMI 1640 with 10% fetal bovine serum (FBS)) for 1 hour at 37 °C. After three washes with medium to remove extracellular calcein and particles, the cells were imaged live by CLSM at 37 °C.

Cell-Growth Assays of Cell Viability

BMDCs were harvested and derived as described in Sec 4.1.4. Day 6 BMDCs ($1x10^6$ cells/well/mL) were plated in a 6-well plate for 2-4 hours to allow the cells to attach to the bottom of the plates. Cells were then incubated with 25 μg/mL of BAC-crosslinked or PEGDMA-crosslinked nanoparticles for 1 hour at 37 °C. After washing three times with complete medium to discard the extracellular nanoparticles, cells were collected, counted, and replated in 96-well plates at a density of $5x10^4$ cells/well. The replated cells were then cultured for an additional three days, and the number of cells grown out in these cultures was determined by the CyQUANT® NF Cell Proliferation Assay Kit at 488 nm/530 nm using a fluorescence microplate reader (SPECTRAmax™ GEMINI, Molecular Devices Corp.)

Degradation *In Vitro*

To enable tracking of dissolution of the particle cores in live cells, nanoparticles were labeled by poly fluorTM 570 methacryloxyethyl thiocarbamoyl rhodamine B in

the core. This fluorescence dye was dissolved in EtOH (50 mg/mL) and added to comonomer and BAC mixture (10 μL in 1 mL) before the synthesis.

Day 6 BMDCs ($1.2x10^5$ cells/well) were plated in Lab-Tek™ chambers and cultured overnight (~ 18 hours). Cells were treated with or without 25 μg/mL of BAC nanoparticles in complete medium for 1 hour at 37 °C. After three washes with medium to remove extracellular particles, the cells were imaged live by CLSM at 37 °C. The cells were then cultured and imaged live by CLSM at 37 °C over 24 and 48 hours.

6.2 Design of Biodegradability

An important consideration for clinical application of this polymeric drug delivery systems is the ultimate fate of the polymeric materials, which will be determined by its method of synthesis, its subsequent degree of purity, its behavior on administration into the individual biological system, and its biodistribution.[115] The biodegradability of nanoparticles used for drug delivery is of great concern, as the blood circulation and final accumulation of the polymeric materials and the by-products could potentially cause serious toxicity or immune response.[115]

Biodegradability can be defined as the capability of the material to be broken down *in vivo* into excretable or metabolized products. An efficient process inside the body to disassociate the nanoparticles from the drugs, and then break them down into inert or harmless chemicals that can exit the body quickly is needed for a

biodegradable drug delivery system.

Hydrolysis is used as a major mechanism to degrade polymeric systems, for example, polymers with ester linkages such as the poly(lactide-co-glycolide) (PLGA) family.[39] In general, an ester link can be slowly broken down in water into a hydroxyl functional group and a carboxylic acid functional group. With the aid of dilute acid to protonate the carbonyl group, the acid-catalysed hydrolysis can be much more efficient. However, it has been reported that PLGA has poor stability in endolysosomes,[33, 116] as drugs cargoes are often degraded in acidic microclimate before it can be successfully released to the cytosol.[39, 40] Hydrolysis process is not suitable to design the biodegradability of our nanoparticles. If the nanoparticles were degradable in acidic environment under hydrolysis, their pH-responsive function could be compromised.

Enzymatic degradation[31, 32, 72, 73] is another commonly used mechanism for biodegradation. Almost all processes in a biological cell need enzymes. In an enzymatic reaction, the substrate could be converted into different molecules selectively by specific enzyme(s) at a significant rate. However, enzymes are rich in endosomes, and especially lysosomes. As the kinetics of endolysosomal escape is not clear, the cytosolic delivery could happen by the disruption of the endosomes or lysosomes. If the nanoparticles could be located in the lysosomes for certain period of time, the enzymes could digest the nanoparticles and drug cargos there efficiently, unless we could make use of a specific enzymatic reaction in the cytosol. Instead of locating a specific enzyme that only present in cytosol of certain cell types, we

explored a specific chemical reaction as an alternative mechanism for nanoparticles degradation.

Cytosolic Environment and Degradable Crosslinker

Glutathione is a small molecule made up of three amino acids, which exists in almost every cell of the body (Figure 6.1). Thiol groups (~ 5 mM) are usually kept in a reduced state. In effect, glutathione reduces any disulfide bonds formed within cytoplasmic proteins to cysteines by acting as an electron donor. The presence of glutathione is required to maintain the normal function of the immune system, as it is known to play a critical role in the multiplication of lymphocytes which occurs in the development of an effective immune response.[117] Furthermore, glutathione is used to detoxify various chemicals from the body. Glutathione is found almost exclusively in its reduced form in the cytosol since the enzyme glutathione reductase is constitutively active and inducible upon oxidative stress. This enzyme converts oxidized form glutathione disulphide (GSSG) to the sulfhydryl form GSH. In fact, the ratio of reduced glutathione to oxidized glutathione within cells is a measure of cellular toxicity.

Based on these facts, we sought to take advantage of the constant concentration of GSH present in the cell cytosol, and apply disulfide reduction as a mechanism of biodegradability of our nanoparticles.[118-122] With the thiol groups of GSH in cytoplasm, the nanoparticles rich in disulfide links would be broken down to polymer chains by the reducing environment. In addition, since the intracellular GSH

concentration (1-10 mM) is 1000-fold greater than the extracellular level (2 μM),[120, 123-126] the particles could potentially be stable until degradation is carried out in the cytoplasm after endolysosome escape. Thus, a crosslinker BAC[127-129] (Figure 6.1) with a disulfide bond was chosen to synthesize the nanoparticles.

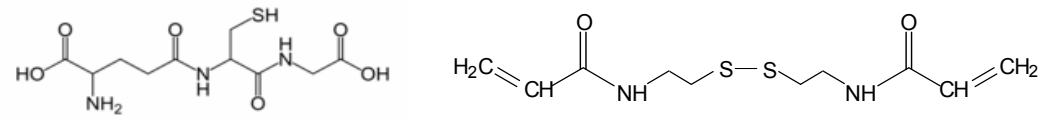

Figure 6.1 Chemical structures of GSH and BAC.

Non-toxic Micelle Formation

Given the hypothesis that nanoparticles crosslinked by disulfides could be degraded by GSH in the cell cytosol, the final components and their cytotoxicity are still of concern. By simply replacing the PEGDMA crosslinker of the 'stable' core-shell nanoparticles with the disulfide-linked BAC, disulfide cleavage would be proposed to produce insoluble polymer chains of PDEAEMA in the cytosol. These PDEAEMA breakdown products could be toxic to cells, as was reported by Zuidam *et al*. in a study of structurally-similar poly(dimethylaminoethyl methacrylate) polymers.[90] We have investigated core-only nanoparticles in Chapter 4, and proved their potential cytotoxicity as well. Although we shield the hydrophobic and slightly cytotoxic core by the hydrophilic AEMA shell, breakdown of the nanoparticles would expose the PDEAEMA polymer to internal membranes of the cell. Similar to core-shell structure used to sequester PDEAEMA in the intact particles, we need a design to 'hide' the PDEAEMA polymer chains in the breakdown products as well.

To achieve this goal, we pursued the approach schematically outlined in Figure 6.2. We hypothesized that copolymerization of DEAEMA with a hydrophilic PEG methacrylate in the core, crosslinked by the disulfide BAC crosslinker, would provide a degradable particle with a nontoxic breakdown structure: each chain of the crosslinked core would have a 'comb' copolymer architecture, with a DEAEMA backbone and short PEG side chains. Cleavage of the crosslinks holding the core together would result in release of individual comb chains. The hydrophobic nature of the DEAEMA backbone units at neutral pH would favor collapse of the backbone units, while the hydrophilic PEG chains would extend into solution, forming a unimolecular micelle. We hypothesized that such a unimolecular micellar breakdown product could be safely eliminated from cells and eliminated from the body, *e.g.*, through the kidneys.

In summary (Figure 6.2), we would crosslink DEAEMA and PEGMA by BAC, which possesses a disulfide bond and can be reduced by GSH in the cytoplasm, to form the degradable nanoparticles. The nanoparticles should still have the capability to disrupt the endolysosomes and release drugs via their pH-sensitivity. After the nanoparticles carrying the drug molecules are released to the cytosol, they would be digested by GSH in the cytoplasm. The breakdown poly(DEAEMA-co-PEGMA) comb polymer chain could form non-toxic micelles by hiding the slightly toxic PDEAEMA to the core while facing the hydrophilic PEG toward cell environment. At the same time, drug molecules would be unpacked from the nanoparticles, and released to the cytosol upon the degradation of drug cargos.

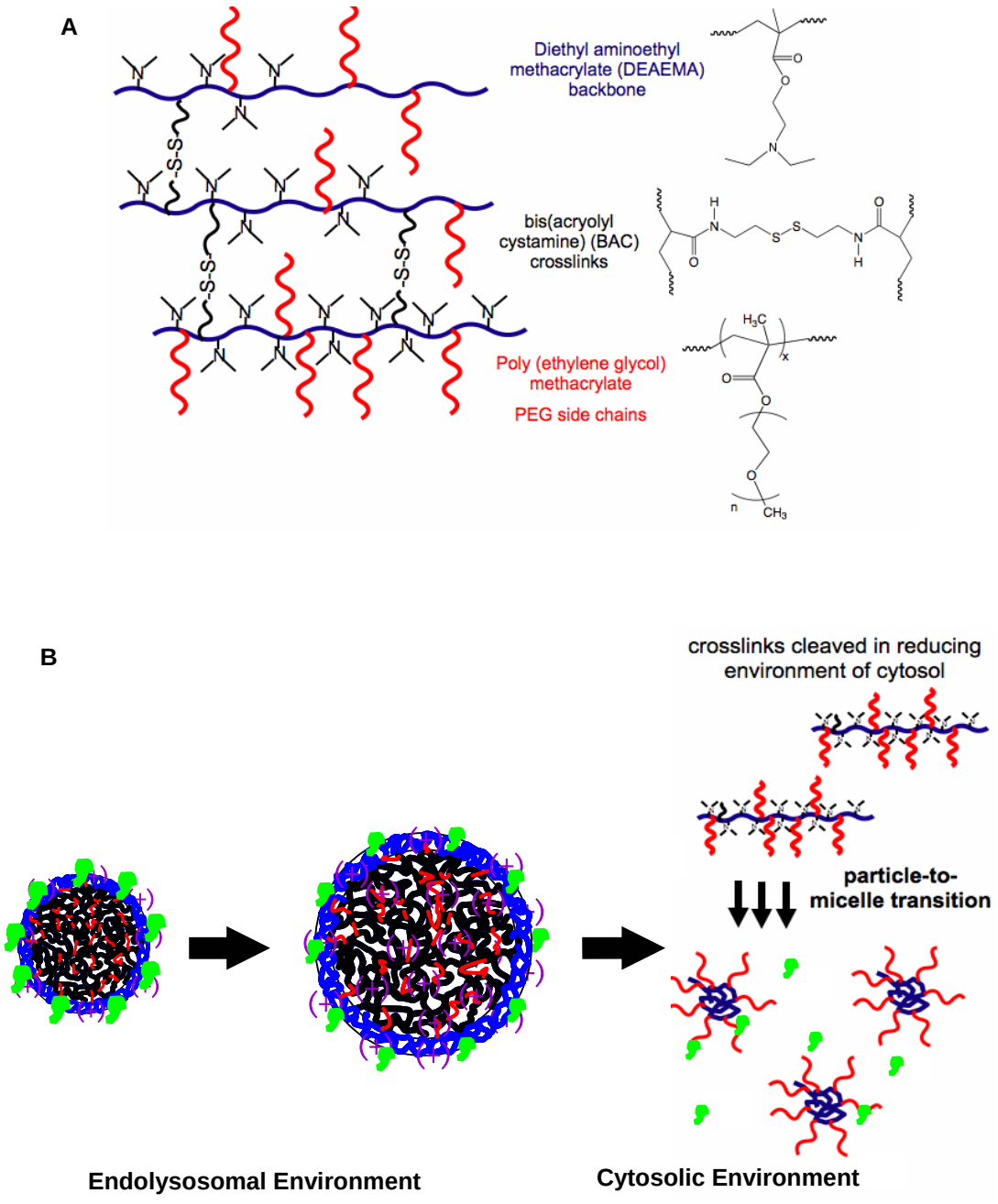

Figure 6.2 Schematic of biodegradable nanoparticles. (A) Chemical architecture of biodegradable nanoparticles. (B) Behavior of biodegradable nanoparticles in cells. At extracellular pH, nanoparticles remain in their deswelled state and bind drug molecules on the shells electrostatically. At endolysosomal pH, the core tertiary amines ionize, and the particles swell and disrupt the endolysosomes, while the drugs

remain bound. In the cytoplasm environment, GSH reduces the disulfide bonds of the crosslinker BAC, and the nanoparticles are digested into non-toxic micelles, which have the hydrophilic PEGMA as outside layer and hydrophobic PDEAEMA as inside core, and the drug molecules are released.

6.3 Degradation of BAC Crosslinked Nanoparticles

As designed above, the degradation of the nanoparticles mainly depends on the concentration of the crosslinker BAC, as the amount of the disulfide bonds in the nanoparticles decides the efficiency of the reduction by GSH. However, parameters such as the molecular weight of comonomer PEGMA, and the ratio of PEGMA to DEAEMA in the comonomer mixture, can impact the solubility and cytotoxicity as we discussed above. To determine how these physical parameters of DEAEMA-PEGMA-BAC hydrogel nanoparticles affect the degradation, we synthesized a range of different nanoparticles as listed in Table 6.1. Note that in this Chapter, all the nanoparticles discussed were core-shell structured unless specified.

Table 6.1 Composition of Degradable Hydrogel Nanoparticles

Sample	DEAEMA (mg)	PEGMA (mg)	BAC (mg)
DB1*	922.0	0	16
DB1.5	922.0	0	25
DB2.5	922.0	0	40
DB3.75	922.0	0	60
DB5	922.0	0	80
DPEG200_10%***	862.1	95.8	16
DPEG400_10%	885.1	98.3	16
DPEG1000_10%	903.6	100.4	16
DPEG1000_20%	885.1	221.3	16
DPEG400_10%_Stable	885.1	98.3	(21.6)**

* D: DEAEMA; B: BAC; 1, the molar ratio of BAC compared to monomer(s)

** PEGDMA200 (mg) used to reach same molar ratio as using 16 mg BAC.

*** 10%: weight ratio of PEGMA

The total monomer concentration for each synthesis was kept constant (~ 5 mmol) as our original nanoparticles, while the weight ratio of PEGMA to DEAEMA was varied from 0:10 to 2:8. Nanoparticles were prepared using PEGMA with different molecular weights (MW_{PEO} = 200, 400, 1000) to determine the role of the PEG side chain length in degradation and cytotoxicity. The crosslinker ratio of BAC was from 0 to 5 mol%. Because BAC was poorly soluble in water or DEAEMA, 300 μL of EtOH was used to dissolve BAC at 70 °C before mixing with the other comonomers (see 6.1.2 for details).

6.3.1 Effect of BAC Concentration on Degradation

As the concentration of GSH in the cytoplasm is constant for most of the cell

types, and maintained ~ 1-10 mM according to different cell types,[94, 126] we first sought to determine whether BAC-crosslinked nanoparticles were sensitive to degradation by such GSH concentrations and assess the impact of crosslink density on particle breakdown. For these initial experiments, we tested the response of core-shell BAC-crosslinked polyDEAEMA nanoparticles (no PEGMA co-monomer) to GSH treatment. This experiment is also to determine whether the presence of sulfate groups on the chain ends of emulsion-polymerized polyDEAEMA chains and/or pendant sulfhydryls groups would impart solubility to the breakdown products at neutral pH. Nanoparticles were synthesized with varying concentrations of BAC (1-5 mol% relative to DEAEMA). The particles (~ 0.5 mg) were then suspended in different buffers (1 mL) at 37 °C for 24 hrs with mild shaking. Absorbance of the suspensions at 450 nm was measured to evaluate turbidity as a first-order readout for the presence of intact particles. PBS (pH 7.4) was used as a control sample, since the nanoparticles were stable without any size change when incubated in PBS for 24 hours (data not shown). As shown in Figure 6.3, particles suspended in GSH-containing serum-free medium (GSHM, 10 mM GSH) gave a similar transparency to those in PBS. This result was not completely unexpected since polyDEAEMA homopolymers is not normally soluble at pH 7.4 in aqueous solutions. To confirm that the lack of transparency of the particles suspensions was a result of polymer chain insolubility but not failure of GSH to cleave the disulfide crosslinks, we tested the particle suspension in GSH-supplemented deionized water (GSHW, 10 mM GSH). Besides reducing capability, this solution provided an acidic

environment (pH ~ 3) that could protonate and thus dissolve PDEAEMA chains completely following crosslink degradation. In this case, the BAC-crosslinked samples were totally transparent (Figure 6.3). This result suggested the BAC concentrations used were sufficient to respond to the GSH, while improvement of the solubility of break-down components was needed. Unless specified otherwise, 1 mol% of BAC (16 mg) was used in the further studies testing the effect of other parameters on the degradability.

As we mentioned, due to the solubility of BAC, EtOH was used to achieve a homogenous monomer/crosslinker mixture before adding to the water bath. The addition of EtOH could reduce the hydrophobicity of the monomer, and thus affect the emulsion polymerization. The inefficient crosslinking between BAC and the monomer could result in homopolymer nanoparticles, which would consist of only PDEAEMA chains instead of crosslinked hydrogels. In this case, the PDEAEMA chains would dissolve in acidic conditions irreversibly. To test this hypothesis, we simply suspended the particles into phosphate buffer at pH 4.86, and detected their turbidity. We then added NaOH to bring the pH back to 7.4, and checked the turbidity of the solution again. In all the cases (data not shown), the nanoparticle suspension looked transparent (absorbance at 450 nm < 0.25) when incubated in phosphate buffer at pH 4.86 while the absorbance was restored when the pH was adjusted to 7.4 by NaOH. This result indicated that the nanoparticles were formed with BAC crosslinker. Otherwise, the solution would have remained transparent (absorbance < 0.25) when the pH was changed back to pH 7.4 as the non-crosslinked

polymer chains were dissolved in acid irreversibly.

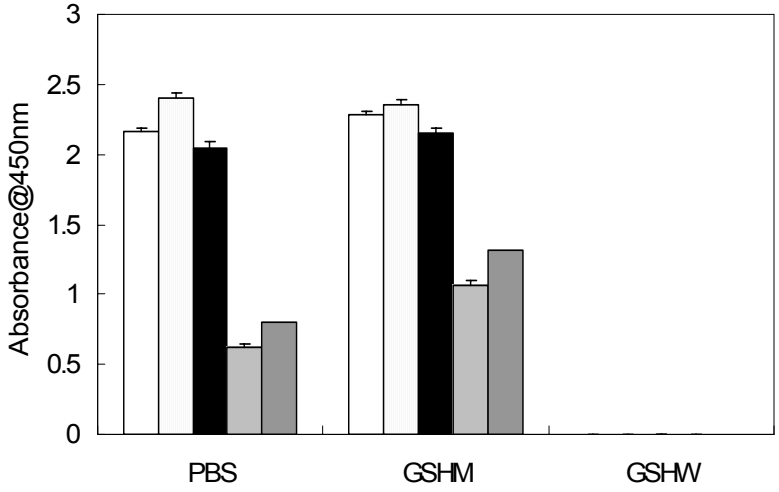

Figure 6.3 Effect of crosslinker ratio on degradability. BAC-crosslinked polyDEAEMA nanoparticles were synthesized with different concentration of crosslinker: 1 (white), 1.5 (dot), 2.5 (black), 3.75 (stripe), 5 (grey) mol% BAC (~ 5 mmol total monomer DEAEMA). Nanoparticles were suspended in PBS, GSH in serum free medium (GSHM, pH 7.4), or GSH in water (GSHW, pH 3.0). The UV absorbance of the particle suspensions were measured after 24 hours of shaking at 37 °C. Shown are mean ± S.D. of triplicate samples.

6.3.2 Effect of PEGMA on Degradability

The initial degradation measurements described in 6.3.1 suggested that pure polyDEAEMA nanoparticles do not have sufficient solubility for dissolution following crosslink degradation. To impart solubility to the nanoparticle polymer, we synthesized copolymer particles using DEAEMA and PEGMA as comonomers. PEGMA with different molecular weights could provide different chain lengths with

different hydrophilicity, thus affecting the degradability of the nanoparticles and their cytotoxicity. We synthesized nanoparticles of DEAEMA with no PEGMA, and compared to copolymer particles prepared with DEAEMA and PEGMA200, PEGMA400, or PEGMA1000 at a fixed weight ratio of 90:10 of DEAEMA:PEGMA (as summarized in Table 6.1). The same amount of BAC (1 mol% relative to monomers) was used in each condition. The particles (~ 0.5 mg) then suspended in PBS or GSHM (1 mL) at 37 °C with mild shaking before absorbance measurements. Particles with PEGMA400 and PEGMA1000 showed obvious degradation after one day of incubation, as the absorbance of these samples was decreased in GSHM when compared to those in PBS (Figure 6.4); the absorbance of PEGMA1000 copolymer particles was only 26.3% of the initial suspension. This result suggested that longer PEG side chains provided enhanced solubility relative to shorter PEG in these DEAEMA-PEGMA copolymers. For PEGMA200 sample, the absorbance in GSHM was much higher than that in PBS. The reasons for this discrepancy are unclear but could reflect improved access of GSH to the core of the particles due to PEG enabling water/GSH penetration to the particles. Without substantially enhancing the solubility of freed polymer chains, this process favored particle aggregation rather than dissolution, thus resulting in the larger value of absorbance as indicated in Figure 6.4.

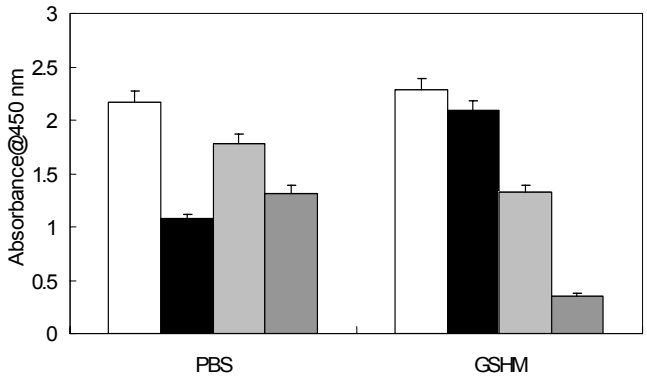

Figure 6.4 Effect of PEGMA molecular weight on degradability. Nanoparticles were synthesized by DEAEMA alone (white) or DEAEMA and PEGMA (MW_{PEO} = 200 g/mol (black), 400 g/mol (stripe), or 1000 g/mol (grey)) at the weight ratio of 90:10. 1 mol% of BAC was used as crosslinker. Nanoparticles were suspended in PBS or GSH in serum free medium (GSHM, pH 7.4). The UV absorbance of the particle suspensions was detected after 24 hours shaking at 37 °C. Shown are mean ± S.D. of triplicate samples.

In the discussion above, we used the turbidity of the solution to monitor the degradation of the nanoparticles, as it was a simple method to infer changes in the particles under different conditions. However, such measurements are only useful as first-order analyses as particle swelling may reduce absorbance without reflecting actual permanent particle dissolution. We thus employed dynamic light scattering (DLS) measurements to provide further insight into the effect of GSH treatment on BAC-crosslinked nanoparticle breakdown. Stable nanoparticles crosslinked by PEGDMA200 (as used in the studies of Chapters 3-5) at the same monomer:crosslinker ratio (1 mol% crosslinker) were prepared for comparison with

copolymer nanoparticles (DEAEMA and PEGMA400 at a weight ratio of 90:10). As shown in Figure 6.5, the mean hydrodynamic diameter of degradable nanoparticles decreased dramatically after incubation in GSHM (from ~ 500 nm to ~ 100 nm), while the size of stable nanoparticles remained constant (~ 350 nm). To further favor particle breakdown/polymer solubility, we tested nanoparticles synthesized with an 80:20 mass ratio of DEAEMA:PEGMA1000. As shown in the CryoEM examination of these particles shown in Figure 6.6A, we confirmed that inclusion of this increased quantity of hydrophilic PEGMA1000 units in the particles did not interfere with particle formation/particle monodispersity. DLS measurements following incubation of these particles in PBS for 48 hours (solid circles Figure 6.6B) showed the particles were slightly swollen, and the size distribution had a sharp peak at ~ 230 nm. In contrast, incubation of the particles in GSHM (empty circles Figure 6.6B) led to the development of two populations according to the size distribution. One was at ~ 100 nm, at which particles had a relatively broad distribution, with a half width of the peak being ~ 40 nm. A second smaller peak in the size distribution was found at ~ 20 nm, a size consistent with individual solubilized polymer chains in a unimolecular micelle configuration. This distribution curve confirmed our design that particles could degrade in GSHM with the disulfide reduction, and confirmed the possibility of forming solubilized (presumably micellar) breakdown products when PEGMA was used to increase hydrophilicity and solubility.

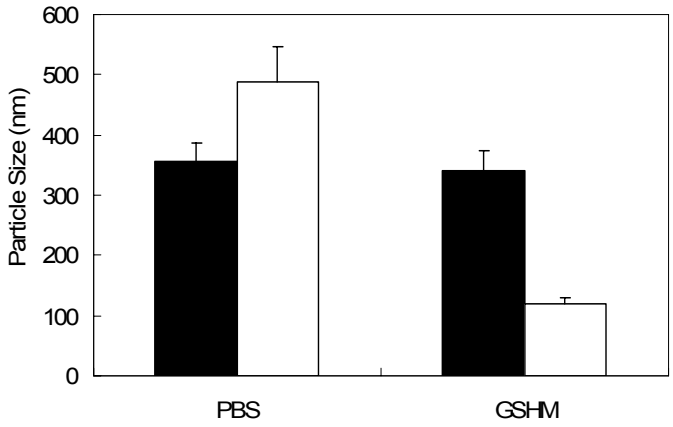

Figure 6.5 Degradability of nanoparticles by DLS. Nanoparticles synthesized with DEAEMA and PEGMA 400 at a weight ratio of 90:10. PEGDMA200 (black) and BAC (white) were used as crosslinker (1 mol%). Nanoparticle size was measured by DLS after suspending in PBS, or GSH in serum free medium (GSHM, pH 7.4) for 24 hours at 37 °C with mild shaking. Shown are mean ± S.D. of triplicate samples.

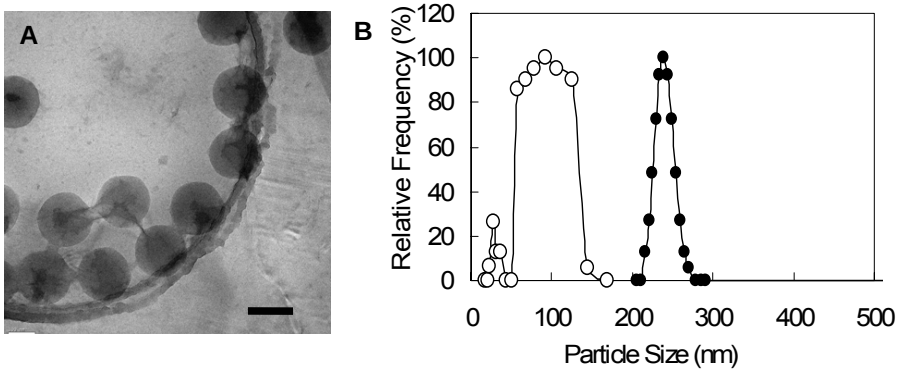

Figure 6.6 Size studies of biodegradable nanoparticles by CryoEM and DLS. Particles were synthesized with DEAEMA and PEGMA1000 at a weight ratio of 80:20, and the BAC was kept 1 mol%. (A) CryoEM of BAC-crosslinked nanoparticles. Scale bar 200 nm; (B) Size distributions of BAC-crosslinked nanoparticles by DLS. Particles were suspended in PBS (filled circles) or GSHM (open circles) for 48 hours at 37 °C.

In conclusion, we proved that using BAC as crosslinker could provide degradability to the nanoparticles, and including PEGMA with high molecular weight could increase the solubility of the break-down components. At the specific conditions we tested above (DPEG1000_20%, with BAC 1 mol%), the size distribution of nanoparticles degrading in GSHM for two days indicated the micelle's formation as we expected.

6.4 Biological Characterization of Biodegradable Nanoparticles

We were able to synthesize biodegradable nanoparticles using BAC crosslinker and PEGMA1000 as comonomer. As discussed above, the nanoparticles (DPEG1000_20%) showed promising degradation in two days in GSHM at 37 °C. Further investigation of the pH-sensitivity and degradation *in vitro* in live cells were performed.

6.4.1 Endolysosomal Disruption by pH-Sensitivity

We first sought to confirm that the significant changes in nanoparticle structure described above (change in crosslinker and inclusion of PEGMA for solubility) did not affect the endosome disruption activity of the particles. Here, we used calcein delivery to examine the capability of endolysosomal disruption by the biodegradable

nanoparticles (DPEG1000_20%, BAC 1 mol%).

Calcein delivery with biodegradable BAC nanoparticles was carried out as described in Section 6.1.4. DC2.4 cells ($1.2x10^5$ cells/well) were plated in Lab-Tek™ chambers for 18 hours, and then calcein (150 μg/mL, 0.24 mM) was added to the cells with or without BAC nanoparticles (25 μg/mL) in complete medium for 1 hour at 37 °C. After three washes with medium to remove extracellular calcein and particles, the cells were imaged live by CLSM at 37 °C. As shown in Figures 6.7 A/C, cells treated with calcein alone showed a punctuate distribution of fluorescence, indicative of endolysosomal compartmentalization of the dye. Cells co-incubated with calcein and BAC nanoparticles exhibited calcein fluorescence throughout the cytosol and nucleus (Figure 6.7 B/D). This result was similar as that observed in Figures 4.1 B/E/H, which showed efficient calcein delivery by stable crosslinked nanoparticles. It confirmed that although changes had been made in the chemical composition, BAC nanoparticles still possessed substantial pH-sensitivity, providing efficient endolysosomal disruption and calcein delivery to the cell cytosol.

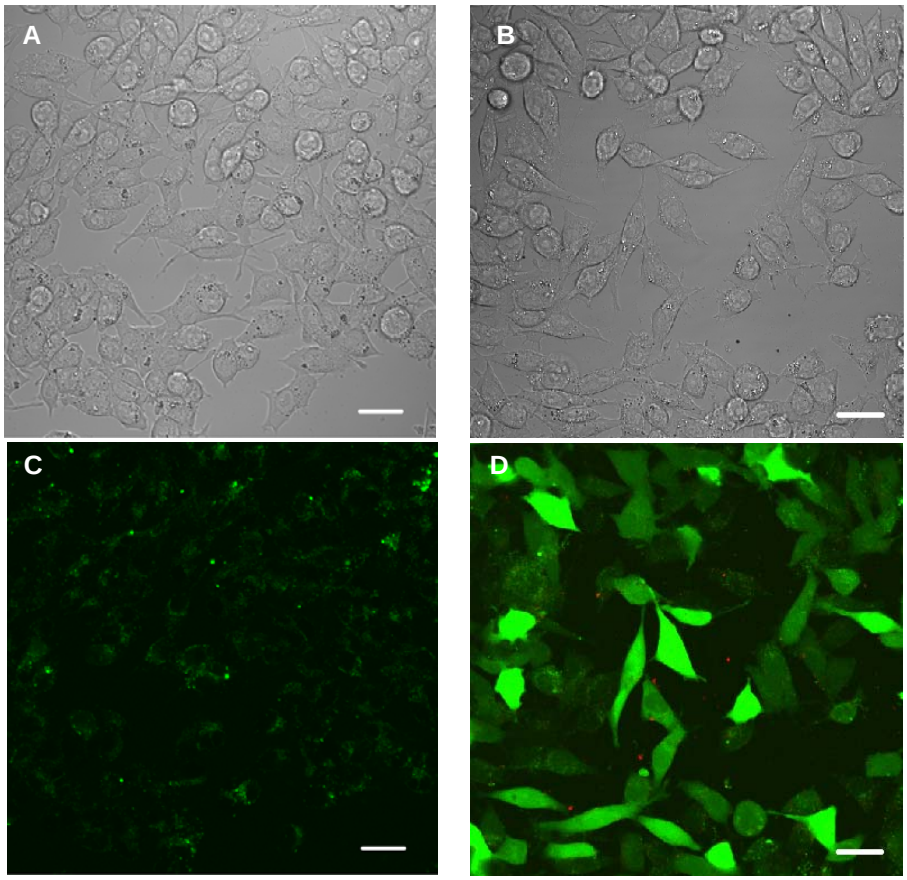

Figure 6.7 Calcein delivery to DC2.4 cells with biodegradable BAC nanoparticles. Calcein alone (A, C) or calcein with 25 μg/mL of BAC nanoparticles (B, D) were incubated with DC2.4 for 1 hour, and then imaged live at 37 °C by CLSM at 40X. Shown are brightfield (A, B) and fluorescence overlays (red, nanoparticles; green, calcein fluorescence) (C, D). Scale bars 20 μm.

6.4.2 Cytotoxicity in Primary Dendritic Cells

Another concern of using the BAC nanoparticles for the biological system was their cytotoxicity. As we discussed in Section 6.2, the design for biodegradability was to facilitate safe elimination of the nanoparticles (for eventual *in vivo* application)

and decrease any toxicity or side effects that accumulation of stable nanoparticles might cause in cells/tissues. To assess the cytotoxicity of the BAC-crosslinked degradable particles, the viability of bone marrow-derived dendritic cells (BMDCs) treated with BAC nanoparticles was assessed.

Using the cell-growth assay described in section 6.1.4, day 6 BMDCs were incubated with 25 μg/mL of BAC-crosslinked or PEGDMA-crosslinked nanoparticles for 1 hour at 37 °C. After washing three times with complete medium to remove extracellular nanoparticles, cells were collected, counted, and replated in 96-well plates at a density of $5x10^4$ cells/well. The replated cells were then cultured for three days, and the number of cells grown out in these cultures was determined. Stable nanoparticles crosslinked with PEGDMA had very low cytotoxicity, nanoparticle-treated cells expanded to a level of 85% of untreated control cells following three days' growth (Figure 6.8). Likewise, biodegradable nanoparticles crosslinked with BAC also had low toxicity: at nanoparticle concentrations of 25 μg/mL that provided efficient intracellular delivery of calcein as shown in Figure 6.7, cells expanded to a level of 95% of controls (Figure 6.8).

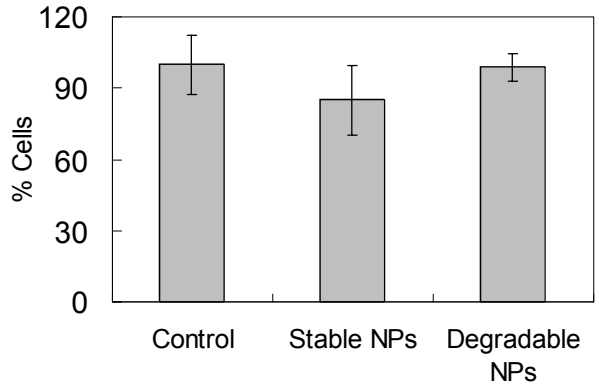

Figure 6.8 Cell viability post biodegradable nanoparticles treatment. Day 6 BMDCs

were incubated with 25 μg/mL stable nanoparticles (PEGDMA as crosslinker), biodegradable nanoparticles (BAC as crosslinker), or no particles (control) for 1 hour, washed three times, then replated at $5x10^4$ cells/well and allowed to grow for three days. The number of cells grown out for each condition was then quantified. Shown are mean ± S.D. of triplicate samples.

We further investigated another two conditions in the similar study: the nanoparticles synthesized with DEAEMA and BAC without any PEGMA (DB1), and nanoparticles of DPEG1000_20% without AEMA shell. Here, for the DB1 core-shell nanoparticles, we observed very strong toxicity (~ 50% cells were dead; Figure 6.9). Although the shell could decrease cytotoxicity by shielding the DEAEMA core inside, the degradable nanoparticles with BAC crosslinker were broken down to PDEAEMA polymer chain in the cell cytosol by GSH. The shell was also expected to dissolve in this process, and could not provide a shield to the PDEAEMA anymore. Including PEGMA as the comonomer to provide hydrophilicity and solubility to the PDEAEMA after degradation was necessary. This contrasts with the lack of toxicity from BAC-crosslinked poly(DEAEMA-co-PEGMA) core-shell particles (DPEG1000_20%), where DEAEMA units from the core are still shielded from interactions with intracellular components following breakdown/dissolution of the shell by the presence of the PEGMA units on each core copolymer chain (shown in Figure 6.2). As shown in Figure 6.9, the low toxicity of the poly(DEAEMA-co-PEGMA) particle core in fact

makes the shell layer unnecessary to avoid toxicity. Thus, tuning of the particle core composition to facilitate biodegradation also allows the option of simplifying the overall design of the particles (from core-shell to core-only), as long as a suitable drug binding/loading method could be designed.

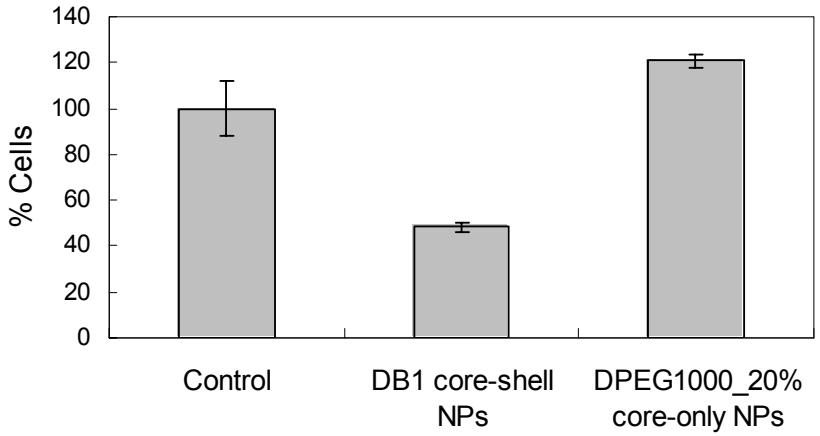

Figure 6.9 Effect of shell or PEGMA of biodegradable nanoparticles on cell viability. Day 6 BMDCs were incubated with 25 μg/mL DB1 core-shell nanoparticles, DPEG1000_20% core-only nanoparticles, or no particles for 1 hour, washed three times, then replated at $5x10^4$ cells/well and allowed to grow for three days. The number of cells grown out for each condition was then quantified. Shown are mean ± S.D. of triplicate samples.

6.4.3 Degradation *In Vitro*

Finally, we examined the degradability of BAC-crosslinked nanoparticles in dendritic cells. Instead of labeling the shell with Cy3 mono-NHS ester, nanoparticles were labeled by poly fluorTM 570 methacryloxyethyl thiocarbamoyl

rhodamine B in the core, to enable tracking of dissolution of the particle cores in live cells. By labeling the core, we expected that particle fluorescence would only take on a diffuse cytosolic distribution (or be eliminated from the cells altogether) when the core was totally dissolved in the cytosol, since as shown in Chapter 4, the intact particles remain within DCs for several days without exocytosis.

Day 6 BMDCs ($1.2x10^5$ cells/well) were plated in Lab-Tek™ chambers and cultured overnight (~ 18 hours). Cells were incubated with or without 25 μg/mL BAC nanoparticles (DPEG1000_20% core-shell) in complete medium for 1 hour at 37 °C. After three washes with medium to remove extracellular calcein/particles, the cells were imaged live by CLSM at 37 °C. The BAC particles were observed in the cells after 1 hour of incubation (Figure 6.10 B/F), which indicated the endocytosis and/or endolysosomal escape of the nanoparticles compared to the control (Figure 6.10 A/E). However, after 24 hours and 48 hours of incubation, punctuate fluorescence of the nanoparticles still remained in the cytosol (Figure 6.10 C/G and D/H), in a manner that was qualitatively indistinguishable from the observations after only 1 hour incubation.

This result indicated that the nanoparticles do not appear to be degraded efficiently in BMDCs. We observed the nanoparticles' degradation in GSHM in two days with forming micelles; however, there were still remaining particles around 100 nm as the size distribution curve showed. Thus the BAC particles we used in the cell study could still be around 100 nm in size after two days of degradation. Second, the study discussed in Section 6.2 was carried out in 10 mM GSH medium,

while the concentration of GSH in cell cytosol varied in different cell types from 1-10 mM. The nanoparticles might encounter GSH concentration lower than 10 mM in BMDCs, thus the degradation would be less efficient. Furthermore, there are a lot of proteins present in cell cytosol, which could agglomerate with our nanoparticles and prevent the GSH diffusion into the nanoparticles. Alternatively the aggregation of break-down polymer chains with protein could prevent their ultimate solubility. We observed large size (>500 nm, data not shown) of breakdown components when incubating the BAC-crosslinked nanoparticles in GSH in complete medium containing serum protein (10% FCS, 10 mM GSH). Optimization of the chemical composition of these particles to obtain faster/more complete degradation is still ongoing, and represents an important goal for future work.

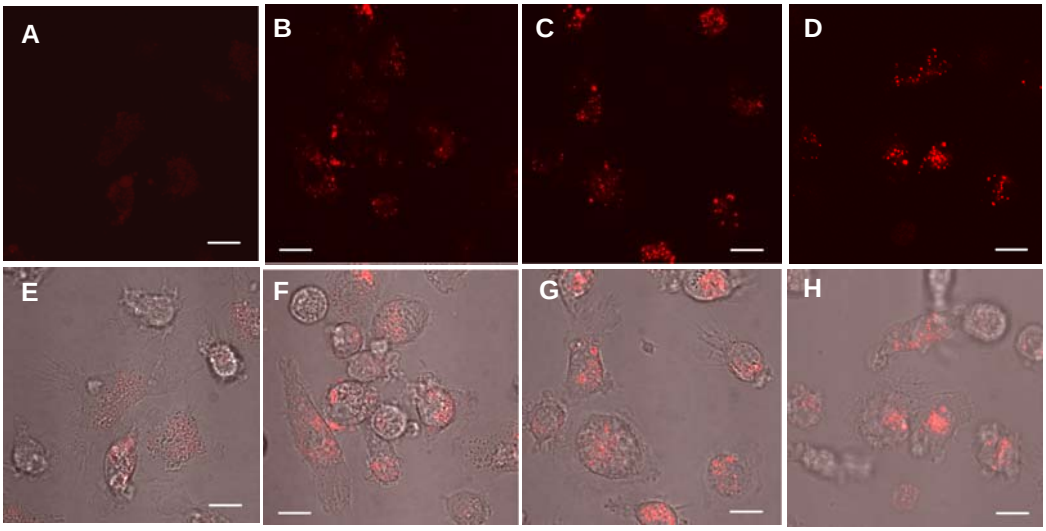

Figure 6.10 BAC nanoparticles in BMDCs. BMDCs were incubated without (A, E) or with BAC nanoparticles for 1 hour, and then imaged live at 37 °C by CLSM at 100X (B, F). The cells were then cultured an additional 24 hours (C, G), and 48 hours (D, H) and imaged again to determine whether nanoparticles degraded.

Shown are fluorescent images (A-D) and overlays (E-H) of nanoparticle fluorescence (red) and cells (brightfield). Scale bars 10 μm.

In conclusion, we designed and synthesized biodegradable nanoparticles using BAC, a crosslinker with a disulfide bond, which could be digested by GSH in cell cytosol. PEGMA was included as comonomer to provide the system with more hydrophilicity and solubility after degradation. The preliminary study showed promising degradation results in GSHM, and DLS data indicated that the DEAEMA-co-PEGMA polymer chains formed micelle-sized components, which was proved non-toxic in BMDCs by a 3-day cell growth assay. These BAC nanoparticles possessed pH-sensitivity and were able to delivery calcein efficiently to cell cytosol. However, via CLSM we did not observe BAC-crosslinked nanoparticle breakdown in BMDCs after two days. Further studies on the compositions which could provide more efficient and faster degradation are ongoing. The development of fully biodegradable nanoparticles could potentially lead to *in vivo* testing in animal models for immunotherapy.

7 Conclusions and Future Directions

7.1 Novel Designs for Intracellular Drug Delivery

In this thesis, we systemically studied the swelling behavior of a hydrogel system formed by diethyl amino ethyl methacrylate (DEAEMA), and explored the possibility of taking advantage of its pH-sensitivity as a drug delivery system in a reducing pH environment. By emulsion polymerization, we successfully synthesized monodisperse pH-sensitive PDEAEMA-core/PAEMA-shell nanoparticles whose size was around 200 nm. We further demonstrated that these core-shell nanoparticles were capable of efficient cytosolic delivery of membrane-impermeable molecules (such as calcein, OVA protein, Influenza A, or siRNA) to dendritic cells via the 'proton sponge effect'. These nanoparticles showed significant improvement in cross presentation of Class I MHC molecules and T cell activation by delivering the antigen protein OVA to BMDCs, and promising knockdown of mRNA by delivering siRNA to epithelial cells for gene silencing. These preliminary applications indicated that those nanoparticles may be of utility for delivery of membrane impermeable drug compounds or oligonucleotides to the cytosol of dendritic cells for immunotherapy, and other cell types for gene therapy.

The pH-sensitivity of polymers for endosome escape has been widely used to design intracellular drug delivery system. However, different from typical polymeric drug delivery systems which are formed by physical complexation of the polymer and drug molecules, our strategy is to use monodisperse crosslinked hydrogel

nanoparticles whose size, stability, and properties are predefined and under control. This modification demonstrated the highly improved efficiency for intracellular drug delivery in different cell types, as the hydrogel nanoparticles potentially improved the cellular uptake efficiency and the stability of the drug delivery system besides endolysosomal escape function.

We further introduced core-shell structure to the nanoparticles. By sequestering the slightly hydrophobic, pH-buffering component of the polymer particles within the core by a more hydrophilic shell composition, these nanoparticles effectively disrupted endolysosomes and delivered molecules to the cytosol of cells without overt cytotoxicity, which was often observed by polymeric drug delivery systems that could disrupt endolysosomes. This design proved a method to reduce cytotoxicity by 'hiding' toxic components from contacting cells. This simple concept could potentially be applied widely to any drug delivery system suffering cytotoxicity. In addition, the segregation of drug/cell binding function of the shell from the pH-sensitivity and endolysosomal escape function of the core provided flexibility to tune the surface charge and charge density to desirable drug molecules, and to chemically modify the shell structure with targeting functions.

The extension to biodegradable nanoparticles that quickly dissolve to nontoxic soluble components upon reaching the cytosol is under investigation. The biodegradability could promote efficient unpacking of drugs carried to the cytosolic compartments, and lead to further *in vivo* test. Different from hydrolysis or enzymatic degradation, we designed the degradability by using reducible crosslinker

which could be digested in the cytosolic environment. Similar as PEGylation of a polymer, we applied PEGMA as a comonomer to the hydrogel, and demonstrated that the break-down polymer chains turned into nontoxic soluble components. This idea may be of use in designing nontoxic polymeric materials for biological applications.

7.2 Future Directions

7.2.1 Shell Structures for Drug Loading and Targeting

In this thesis, we mostly focused on evaluating the delivery efficiency of the nanoparticles. Our effort was to demonstrate the pH-sensitivity and endolysosomal escaping function of the core. We have proved that the shell structure, which is a very important part of the design, decreased the cytotoxicity significantly. Further studies of the shell structure need to be carried out. We could investigate the shell formation and the surface charge density on the shells by exploring the emulsion polymerization process. These characters of shell structure would help us understand drug binding and cell binding efficiency of the nanoparticles. In addition, the segregation of core and shell according to their functions provides us opportunities to alternate the shell structure without affecting the endolysosomal disrupting function. Exploring the use of different polymers as the shell structure to provide different binding properties would be very interesting. For instance, most studies have focused on using polycationic polymers to bind DNA or negatively charged proteins, but few systems have been reported for delivering a positively charged drug

molecules. A shell with carboxyl group could be used for this function. This investigation could potentially increase the application of our nanoparticles to a larger variety of drug types.

Another aspect that would be interesting to explore would be alternative methods for drug loading. Currently, the drug molecules bind to the shell of nanoparticles electrostatically. The binding efficiency could decrease by competitive binding of proteins in biological systems. A method to protect the drug molecules from this effect would be very practical, as it could reduce the drug dosage and avoid repeating drug treatment if the drug could be carried and delivered efficiently. A strategy to load the drug in the shell, between the shell and core, or in the core could be very useful and important to improve this system's efficiency.

Furthermore, the capability of targeting specific cell types could be added to the shell structure of the nanoparticles. An advantage to use polymeric materials for drug delivery system is their tunable chemistry. Conjugating targeting ligands or peptide sequences is achievable with our shell structure. Again, the core-shell structure makes this modification very flexible, without affecting the endolysosomal escaping function.

7.2.2 Study on Biodegradability

Our preliminary study showed promising results on the biodegradability of the nanoparticles *in vitro*. However, we have not proven the thoroughly degradation of

nanoparticles in cell cytosol by CLSM. It has been reported that although GSH is present in all mammalian cells, the concentration of GSH varies in different cell types.[120, 125] This fact could potentially limit the application of biodegradable nanoparticles since the degradation efficiency would be affected by the concentration of GSH in cells. So far, 10 mM of GSH was used for our study to detect the degradation, and it would be worth to evaluate the cellular GSH level in the cell types we are interested in. Other the other hand, the chemical compositions which could achieve more fast/efficient degradation in lower GSH concentrations (5 mM in general) could be a major task. Further applications using biodegradable nanoparticles as an intracellular drug delivery system should be investigated.

7.2.3 A Practical Intracellular Drug Delivery System

Overall, we have designed and demonstrated the capability of the core-shell nanoparticles for a variety of intracellular delivery applications. The final goal would be to test the biodegradable nanoparticles *in vivo*. To perform the animal study, the first step is to investigate the toxicity of the nanoparticles and understand its biodistribution with different administrations. The fluorescent or radioactive tracing and the histology samples of different organs could be used to identify the pathway and toxicity of nanoparticles and to prove their clearance or degradation.

Combining the targeting and improved drug binding property, we believe this system may be of great utility as a practical delivery system in market in the near

future. In addition, the concepts of pH-sensitivity for endolysosomal escaping, core-shell structure for non-toxicity and drug/cell binding, reducible crosslinker for biodegradablilty, and PEGylation to shield the toxic elements are significant contributions for designing intracellular drug delivery systems.

Appendix 3D Periodic Porous pH-Sensitive Hydrogels for Drug Delivery

As we discussed in Chapter 2, pH-sensitive hydrogels could be used as a controlled drug release system responding to a change in the environmental pH. A mechanism to load the drug molecules into the hydrogels and to release drug in a controlled manner is necessary. Current strategies include encapsulation of drug molecules in the hydrogel[130-133] or conjugation of drug molecules to the polymer chain constructing the hydrogels.[72, 133] In these methods, the drug loading is very limited, and drug molecules are released slowly via diffusion through the mesh of the hydrogels or upon the hydrogel erosion/degradation. In this Appendix, we present an alternative method of forming porous hydrogels that would help load macromolecule drugs such as DNA, siRNA, or protein into the porous structure of the hydrogels. Those connective pores could potentially form the basis for the better storage and protection of drug molecules. Drugs can be released in a controlled manner when the pore size changes corresponding to the environmental pH changes.

A.1 Porous pH-Sensitive Hydrogels

A.1.1 Porous Structure in a Hydrogel Matrix

There are several methods to create porous structures in hydrogels. Microsyneresis is a phenomenon where a phase separation occurs during the

polymerization and a heterogeneous polymer network is formed consisting of domains of highly crosslinked microgels which are connected by loosely crosslinked chains. It happens if the amount of water present in the monomer solution is greater than the water content corresponding to the equilibrium degree of swelling.[134, 135] The pores generated in this way are relatively large, and can used as microreservoirs. Porogen is a method to create pores by gas foaming[136] or leaching solid crystal such as NaCl.[137] To obtain high pore interconnectivity, a porosity of 95 v% needs to be introduced to the matrix.[138-140] It therefore makes this method only suitable for stiff materials. Crystalline arrays of monodispersed spherical colloids have been demonstrated or proposed for use in a wide variety of areas, such as templates to generate porous materials with highly ordered structures. In this method (Figure A.1), the colloidal crystals are assembled to serve as templates, the voids of which are infiltrated by materials that solidify/polymerize there. The original colloidal particles are subsequently removed, leaving behind a new material with pores that preserve the most valuable property of the colloidal crystals: the well-defined long ranged periodic structure. The colloidal crystal template method has the advantage of being able to control the dimensions of the pores easily, by varying the size of the beads in the templates. The close-packing porous structure results in a number of useful properties such as maximal packing density, high surface to volume ratio, tightly controlled thickness, and sufficiently large domain size. This method originally has been used to gain the structure for optical diffraction and photonic band gaps for stiff materials such as inorganic oxides, carbons, and polyurethane.[141] Our

lab has been able to synthesize the bioactive hydrogel of poly ethylene glycol (PEG) or gelatin with interconnecting macropores for tissue engineering.[138, 140] This provides a good foundation for applying this method to our porous pH-sensitive hydrogel as a drug delivery system.

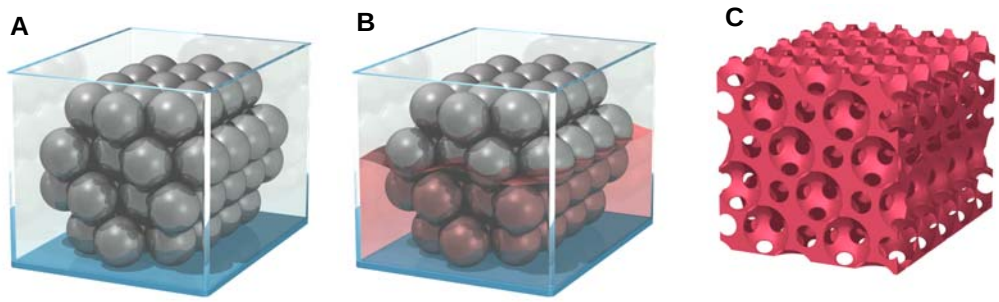

Figure A.1 Schematic illustration of constructing colloidal crystal templating for porous hydrogels. A) Patterning; B) Templated polymerization of hydrogel; C) Template removal.

A.1.2 Porous pH-Sensitive Hydrogels as Drug Delivery System

Discussed in Chapter 2, pH-sensitive hydrogels have been widely used for drug delivery. They have the potential to provide drug molecules with hydrophilic surroundings. The gels' swelling/deswelling abilities according to environmental pH could be applied as a trigger to encapsulate or release the drug molecules. In this Appendix, colloidal crystal templating is applied to create periodic porous structures in the pH-sensitive hydrogels. Drug molecules are expected to move among these periodic pores via the connective windows to their nearest neighbors (Figure A.2). Importantly, the porous gels are expected to swell/deswell rapidly because of

extensive contact area to water.[133, 134] We hypothesized that the pH-sensitivity of the hydrogel could potentially work as a 'valve' for drug release (in Figure A.2). When environmental pH is above the pK_b of the gel, (for the poly(DEAEMA-co-PEGMA chosen, the pK_b is slightly lower than physiological pH 7.4), the gel is in a collapsed state, and the connective windows and pores are in their minimal sizes. Thus drug molecules will be highly restricted in the porous structure. When the environmental pH is below pK_b of the gel, the gel is in the swelled state and the connective windows and pores will be enlarged, resulting in the drug's rapid movement toward the surface of the gel, allowing it to escape. In this manner, the hydrogel protects drugs in a hydrophilic environment from degradation, and releases them with its pH-sensitivity.

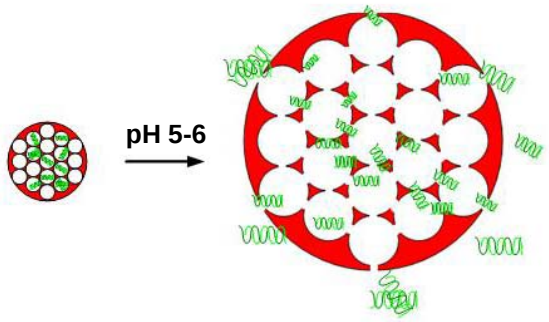

Figure A.2 Schematic of pH-sensitive 'valve' for drug encapsulation and release in a porous pH-sensitive hydrogel.

Drug release from bulk gels can be fundamentally very interesting besides its potential applications. Through detailed characterization of the pH-sensitivity and the porous structure of hydrogels, we seek to gain a fundamental knowledge of the importance of these parameters as a general drug delivery system. In contrast to

typical cationic polymer DNA/drug delivery systems (such as PEI), we hypothesize that porous gels would facilitate DNA/drug release rapidly responding to pH changes instead of entrapping DNA/drug tightly via electrostatic force on the positively charged polymer chains. Although the monomer chains of gels will be positively charged in the swelled state at reduced pH, the counterions (in this case, Cl^-) in water rather than the negatively charged drug molecules will be attracted to them. Thus the porous structure eliminates the direct contact between DNA/drug molecules and the ionized groups comparing to other cationic polymeric drug delivery systems.

A.2 Materials and Experiments

A.2.1 Materials

All reagents were used as received without further purification. 2-diethylamino ethyl methacrylate (DEAEMA), tetraethylene glycol dimethacrylate (TEGDMA), ammonium peroxodisulfate (APS), and micro particles based on poly methyl methacrylate (PMMA) (4 μm) were purchased from Sigma-Aldrich Chemical Co. Poly (ethylene glycol) monomethacrylate (PEGMA, MW_{PEO} = 200 g/mol), and poly fluor™ 570 methacryloxyethyl thiocarbamoyl rhodamine B were purchased from Polysciences Inc. Polydimethylsiloxane (PDMS) were made from Sylgard® 184 Silicone Elastomer Kit, Dow Corning Corporation.

A.2.2 Colloidal Crystal Templating for 3D Porous pH-Sensitive Hydrogels

Monodisperse PMMA microparticles (4 μm) solution (2.6 wt%) was centrifuged down at 15,000 x*g* for 10 min. The particles were re-suspended in 70 wt% EtOH to make the final concentration of 20 wt%. After 15 min sonicating to avoid the aggregation, 200 μL of condensed particle suspension was added to the PDMS ring holder (H = 5 mm, R = 2.5 mm, cut by revolving punch, Small Parts Inc.) adhered to the glass slide with plasma treatment. The particles were then dried and close-packed on top of a reciprocating shaker (Lab Rotator 2314Q, Barnstead International) operated at 250 rpm for about 4 hours at room temperature.

A hydrogel precursor solution was prepared as described in Section 2.1.2. In a typical polymerization process, 103 μL DEAEMA (0.5 mM), 155 μL PEGMA 200 (0.5 mM), and 1.5 μL TEGDMA (0.5% mol crosslinker/mol comonomers) were mixed in 269 μL 25 v% EtOH, giving a final solution containing 50 wt% comonomers. For fluorescent labeling of gels, 10 μL poly fluor^{TM} 570 methacryloxyethyl thiocarbamoyl rhodamine B stock solution (50 mg/mL in 25% EtOH) was included in the precursor solution. The initiator APS (20 μL of 200 mg/mL APS in water, freshly made) was added, and 50 μL of the fluorescent labeled precursor solution was gently pipetted onto the colloidal crystal template formed by PMMA microspheres, and perfused by centrifugation (5 min, 2000 x*g*).

After polymerizing at 45 °C (covered by glass slide to avoid solvent evaporation) for 20 min, the polymerized construct was taken out from the PDMS ring holder and

transferred to excessive acetone for three days in order to etch the microsphere and form the porous structure. The templated gels were further cleaned by soaking in EtOH for one day to dilute all the acetone and remove the dissolved PMMA. After swelling in water for another three days, the porous gels were stored in clean water for further characterization.

A.2.3 Morphology of the Porous Hydrogels

The porous gel discs were dehydrated serially in 25, 50, 75, 95 wt% EtOH for 30 min each, and 100 wt% EtOH overnight. The gel discs were air-dried for 24 hours in the presence of desiccant. After sputter coating (Desk II cold sputter/etch unit, Denton Vacuum LLC) of gold particles with 10 nm thickness, the porous gels were imaged using a JEOL 6060SEM (JEOL, Ltd., Japan) at 5kV.

Fluorescent porous gels were observed using a confocal laser scanning microscope (CLSM, Zeiss LSM 510) with 40X or 100X Apochromat oil objectives with the presence of PBS.

A.2.4 pH-sensitivity of the Porous Hydrogels

Poly(DEAEMA-co-PEGMA) hydrogel discs were transferred to a 6-well plate, and immersed in phosphate buffers of varying pH (100 mM ionic strength, 3 mL) with mild agitation in a Jitterbug shaker (Boekel Scientific, Model 130000). The

wet mass of each sample was measured for each condition to determine the mass swelling ratio (Q), defined as the mass of the gel in the swelled state divided by the mass of gel in the deswelled state at pH 9. To assess equilibrium swelling, the gels were allowed to equilibrate for up to 24 hours. The mass of the gels was assessed at different time points (swelling over 2, 4, 8, and 24 hours) to confirm that swelling had reached equilibrium. The pore size under different pH conditions was examined by CLSM. During the imaging process, porous gel discs were confined in a PDMS ring holder adhered to a glass slide after reaching equilibrium. Buffers with different conditions were added in the PDMS holder to keep the gels in desired environment/pH.

To assess swelling kinetics, the hydrogel discs were first equilibrated in a pH 7.48 buffer. For the swelling phase, gels were transferred to a pH 5.66 buffer, and the masses of the gels were measured every 10 min for the first hour, every 20 min for the second hour, and every 30 min until it reached equilibrium. For the deswelling phase, gels were then transferred back to a fresh pH 7.48 buffer, and the masses of gels were measured every 10 min for 1 hour, and then measured at 8 hours.

A.3 Results and Discussion

A.3.1 Fabrication of Porous Hydrogels

Colloidal crystal template was referred as the fabrication of three dimensional (3D) porous materials by employing monodisperse colloid spheres as the building

blocks.[142-144] Choosing a type of colloidal sphere as the template and patterning the spheres in a close-packed manner is crucial to generate periodic pore structures with high interconnectivity.

PMMA particles of 4 μm were used here as they are commercially available and relatively inexpensive, and most importantly, possess good monodispersity, which affects the patterning and therefore the porous structure in the hydrogel. In addition, proper solvents were needed for etching the particle templates after polymerization to obtain the final porous structure. It is necessary for the solvent to be able to dissolve the particle materials without destroying the polymer matrix. It was also important that the solvent is miscible with water to facilitate solvent removal and exchange into aqueous solutions for future experiments. Acetone, which was used for etching the PMMA particles template, satisfied these requests. Therefore, choosing PMMA particles was suitable for both templating and etching processes.

The template particle size dictates the pore size, interconnectivity, window size, void percentage for polymer loading, and therefore the mechanical properties of the gels and the affine deformation when the resulting gels respond to varying pH. For these reasons, templates with particle sizes of 4 μm were formed to allow systematic studies of the effect of 3D porous structure on the soft hydrogel properties and the pH-sensitivity of the hydrogel as the potential control of the pore size changes.

Monodisperse colloid spheres were self-assembled into an ordered 3-D pattern. There are a variety of approaches to help with self assembly, such as sonicate packing,[145] patterned sedimentation,[146] controlled evaporation,[147] centrifugation,

pressing, filtration, or slit filling.[144] In this Appendix, we used controlled evaporation to generate compact packing from the self-assembly of high monodisperse PMMA colloidal spheres. To provide a defined macroscopic shape to templates, PDMS molds of disc shape were used to confine the template assembly on top of a glass substrate. Parameters such as the particle concentration/density of colloidal spheres, the property of the suspending solution, and the evaporation rate (the concentration of the EtOH, the shaker speed etc.) were practiced to optimize close packing qualities, which are not discussed in detail here.

It is very important to remove the deposition solvent from the template interstices, and make space for the polymer solution. Failure to dry the template might cause the collapse of patterned particles, and the beads might re-suspend in monomer solution without patterning. In addition, polymer precursor could only cover the voids partially if some of them were occupied by the solvent of colloidal crystal suspension. Our template was dried at room temperature, as we found that high temperatures tended to change the self-assembled close-packing template, or even melt the PMMA particles. It has been found that applying centrifugation facilitates the penetration of the gel precursor solution into the template.

A.3.2 Morphology of Porous Hydrogels

The morphology of the resulting porous hydrogels was characterized by optical, fluorescent and scanning electron microscopy extensively. Shown in Figure A.3 are

some typical images from each approach.

In SEM images of dehydrated gels (Figure A.3 A-D), a two-layer gel membranes were examined. Shown in Figure A.3 A is the free surface of the hydrogel. On the left half of the image, the pattern of well ordered hexagons was observed. The diameter of these hexagons was about 3 μm, indicated the pores formed by etching the particles themselves. The smaller size compared to the original 4 μm was caused by the dehydration of the hydrogel sample in the SEM sample preparation process. On the right half of the image, only unconnected pores of much smaller size (about 1 μm) were observed. Those pores were formed by the cotangent points between the particles and the contacting substrate, or the free surface of the gel where the polymer solution covering the top of the particles. After etching, these smaller inter-pores were formed at the cotangent points where the polymer solution could not infiltrate. As reported, those inter-pores usually take the size of about 1/4 of the original packing colloidal particle size.[140] In Figure A.3 B, by tilting the sample mount to 20°, we observed the cross section of the porous gel, where, the two layers of patterned pores are seen clearly. The free end was mainly sealed, but some of the inter-pores could be seen. More inter-pores were shown in Figure A.3 C. In this image, each pore formed by taking space of original colloidal particles was connected to the next layer with three smaller inter-pores, which indicates the FCC assembly pattern where the second layer of particles would fall on top of the void of three contacting particles on the first layer. In a zoomed image (in Figure A.3 D), the inter-pore size was measured as 0.9 μm ± 0.2 μm, while the pore size was 3.3 μm ±

0.2 μm.

Under optical microscope, usually two to ten layers of well-ordered pores could be clearly resolved. A two-layered porous gel with its pores hexagonally closed-packed over a long range was shown in Figure A.3 E. The white lines indicated the first layer in the focal plane, while the dark lines were the second layer underneath. Since the particles self-assembled in a FCC pattern, the cotangent points between each particle on the lower layer were clearly observed in the center of the upper layer. It was obvious that the pore size was slightly larger than the original particle size (4 μm) due to the slight swelling status of the hydrogels compared to its as-synthesized size. In the up-right and down-left corners of the images, two patchy areas, where only one layer was observed, indicated that the inefficient close packing had occurred. The infiltrated precursor solution occupied these areas, and formed a solid gel region instead of a porous structure.

Using CLSM with serials scanning on the z-direction, we could potentially study the 3D porous structure in depth. In Figure A.3 F, a swollen porous hydrogel at pH 4.79 buffer was examined. Similar to the schematic shown in Figure A.1, the pore was connected with six other pores (as indicated by the arrows) at the same layer through inter-pores formed by blocking the infiltration of precursor solution and further polymerization by the cotangent points of the particles. A porous gel with seven to eight layers was examined by CLSM with the intervals of 0.43 μm in the z-direction. The x-y, y-z, x-z planes at random cross sections are shown in Figure A.3 G. Each plane clearly showed the FCC pattern of the close packing. By using

Volocity (Improvision Inc), the CLSM images were reconstructed to a 3D image of the porous hydrogel. In Figure A.3 H, the inter-pores could be seen through clearly for several layers, demonstrating the high connectivity of these 3D porous hydrogels.

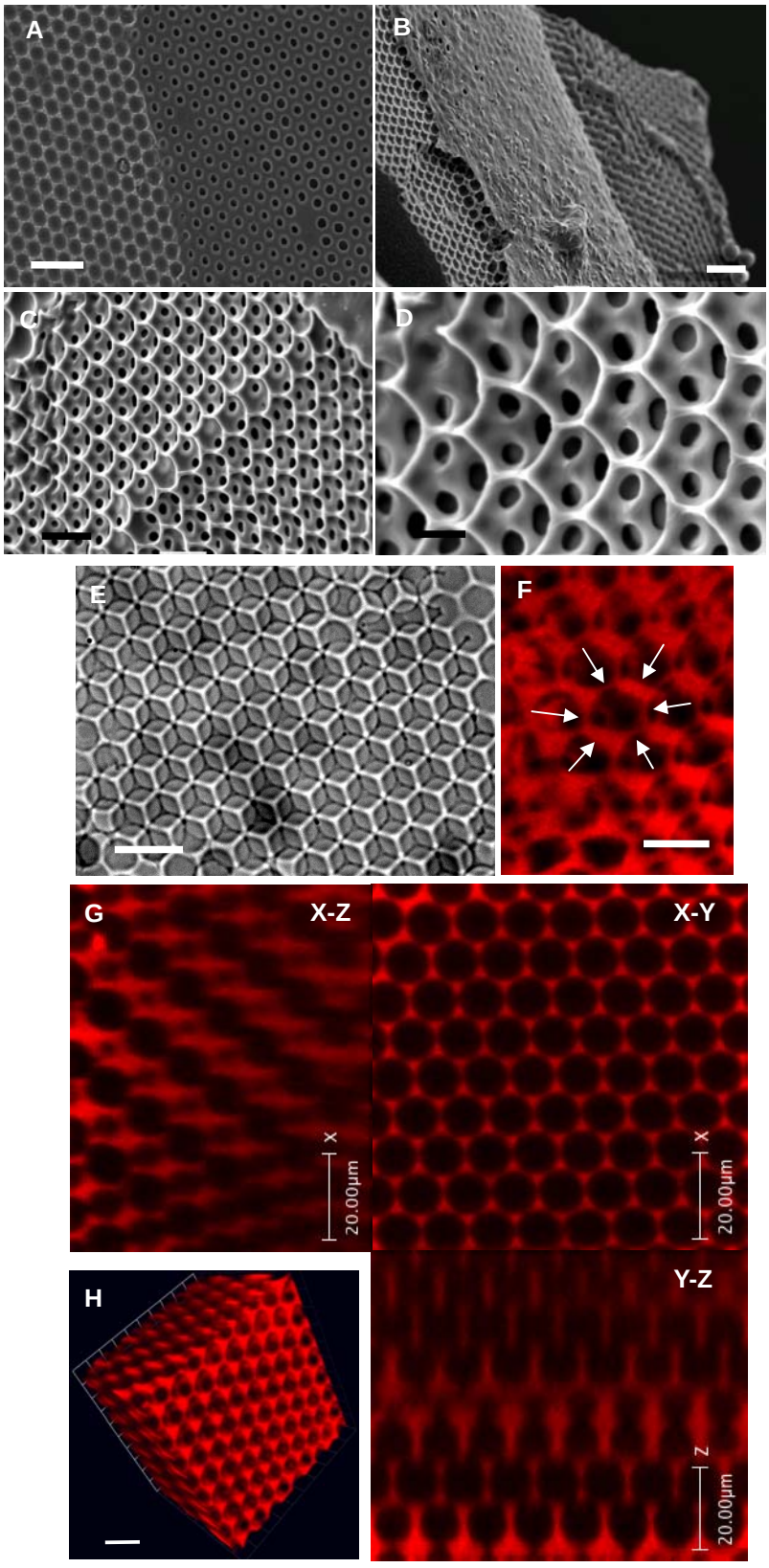

Figure A.3 Morphology of porous hydrogels. (A-D) SEM image of the dehydrated

porous gels. Porosity/inter-pores at the free surface of hydrogel (A, scale bar 10 μm); intersection showing at least two layers of patterned pores etched from PMMA spheres (B, scale bar 10 μm); a section of close-packed porous structure (C, scale bar 5 μm); cross-sectional image of well ordered pores and inter-pores (D, scale bar 2 μm). (E) Brightfield optical image with 100X object lens showing two layers of ordered pores. Scale bar 10 μm. (F-H) CLSM images of fluorescence-labeled swelled hydrogels (in a pH 4.79 phosphate buffer). Images of the 3D structure of the hydrogel lattice after etching (F, scale bar 10 μm); image of 3D structure of a well-patterned porous hydrogel examined in x-y, y-z, and x-z planes (G, scale bars 20 μm); 3D reconstruction of CLSM images of a well-patterned porous hydrogel in the swelled state created using Volocity (H, scale bar 20 μm).

In this Appendix, although we did not examine the mechanical properties of the hydrogels with high porosity, the swollen gels shown in Figure A.3 F-H would be able to support itself very well in any characterization process such as microscopy or weighing. These swollen gels were with very high water content as the pore size were enlarged ~ 2-fold as their original size while the polymer content was less than 25% of the total volume. We did not observe any collapse of the hydrogel lattice in the swelled state. At high pH of 9.5, the hydrogel shrank noticeably, and the pores in the gel lattice appeared to have slight deformation.

Together these approaches guided us in how to obtain repeatable high quality patterning of 3D colloidal crystals template, and also proved that we successfully

fabricated periodic 3D porous hydrogel with self-assembled colloidal template.

A.3.3 Effect of pH Sensitivity on Pore Size Changes

The swelling capability of solid bulk hydrogels with different chemical compositions has been discussed extensively in Section 2.2.2. Here, we evaluated the pH sensitivity of porous gels by comparing to the bulk gel formed with the same chemical composition. As we described in Section A.2.2, the precursor solution only infiltrated into the voids between colloidal beads. Thus, the swelling ability could be strongly affected, as the fraction of polymer in a porous hydrogel (less than 25 v%) was much lower than that of a solid gel (100%) due to its high porosity. To investigate this effect on pH sensitivity, we compared the equilibrium mass swelling ratio (Q) of porous gels and bulk gels at different pH. Bulk gels and porous gels made in the same geometry in the PDMS ring holder were soaked in phosphate buffers at pH ranging from 4.8 to 9.0 to reach their equilibrated swelled state before being weighed. As expected, the porous hydrogel still possessed the swelling property as a bulk hydrogel; however, the swelling capability was highly reduced due to its low content of polymer fraction in its total volume (Figure A.4 A). The solid bulk hydrogel swelled reaching 18-fold mass/volume changes at pH 4.8, while porous gels could only swell by 8-fold. Two kinds of gels had the similar transition point about pH 7.4 to perform their reversible swelling/deswelling. This consistency proved that gel pK_b decides the transition pH.

In addition, the effect of pH sensitivity on pore size and inter-pore size was evaluated by CLSM. The pore size at different pH was plotted together with the mass swelling ratio *Q* (Figure A.4 B), and some of the CLSM images of porous hydrogels are shown in Figure A.4 C. The pore size was enlarged to 7 μm at pH 4.9, while it collapsed to 3.7 μm at pH 9.0. The pore size changes due to the pH change also induced the inter-pore size changes, which was reported as 1/4 of the pore.[140] This effect of the pore and inter-pore size enlargement at reduced pH could work as the 'pH valve' as we hypothesized in Figure A.2, and help release the drug molecules which loaded in the pores before swelling. Interestingly, the change of pore size was approximately linear according to the pH change, instead of showing sharp transition at pK_b. The exact reason is still under investigation.

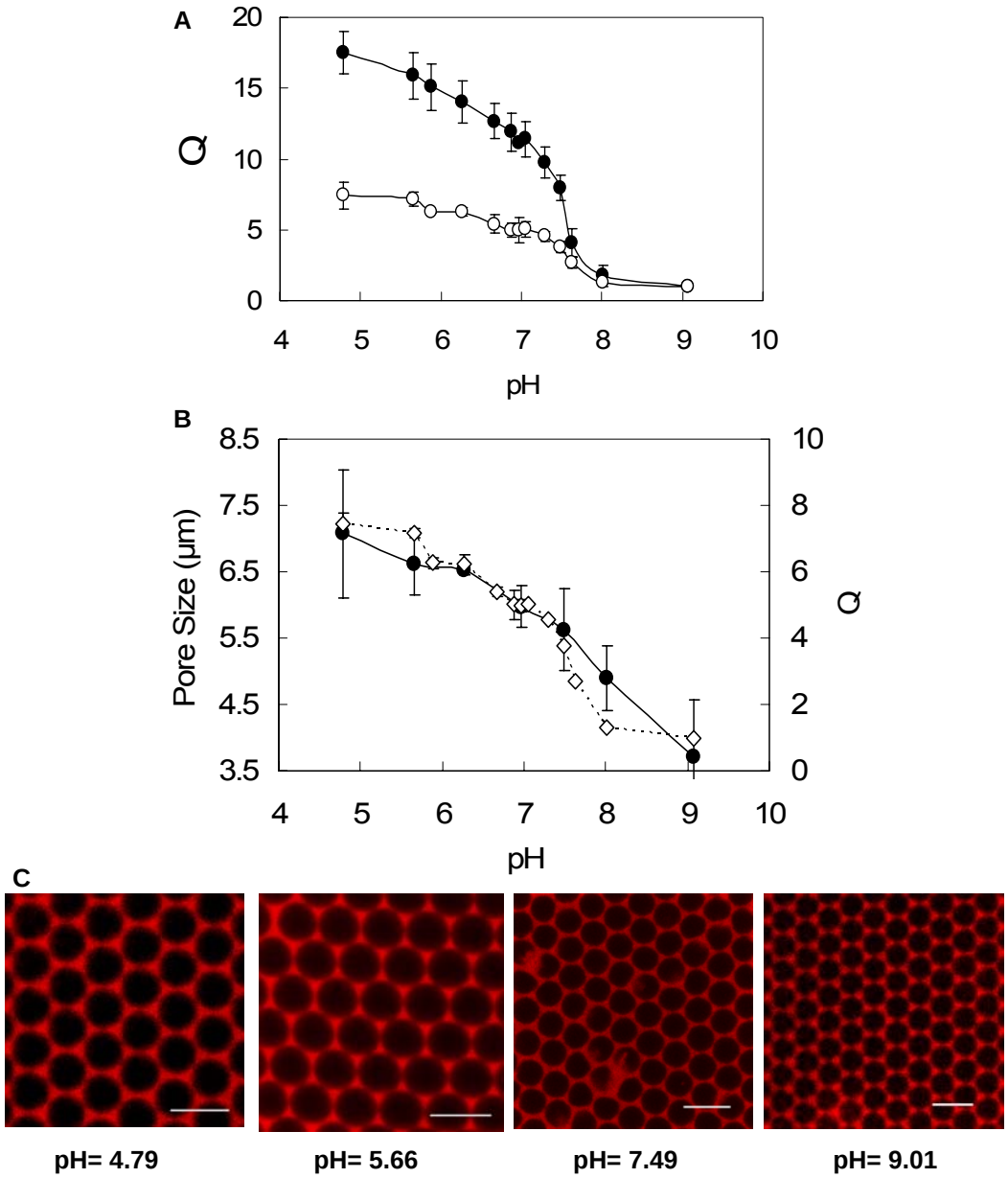

Figure A.4 pH sensitivity and pore size of porous hydrogel at 37 °C. (A) Mass swelling ratio (Q) of both bulk (solid dots) and porous (empty dots) hydrogels (PEG200_50% with 0.5 mol% crosslinker) at different pH. Shown are average ± S.D. of triplicate samples. (B) Pore size (filled dots with solid line, y axis on the left) of porous hydrogels according to mass swelling ratio (open dots with dashed line, y axis on the right). Error bars of pore size measurement showed standard deviation of

20 pores examined at each condition. (C) CLSM images of porous structure of same gel sample at different pHs. Shown are all x-y planes. Scale bars 10 μm.

A.3.4 Dynamic Swelling of pH-Sensitive Porous Hydrogels

As discussed in Section 2.2.3, it is necessary to define and calculate the characteristic response time of gels, as this will be a significant parameter controlling drug loading and release profiles from gels used for drug delivery. Different from bulk hydrogels, porous gels possessed periodic pores which provide extensive contact to water/solvent and ions. Since the swelling kinetics are typically dominated by diffusion times for the ions in the solution,[80] the pore size and porosity could significantly affect the response rate, due to the efficient transport of water and ions, and the ionic interactions in the porous structure.

The dynamic swelling of solid bulk hydrogels has been shown in Figure 2.7. Here, we compared it with the porous hydrogels formed with the same chemical composition. Similar to the bulk gel studies, changes in the mass swelling ratio as a function of time were measured following transfer of porous gels equilibrated at extracellular pH/ionic strength conditions to acidic pH conditions and *vice versa*.

Porous hydrogels were able to respond to the environmental pH change immediately. Within twenty minutes, the porous gels could reach their equilibrium swelling when located in pH 5.66 buffer (Figure A.5 A). As expected, porous gels had much more contact with water, and reached equilibrium swelling much faster (in

20 min) than solid gels (in 60 min). Swelling of the porous gels was also reversible, as hydrogels were able to shrink to the original size when put back in pH 7.48 buffer. As in Figure A.5 B, deswelling reached 95% of equilibrium within 60 min. Interestingly, the deswelling process happened in a similar pattern for both type of gels. This similarity indicated that the driving force for removing the protons from the hydrogel was not affected by the porous structure significantly. These comparisons between the two types of gels again indicated that the swelling and deswelling processes were controlled by a different mechanism. This information could be instructive for the future design of a drug loading process and drug releasing profile using porous gels.

In addition, both solid and porous hydrogels were able to shrink to their original size after a swelling cycle in pH 5.66 and in pH 7.48 buffer, which ensured that the hydrogels respond reversibly at different pHs.

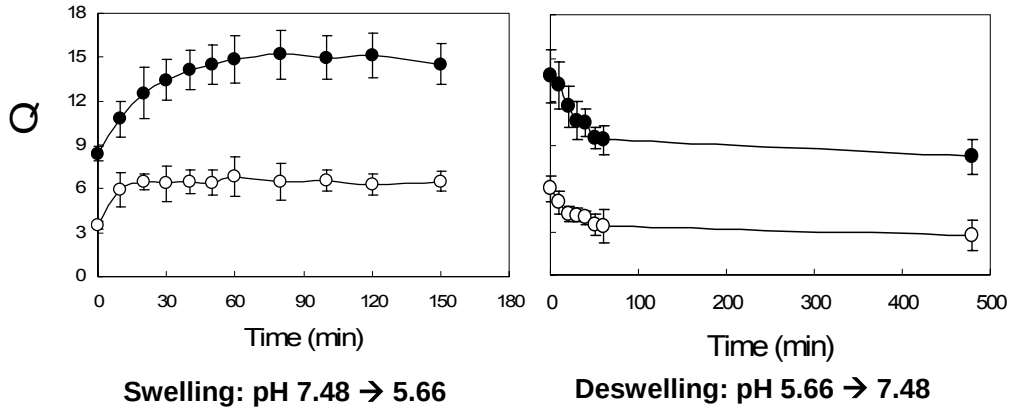

Figure A.5 Dynamic swelling of bulk and porous hydrogels at 37 °C. Hydrogels (PEG200_50% with 0.5 mol% crosslinker) were equilibrated in pH 7.48. (A) Swelling ratio in pH 5.66. Hydrogels were transferred to pH 5.66 phosphate buffer

with 100 mM ionic strength, and weighed every 10 min for an hour, every 20 min for another hour, and every 30 min before reaching equilibrium. (B) Deswelling of the same gels from (A) when transferred back to a buffer at pH 7.48. Hydrogels were transferred to pH 7.48 phosphate buffer at 100 mM ionic strength, and weighed every 10 min for the first hour, and then at eight hours. The average ± S.D. of triplicate samples are shown.

In conclusion, we have successfully fabricated pH-sensitive porous hydrogels which possess 3D periodic pores with controlled size and extensive inter-pores. This porous structure together with pH-sensitivity of the hydrogels could be potentially used as drug delivery system, which can achieve desirable drug loading and drug protection in the pores, as well as a controlled release profile by pore/inter-pore size changes responding to the environmental pH. The future work will focus on the design and understanding the drug loading process and release profile. In addition, using a colloid crystal template to form porous hydrogels with different pore and inter-pore sizes could provide a feasible template working with drug molecules with different size, and provide a variety of different drug dosage and release profiles.

Bibliography

1. Medina-Kauwe, L. K.; Xie, J.; Hamm-Alvarez, S., Intracellular trafficking of nonviral vectors. *Gene Therapy* **2005,** 12, (24), 1734-1751.
2. Putnam, D., Polymers for gene delivery across length scales. *Nature Materials* **2006,** 5, (6), 439-451.
3. Wagner, E.; Kloeckner, J., Gene delivery using polymer therapeutics. *Polymer Therapeutics I: Polymers as Drugs, Conjugates and Gene Delivery Systems* **2006,** 192, 135-173.
4. Tagami, T.; Barichello, J. M.; Kikuchi, H.; Ishida, T.; Kiwada, H., The gene-silencing effect of siRNA in cationic lipoplexes is enhanced by incorporating pDNA in the complex. *International Journal of Pharmaceutics* **2007,** 333, (1-2), 62-69.
5. Devalapally, H.; Shenoy, D.; Little, S.; Langer, R.; Amiji, M., Poly(ethylene oxide)-modified poly(beta-amino ester) nanoparticles as a pH-sensitive system for tumor-targeted delivery of hydrophobic drugs: part 3. Therapeutic efficacy and safety studies in ovarian cancer xenograft model. *Cancer Chemotherapy and Pharmacology* **2007,** 59, (4), 477-484.
6. Borghouts, C.; Kunz, C.; Groner, B., Current strategies for the development of peptide-based anti-cancer therapeutics. *Journal of Peptide Science* **2005,** 11, (11), 713-726.
7. Son, Y. J.; Jang, J. S.; Cho, Y. W.; Chung, H.; Park, R. W.; Kwon, I. C.; Kim, I. S.; Park, J. Y.; Seo, S. B.; Park, C. R.; Jeong, S. Y., Biodistribution and anti-tumor efficacy of doxorubicin loaded glycol-chitosan nanoaggregates by EPR effect. *Journal of Controlled Release* **2003,** 91, (1-2), 135-145.
8. Schweichel, D.; Steitz, J.; Tormo, D.; Gaffal, E.; Ferrer, A.; Buchs, S.; Speuser, P.; Limmer, A.; Tuting, T., Evaluation of DNA vaccination with recombinant adenoviruses using bioluminescence imaging of antigen expression: impact of application routes and delivery with dendritic cells. *Journal of Gene Medicine* **2006,** 8, (10), 1243-1250.

9. Determan, A. S.; Wilson, J. H.; Kipper, M. J.; Wannemuehler, M. J.; Narasimhan, B., Protein stability in the presence of polymer degradation products: Consequences for controlled release formulations. *Biomaterials* **2006,** 27, (17), 3312-3320.
10. Asokan, A.; Cho, M. J., Exploitation of intracellular pH gradients in the cellular delivery of macromolecules. *Journal of Pharmaceutical Sciences* **2002,** 91, (4), 903-913.
11. Akinc, A.; Langer, R., Measuring the pH environment of DNA delivered using nonviral vectors: Implications for lysosomal trafficking. *Biotechnology and Bioengineering* **2002,** 78, (5), 503-508.
12. Wu, G. Y.; Wu, C. H., Receptor-Mediated Gene Delivery and Expression Invivo. *Journal of Biological Chemistry* **1988,** 263, (29), 14621-14624.
13. Leong, K. W.; Mao, H. Q.; Truong-Le, V. L.; Roy, K.; Walsh, S. M.; August, J. T., DNA-polycation nanospheres as non-viral gene delivery vehicles. *Journal of Controlled Release* **1998,** 53, (1-3), 183-193.
14. Davis, S. S., Biomedical applications of nanotechnology - Implications for drug targeting and gene therapy. *Trends in Biotechnology* **1997,** 15, (6), 217-224.
15. Kabanov, A. V., Taking polycation gene delivery systems from in vitro to in vivo. *Pharmaceutical Science & Technology Today* **1999,** 2, (9), 365-372.
16. Caplen, N. J.; Kinrade, E.; Sorgi, F.; Gao, X.; Gruenert, D.; Geddes, D.; Coutelle, C.; Huang, L.; Alton, E.; Williamson, R., In-Vitro Liposome-Mediated DNA Transfection of Epithelial-Cell Lines Using the Cationic Liposome Dc-Chol/Dope. *Gene Therapy* **1995,** 2, (9), 603-613.
17. Wasungu, L.; Hoekstra, D., Cationic lipids, lipoplexes and intracellular delivery of genes. *Journal of Controlled Release* **2006,** 116, (2), 255-264.
18. Luo, D.; Saltzman, W. M., Enhancement of transfection by physical concentration of DNA at the cell surface. *Nature Biotechnology* **2000,** 18, (8), 893-895.
19. Erbacher, P.; Roche, A. C.; Monsigny, M.; Midoux, P., Glycosylated Polylysine DNA Complexes - Gene-Transfer Efficiency in Relation with the Size and the Sugar Substitution Level of Glycosylated Polylysines and with the Plasmid Size. *Bioconjugate Chemistry* **1995,** 6, (4), 401-410.

20. Zauner, W.; Kichler, A.; Schmidt, W.; Sinski, A.; Wagner, E., Glycerol enhancement of ligand-polylysine/DNA transfection. *Biotechniques* **1996,** 20, (5), 905-913.
21. Midoux, P.; Mendes, C.; Legrand, A.; Raimond, J.; Mayer, R.; Monsigny, M.; Roche, A. C., Specific Gene-Transfer Mediated by Lactosylated Poly-L-Lysine into Hepatoma-Cells. *Nucleic Acids Research* **1993,** 21, (4), 871-878.
22. Pouton, C. W.; Seymour, L. W., Key issues in non-viral gene delivery. *Advanced Drug Delivery Reviews* **1998,** 34, (1), 3-19.
23. Akinc, A.; Thomas, M.; Klibanov, A. M.; Langer, R., Exploring polyethylenimine-mediated DNA transfection and the proton sponge hypothesis. *Journal of Gene Medicine* **2005,** 7, (5), 657-663.
24. Wightman, L.; Kircheis, R.; Rossler, V.; Carotta, S.; Ruzicka, R.; Kursa, M.; Wagner, E., Different behavior of branched and linear polyethylenimine for gene delivery in vitro and in vivo. *Journal of Gene Medicine* **2001,** 3, (4), 362-372.
25. Wang, C.; Ge, Q.; Ting, D.; Nguyen, D.; Shen, H. R.; Chen, J. Z.; Eisen, H. N.; Heller, J.; Langer, R.; Putnam, D., Molecularly engineered poly(ortho ester) microspheres for enhanced delivery of DNA vaccines. *Nature Materials* **2004,** 3, (3), 190-196.
26. Roufai, M. B.; Midoux, P., Histidylated polylysine as DNA vector: Elevation of the imidazole protonation and reduced cellular uptake without change in the polyfection efficiency of serum stabilized negative polyplexes. *Bioconjugate Chemistry* **2001,** 12, (1), 92-99.
27. Goncalves, C.; Pichon, C.; Guerin, B.; Midoux, P., Intracellular processing and stability of DNA complexed with histidylated polylysine conjugates. *Journal of Gene Medicine* **2002,** 4, (3), 271-281.
28. Hoffman, A. S.; Stayton, P. S.; Press, O.; Murthy, N.; Lackey, C. A.; Cheung, C.; Black, F.; Campbell, J.; Fausto, N.; Kyriakides, T. R.; Bornstein, P., Design of "smart" polymers that can direct intracellular drug delivery. *Polymers for Advanced Technologies* **2002,** 13, (10-12), 992-999.

29. Schaffer, D. V.; Fidelman, N. A.; Dan, N.; Lauffenburger, D. A., Vector unpacking as a potential barrier for receptor-mediated polyplex gene delivery. *Biotechnology and Bioengineering* **2000,** 67, (5), 598-606.
30. Godbey, W. T.; Wu, K. K.; Mikos, A. G., Poly(ethylenimine) and its role in gene delivery. *Journal of Controlled Release* **1999,** 60, (2-3), 149-160.
31. Akagi, T.; Wang, X.; Uto, T.; Baba, M.; Akashi, M., Protein direct delivery to dendritic cells using nanoparticles based on amphiphilic poly(amino acid) derivatives. *Biomaterials* **2007,** 28, (23), 3427-3436.
32. Gratzer, P. F.; Santerre, J. P.; Lee, J. M., The effect of chemical modification of amino acid side-chains on collagen degradation by enzymes. *Journal of Biomedical Materials Research Part B-Applied Biomaterials* **2007,** 81B, (1), 1-11.
33. Walter, E.; Moelling, K.; Pavlovic, J.; Merkle, H. P., Microencapsulation of DNA using poly(DL-lactide-co-glycolide): stability issues and release characteristics. *Journal of Controlled Release* **1999,** 61, (3), 361-374.
34. Johnston, S. A.; Anziano, P. Q.; Shark, K.; Sanford, J. C.; Butow, R. A., Mitochondrial Transformation in Yeast by Bombardment with Microprojectiles. *Science* **1988,** 240, (4858), 1538-1541.
35. Wang, B.; Ugen, K. E.; Srikantan, V.; Agadjanyan, M. G.; Dang, K.; Refaeli, Y.; Sato, A. I.; Boyer, J.; Williams, W. V.; Weiner, D. B., Gene Inoculation Generates Immune-Responses against Human-Immunodeficiency-Virus Type-1. *Proceedings of the National Academy of Sciences of the United States of America* **1993,** 90, (9), 4156-4160.
36. Dupuis, M.; Denis-Mize, K.; Woo, C.; Goldbeck, C.; Selby, M. J.; Chen, M. C.; Otten, G. R.; Ulmer, J. B.; Donnelly, J. J.; Ott, G.; McDonald, D. M., Distribution of DNA vaccines determines their immunogenicity after intramuscular injection in mice. *Journal of Immunology* **2000,** 165, (5), 2850-2858.
37. Huang, L.; Huang, M.-C.; Wagner, E., *Nonviral Vector for Gene Therapy* Academic Press: San Diego, 1999.
38. Jordan, M.; Schallhorn, A.; Wurm, F. M., Transfecting mammalian cells: Optimization of critical parameters affecting calcium-phosphate precipitate formation. *Nucleic Acids Research* **1996,** 24, (4), 596-601.

39. Cui, Z. R.; Mumper, R. J., Genetic immunization using nanoparticles engineered from microemulsion precursors. *Pharmaceutical Research* **2002,** 19, (7), 939-946.
40. Fu, K.; Pack, D. W.; Klibanov, A. M.; Langer, R., Visual evidence of acidic environment within degrading poly(lactic-co-glycolic acid) (PLGA) microspheres. *Pharmaceutical Research* **2000,** 17, (1), 100-106.
41. Sakiyama-Elbert, S. E.; Hubbell, J. A., Functional biomaterials: Design of novel biomaterials. *Annual Review of Materials Research* **2001,** 31, 183-201.
42. Thomas, M.; Ge, Q.; Lu, J. J.; Chen, J. Z.; Klibanov, A. M., Cross-linked small polyethylenimines: While still nontoxic, deliver DNA efficiently to mammalian cells in vitro and in vivo. *Pharmaceutical Research* **2005,** 22, (3), 373-380.
43. Jones, R. A.; Cheung, C. Y.; Black, F. E.; Zia, J. K.; Stayton, P. S.; Hoffman, A. S.; Wilson, M. R., Poly(2-alkylacrylic acid) polymers deliver molecules to the cytosol by pH-sensitive disruption of endosomal vesicles. *Biochemical Journal* **2003,** 372, 65-75.
44. Uhrich, K. E.; Cannizzaro, S. M.; Langer, R. S.; Shakesheff, K. M., Polymeric systems for controlled drug release. *Chemical Reviews* **1999,** 99, (11), 3181-3198.
45. Rinne, J.; Albarran, B.; Jylhava, J.; Ihalainen, T. O.; Kankaanpaa, P.; Hytonen, V. P.; Stayton, P. S.; Kulomaa, M. S.; Vihinen-Ranta, M., Internalization of novel non-viral vector TAT-streptavidin into human cells. *Bmc Biotechnology* **2007,** 7.
46. Moelle, K.; Tada, Y.; Shibagaki, N.; Knop, J.; Udey, M. C.; von Stebut, E., TAT-fusion protein-transduced Dendritic Cells (DC) efficiently induce CD8(+) T Cells (TC) and vaccinate against leishmaniasis. *Journal of Investigative Dermatology* **2006,** 126, 130-130.
47. Provoda, C. J.; Stier, E. M.; Lee, K. D., Tumor cell killing enabled by listeriolysin O-liposome-mediated delivery of the protein toxin gelonin. *Journal of Biological Chemistry* **2003,** 278, (37), 35102-35108.
48. Cabiaux, V., pH-sensitive toxins: interactions with membrane bilayers and application to drug delivery. *Advanced Drug Delivery Reviews* **2004,** 56, (7), 987-997.
49. Park, T. G.; Jeong, J. H.; Kim, S. W., Current status of polymeric gene delivery systems. *Advanced Drug Delivery Reviews* **2006,** 58, (4), 467-486.

50. Pun, S. H.; Davis, M. E., Development of a nonviral gene delivery vehicle for systemic application. *Bioconjugate Chemistry* **2002,** 13, (3), 630-639.
51. Little, S. R.; Lynn, D. M.; Ge, Q.; Anderson, D. G.; Puram, S. V.; Chen, J. Z.; Eisen, H. N.; Langer, R., Poly-beta amino ester-containing microparticles enhance the activity of nonviral genetic vaccines. *Proceedings of the National Academy of Sciences of the United States of America* **2004,** 101, (26), 9534-9539.
52. Remaut, K.; Lucas, B.; Raemdonck, K.; Braeckmans, K.; Demeester, J.; De Smedt, S. C., Protection of oligonucleotides against enzymatic degradation by pegylated and nonpegylated branched polyethyleneimine. *Biomacromolecules* **2007,** 8, (4), 1333-1340.
53. Ewert, K. K.; Ahmad, A.; Evans, H. M.; Safinya, C. R., Cationic lipid-DNA complexes for non-viral gene therapy: relating supramolecular structures to cellular pathways. *Expert Opinion on Biological Therapy* **2005,** 5, (1), 33-53.
54. Pack, D. W.; Hoffman, A. S.; Pun, S.; Stayton, P. S., Design and development of polymers for gene delivery. *Nature Reviews Drug Discovery* **2005,** 4, (7), 581-593.
55. Cherng, J. Y.; vandeWetering, P.; Talsma, H.; Crommelin, D. J. A.; Hennink, W. E., Effect of size and serum proteins on transfection efficiency of poly((2-dimethylamino)ethyl methacrylate)-plasmid nanoparticles. *Pharmaceutical Research* **1996,** 13, (7), 1038-1042.
56. Banchereau, J.; Steinman, R. M., Dendritic cells and the control of immunity. *Nature* **1998,** 392, (6673), 245-252.
57. Banchereau, J.; Palucka, K.; Pulendran, B., Dendritic cells: A life story. *Journal of Investigative Dermatology* **2000,** 114, (1), 207-207.
58. Banchereau, J.; Briere, F.; Caux, C.; Davoust, J.; Lebecque, S.; Liu, Y. T.; Pulendran, B.; Palucka, K., Immunobiology of dendritic cells. *Annual Review of Immunology* **2000,** 18, 767-+.
59. Palucka, K.; Banchereau, J., Dendritic cells: A link between innate and adaptive immunity. *Journal of Clinical Immunology* **1999,** 19, (1), 12-25.
60. Zarei, S.; Arrighi, J. F.; Ongaro, G.; Calzascia, T.; Haller, O.; Frossard, C.; Piguet, V.; Walker, P. K.; Hauser, C., Efficient induction of CD8 T-associated immune

protection by vaccination with mRNA transfected dendritic cells. *Journal of Investigative Dermatology* **2003,** 121, (4), 745-750.

61. Raychaudhuri, S.; Rock, K. L., Fully mobilizing host defense: Building better vaccines. *Nature Biotechnology* **1998,** 16, (11), 1025-1031.
62. Diebold, S. S.; Montoya, M.; Unger, H.; Alexopoulou, L.; Roy, P.; Haswell, L. E.; Al-Shamkhani, A.; Flavell, R.; Borrow, P.; Sousa, C. R. E., Viral infection switches non-plasmacytoid dendritic cells into high interferon producers. *Nature* **2003,** 424, (6946), 324-328.
63. Greenland, J. R.; Geiben, R.; Ghosh, S.; Pastor, W. A.; Letvin, N. L., Plasmid DNA Vaccine-Elicited Cellular Immune Responses Limit In Vivo Vaccine Antigen Expression through Fas-Mediated Apoptosis. *J Immunol* **2007,** 178, (9), 5652-5658.
64. Awasthi, S.; Cox, R. A., Transfection of murine dendritic cell line (JAWS II) by a nonviral transfection reagent. *Biotechniques* **2003,** 35, (3), 600-+.
65. Irvine, A. S.; Trinder, P. K. E.; Laughton, D. L.; Ketteringham, H.; McDermott, R. H.; Reid, S. C. H.; Haines, A. M. R.; Amir, A.; Husain, R.; Doshi, R.; Young, L. S.; Mountain, A., Efficient nonviral transfection of dendritic cells and their use for in vivo immunization. *Nature Biotechnology* **2000,** 18, (12), 1273-1278.
66. Yoshinaga, T.; Yasuda, K.; Ogawa, Y.; Takakura, Y., Efficient uptake and rapid degradation of plasmid DNA by murine dendritic cells via a specific mechanism. *Biochemical and Biophysical Research Communications* **2002,** 299, (3), 389-394.
67. Gilboa, E., DC-based cancer vaccines. *Journal of Clinical Investigation* **2007,** 117, (5), 1195-1203.
68. Sharp, P. A., RNA interference - 2001. *Genes & Development* **2001,** 15, (5), 485-490.
69. http://www.nastech.com/img/img_rna_interference.gif.
70. Scranton, A. B.; Peppas, N. A., Modern Hydrogel Delivery Systems - Preface. *Advanced Drug Delivery Reviews* **1993,** 11, (1-2), R7-R8.
71. Siegel, R. A.; Firestone, B. A., Ph-Dependent Equilibrium Swelling Properties of Hydrophobic Poly-Electrolyte Copolymer Gels. *Macromolecules* **1988,** 21, (11), 3254-3259.

72. Podual, K.; Doyle, F. J.; Peppas, N. A., Preparation and dynamic response of cationic copolymer hydrogels containing glucose oxidase. *Polymer* **2000,** 41, (11), 3975-3983.

73. Podual, K.; Doyle, F. J.; Peppas, N. A., Dynamic behavior of glucose oxidase-containing microparticles of poly(ethylene glycol)-grafted cationic hydrogels in an environment of changing pH. *Biomaterials* **2000,** 21, (14), 1439-1450.

74. Engin, K.; Leeper, D. B.; Cater, J. R.; Thistlethwaite, A. J.; Tupchong, L.; McFarlane, J. D., Extracellular Ph Distribution in Human Tumors. *International Journal of Hyperthermia* **1995,** 11, (2), 211-216.

75. Gao, Z. G.; Lee, D. H.; Kim, D. I.; Bae, Y. H., Doxorubicin loaded pH-sensitive micelle targeting acidic extracellular pH of human ovarian A2780 tumor in mice. *Journal of Drug Targeting* **2005,** 13, (7), 391-397.

76. Lee, E. S.; Oh, K. T.; Kim, D.; Youn, Y. S.; Bae, Y. H., Tumor pH-responsive flower-like micelles of poly(L-lactic acid)-b-poly (ethylene glycol)-b-poly(L-histidine). *Journal of Controlled Release* **2007,** 123, (1), 19-26.

77. Lee, A. S.; Gast, A. P.; Butun, V.; Armes, S. P., Characterizing the structure of pH dependent polyelectrolyte block copolymer micelles. *Macromolecules* **1999,** 32, (13), 4302-4310.

78. Lawrence, M. J.; Rees, G. D., Microemulsion-based media as novel drug delivery systems. *Advanced Drug Delivery Reviews* **2000,** 45, (1), 89-121.

79. Schwarte, L. M.; Peppas, N. A., Novel poly(ethylene glycol)-grafted, cationic hydrogels: preparation, characterization and diffusive properties. *Polymer* **1998,** 39, (24), 6057-6066.

80. De, S. K.; Aluru, N. R.; Johnson, B.; Crone, W. C.; Beebe, D. J.; Moore, J., Equilibrium swelling and kinetics of pH-responsive hydrogels: Models, experiments, and simulations. *Journal of Microelectromechanical Systems* **2002,** 11, (5), 544-555.

81. Podual, K.; Peppas, N. A., Relaxational behavior and swelling-pH master curves of poly[(diethylaminoethyl methacrylate)-graft-(ethylene glycol)] hydrogels. *Polymer International* **2005,** 54, (3), 581-593.

82. Amalvy, J. I.; Unali, G. F.; Li, Y.; Granger-Bevan, S.; Armes, S. P.; Binks, B. P.; Rodrigues, J. A.; Whitby, C. P., Synthesis of sterically stabilized polystyrene latex particles using cationic block copolymers and macromonomers and their application as stimulus-responsive particulate emulsifiers for oil-in-water emulsions. *Langmuir* **2004,** 20, (11), 4345-4354.
83. Amalvy, J. I.; Wanless, E. J.; Li, Y.; Michailidou, V.; Armes, S. P.; Duccini, Y., Synthesis and characterization of novel pH-responsive microgels based on tertiary amine methacrylates. *Langmuir* **2004,** 20, (21), 8992-8999.
84. Plunkett, K. N.; Moore, J. S., Patterned dual pH-responsive core-shell hydrogels with controllable swelling kinetics and volumes. *Langmuir* **2004,** 20, (16), 6535-6537.
85. Funhoff, A. M.; van Nostrum, C. F.; Koning, G. A.; Schuurmans-Nieuwenbroek, N. M. E.; Crommelin, D. J. A.; Hennink, W. E., Endosomal escape of polymeric gene delivery complexes is not always enhanced by polymers buffering at low pH. *Biomacromolecules* **2004,** 5, (1), 32-39.
86. Jotwani, R.; Pulendran, B.; Agrawal, S.; Cutler, C. W., Human dendritic cells respond to Porphyromonas gingivalis LPS by promoting a Th2 effector response in vitro. *European Journal of Immunology* **2003,** 33, (11), 2980-2986.
87. Thiele, L.; Rothen-Rutishauser, B.; Jilek, S.; Wunderli-Allenspach, H.; Merkle, H. P.; Walter, E., Evaluation of particle uptake in human blood monocyte-derived cells in vitro. Does phagocytosis activity of dendritic cells measure up with macrophages? *Journal of Controlled Release* **2001,** 76, (1-2), 59-71.
88. Vallhov, H.; Qin, J.; Johansson, S. M.; Ahlborg, N.; Muhammed, M. A.; Scheynius, A.; Gabrielsson, S., The importance of an endotoxin-free environment during the production of nanoparticles used in medical applications. *Nano Letters* **2006,** 6, (8), 1682-1686.
89. Sonawane, N. D.; Szoka, F. C.; Verkman, A. S., Chloride accumulation and swelling in endosomes enhances DNA transfer by polyamine-DNA polyplexes. *Journal of Biological Chemistry* **2003,** 278, (45), 44826-44831.
90. Zuidam, N. J.; Posthuma, G.; de Vries, E. T. J.; Crommelin, D. J. A.; Hennink, W. E.; Storm, G., Effects of physicochemical characteristics of

poly(2-(dimethylamino)ethyl methacrylate)-based polyplexes on cellular association and internalization. *Journal of Drug Targeting* **2000,** 8, (1), 51-+.

91. Shen, Z. H.; Reznikoff, G.; Dranoff, G.; Rock, K. L., Cloned dendritic cells can present exogenous antigens on both MHC class I and class II molecules. *Journal of Immunology* **1997,** 158, (6), 2723-2730.
92. Jain, S.; Yap, W. T.; Irvine, D. J., Synthesis of protein-loaded hydrogel particles in an aqueous two-phase system for coincident antigen and CpG oligonucleotide delivery to antigen-presenting cells. *Biomacromolecules* **2005,** 6, (5), 2590-2600.
93. Heinzen, R. A.; Hackstadt, T., The Chlamydia trachomatis parasitophorous vacuolar membrane is not passively permeable to low-molecular-weight compounds. *Infection and Immunity* **1997,** 65, (3), 1088-1094.
94. Hong, S. P.; Leroueil, P. R.; Janus, E. K.; Peters, J. L.; Kober, M. M.; Islam, M. T.; Orr, B. G.; Baker, J. R.; Holl, M. M. B., Interaction of polycationic polymers with supported lipid bilayers and cells: Nanoscale hole formation and enhanced membrane permeability. *Bioconjugate Chemistry* **2006,** 17, (3), 728-734.
95. Yoshimori, T.; Yamamoto, A.; Moriyama, Y.; Futai, M.; Tashiro, Y., Bafilomycin-A1, a Specific Inhibitor of Vacuolar-Type H+-Atpase, Inhibits Acidification and Protein-Degradation in Lysosomes of Cultured-Cells. *Journal of Biological Chemistry* **1991,** 266, (26), 17707-17712.
96. Drin, G.; Cottin, S.; Blanc, E.; Rees, A. R.; Temsamani, J., Studies on the internalization mechanism of cationic cell-penetrating peptides. *Journal of Biological Chemistry* **2003,** 278, (33), 31192-31201.
97. Pack, D. W.; Putnam, D.; Langer, R., Design of imidazole-containing endosomolytic biopolymers for gene delivery. *Biotechnology and Bioengineering* **2000,** 67, (2), 217-223.
98. van Dijk-Wolthuis, W. N. E.; van de Wetering, P.; Hinrichs, W. L. J.; Hofmeyer, L. J. F.; Liskamp, R. M. J.; Crommelin, D. J. A.; Hennink, W. E., A versatile method for the conjugation of proteins and peptides to poly[2-(dimethylamino)ethyl methacrylate]. *Bioconjugate Chemistry* **1999,** 10, (4), 687-692.

99. Rungsardthong, U.; Ehtezazi, T.; Bailey, L.; Armes, S. P.; Garnett, M. C.; Stolnik, S., Effect of polymer ionization on the interaction with DNA in nonviral gene delivery systems. *Biomacromolecules* **2003,** 4, (3), 683-690.

100. Rungsardthong, U.; Deshpande, M.; Bailey, L.; Vamvakaki, M.; Armes, S. P.; Garnett, M. C.; Stolnik, S., Copolymers of amine methacrylate with poly(ethylene glycol) as vectors for gene therapy. *Journal of Controlled Release* **2001,** 73, (2-3), 359-380.

101. Asayama, S.; Maruyama, A.; Cho, C. S.; Akaike, T., Design of comb-type polyamine copolymers for a novel pH-sensitive DNA carrier. *Bioconjugate Chemistry* **1997,** 8, (6), 833-838.

102. You, Y. Z.; Manickam, D. S.; Zhou, Q. H.; Oupicky, D., Reducible poly(2-dimethylaminoethyl methaerylate): Synthesis, cytotoxicity, and gene delivery activity. *Journal of Controlled Release* **2007,** 122, (3), 217-225.

103. Tan, J. F.; Ravi, P.; Too, H. P.; Hatton, T. A.; Tam, K. C., Association behavior of biotinylated and non-biotinylated poly(ethylene oxide)-b-poly(2-(diethylamino) ethyl methacrylate). *Biomacromolecules* **2005,** 6, (1), 498-506.

104. Kumari, K.; Gulati, S.; Smith, D. F.; Gulati, U.; Cummings, R. D.; Air, G. M., Receptor binding specificity of recent human H3N2 influenza viruses. *Virology Journal* **2007,** 4.

105. Inaba, K.; Inaba, M.; Romani, N.; Aya, H.; Deguchi, M.; Ikehara, S.; Muramatsu, S.; Steinman, R. M., Generation of large number of dendritic cells from mouse bone-marrow cultures supplemented with granulocyte macrophage colony-stimulating factor. *Journal of Experimental Medicine* **1992,** 176, (6), 1693-1702.

106. Clarke, S. R. M.; Barnden, M.; Kurts, C.; Carbone, F. R.; Miller, J. F.; Heath, W. R., Characterization of the ovalbumin-specific TCR transgenic line OT-I: MHC elements for positive and negative selection. *Immunology and Cell Biology* **2000,** 78, (2), 110-117.

107. Larsson, M.; Messmer, D.; Somersan, S.; Fonteneau, J. F.; Donahoe, S. M.; Lee, M.; Dunbar, P. R.; Cerundolo, V.; Julkunen, I.; Nixon, D. F.; Bhardwaj, N., Requirement of mature dendritic cells for efficient activation of influenza

A-specific memory CD8(+) T cells. *Journal of Immunology* **2000,** 165, (3), 1182-1190.

108. Swanson, M. S.; Isberg, R. R., Identification of Legionella pneumophila mutants that have aberrant intracellular fates. *Infection and Immunity* **1996,** 64, (7), 2585-2594.
109. Refolo, L. M.; Sambamurti, K.; Efthimiopoulos, S.; Pappolla, M. A.; Robakis, N. K., Evidence that secretase cleavage of cell-surface Alzheimer Amyloid precursor occurs after normal endocytic internalization *Journal of Neuroscience Research* **1995,** 40, (5), 694-706.
110. Schleiss, M.; Lacayo, J.; Belkaid, Y.; McGregor, A.; Stroup, G.; Rayner, J.; Alterson, K.; Chulay, J.; Smith, J., Vaccination as an antiviral strategy for control of cytomegalovirus (CMV) disease: A vectored vaccine approach targeting the UL83 (pp65) homolog protects against congenital CMV disease in the guinea pig model. *Antiviral Research* **2007,** 74, (3), A42-A42.
111. Wills, M. R.; Carmichael, A. J.; Mynard, K.; Jin, X.; Weekes, M. P.; Plachter, B.; Sissons, J. G. P., The human cytotoxic T-lymphocyte (CTL) response to cytomegalovirus is dominated by structural protein pp65: Frequency, specificity, and T-cell receptor usage of pp65-specific CTL. *Journal of Virology* **1996,** 70, (11), 7569-7579.
112. Tabi, Z.; Moutaftsi, M.; Borysiewicz, L. K., Human cytomegalovirus pp65-and immediate early 1 antigen-specific HLA class I-restricted cytotoxic T cell responses induced by cross-presentation of viral antigens. *Journal of Immunology* **2001,** 166, (9), 5695-5703.
113. Brignone, C.; Grygar, C.; Marcu, M.; Perrin, G.; Triebel, F., IMP321 (sLAG-3) safety and T cell response potentiation using an influenza vaccine as a model antigen: A single-blind phase I study. *Vaccine* **2007,** 25, (24), 4641-4650.
114. Walker, E. B.; Haley, D.; Miller, W.; Floyd, K.; Wisner, K. P.; Sanjuan, N.; Maecker, H.; Romero, P.; Hu, H. M.; Alvord, W. G.; Smith, J. W.; Fox, B. A.; Urba, W. J., gp100(209-2M) peptide immunization of human lymphocyte antigen-A2(+) stage I-III melanoma patients induces significant increase in antigen-specific

effector and long-term memory CD8(+) T cells. *Clinical Cancer Research* **2004,** 10, (2), 668-680.

115. Moghimi, S. M.; Hunter, A. C.; Murray, J. C., Long-circulating and target-specific nanoparticles: Theory to practice. *Pharmacological Reviews* **2001,** 53, (2), 283-318.
116. Jilek, S.; Zurkaulen, H.; Pavlovic, J.; Merkle, H. P.; Walter, E., Transfection of a mouse dendritic cell line by plasmid DNA-loaded PLGA microparticles in vitro. *European Journal of Pharmaceutics and Biopharmaceutics* **2004,** 58, (3), 491-499.
117. Murata, Y.; Ohteki, T.; Koyasu, S.; Hamuro, J., IFN-gamma and pro-inflammatory cytokine production by antigen-presenting cells is dictated by intracellular thiol redox status regulated by oxygen tension. *European Journal of Immunology* **2002,** 32, (10), 2866-2873.
118. Han, G.; Chari, N. S.; Verma, A.; Hong, R.; Martin, C. T.; Rotello, V. M., Controlled recovery of the transcription of nanoparticle-bound DNA by intracellular concentrations of glutathione. *Bioconjugate Chemistry* **2005,** 16, (6), 1356-1359.
119. Han, G.; Hong, R.; Fernandez, J.; Kim, B. J.; Forbes, N. S.; Rotello, V. M., Glutathione-mediated drug release using monolayer protected nanoparticle carriers. *Abstracts of Papers of the American Chemical Society* **2006,** 231, 1.
120. Hong, R.; Han, G.; Fernandez, J. M.; Kim, B. J.; Forbes, N. S.; Rotello, V. M., Glutathione-mediated delivery and release using monolayer protected nanoparticle carriers. *Journal of the American Chemical Society* **2006,** 128, (4), 1078-1079.
121. Giri, S.; Trewyn, B. G.; Stellmaker, M. P.; Lin, V. S. Y., Stimuli-responsive controlled-release delivery system based on mesoporous silica nanorods capped with magnetic nanoparticles. *Angewandte Chemie-International Edition* **2005,** 44, (32), 5038-5044.
122. Kam, N. W. S.; Liu, Z.; Dai, H. J., Functionalization of carbon nanotubes via cleavable disulfide bonds for efficient intracellular delivery of siRNA and potent gene silencing. *Journal of the American Chemical Society* **2005,** 127, (36), 12492-12493.
123. Hassan, S. S. M.; Rechnitz, G. A., Determination of Glutathione and Glutathione-Reductase with a Silver Sulfide Membrane-Electrode. *Analytical Chemistry* **1982,** 54, (12), 1972-1976.

124. Jones, D. P.; Carlson, J. L.; Samiec, P. S.; Sternberg, P.; Mody, V. C.; Reed, R. L.; Brown, L. A. S., Glutathione measurement in human plasma Evaluation of sample collection, storage and derivatization conditions for analysis of dansyl derivatives by HPLC. *Clinica Chimica Acta* **1998,** 275, (2), 175-184.
125. Anderson, M. E.; Luo, J. L., Glutathione therapy: From prodrugs to genes. *Seminars in Liver Disease* **1998,** 18, (4), 415-424.
126. Anderson, M. E., Glutathione: an overview of biosynthesis and modulation. *Chemico-Biological Interactions* **1998,** 112, 1-14.
127. Burnham, M. R.; Turner, J. N.; Szarowski, D.; Martin, D. L., Biological functionalization and surface micropatterning of polyacrylamide hydrogels. *Biomaterials* **2006,** 27, (35), 5883-5891.
128. Hiratani, H.; Alvarez-Lorenzo, C.; Chuang, J.; Guney, O.; Grosberg, A. Y.; Tanaka, T., Effect of reversible cross-linker, N,N '-bis(acryloyl)cystamine, on calcium ion adsorption by imprinted gels. *Langmuir* **2001,** 17, (14), 4431-4436.
129. Emilitri, E.; Ranucci, E.; Ferruti, P., New poly(amidoamine)s containing disulfide linkages in their main chain. *Journal of Polymer Science Part a-Polymer Chemistry* **2005,** 43, (7), 1404-1416.
130. Serra, L.; Domenech, J.; Peppas, N. A., Drug transport mechanisms and release kinetics from molecularly designed poly(acrylic acid-g-ethylene glycol) hydrogels. *Biomaterials* **2006,** 27, (31), 5440-5451.
131. Wang, Y. J.; Jiang, H. L.; Hu, Y. Q.; Zhu, K. J., Biodegradable heparin/ampholytic chitosan complexes for pH-sensitive release of proteins. *Acta Polymerica Sinica* **2005**, (4), 524-528.
132. Ward, J. H.; Peppas, N. A., Preparation of controlled release systems by free-radical UV polymerizations in the presence of a drug. *Journal of Controlled Release* **2001,** 71, (2), 183-192.
133. Peppas, N. A., Devices based on intelligent biopolymers for oral protein delivery. *International Journal of Pharmaceutics* **2004,** 277, (1-2), 11-17.
134. Peppas, N. A.; Khare, A. R., Preparation, Structure and Diffusional Behavior of Hydrogels in Controlled-Release. *Advanced Drug Delivery Reviews* **1993,** 11, (1-2), 1-35.

135. Khare, A. R.; Peppas, N. A., Release Behavior of Bioactive Agents from Ph-Sensitive Hydrogels. *Journal of Biomaterials Science-Polymer Edition* **1993,** 4, (3), 275-289.
136. Sheridan, M. H.; Shea, L. D.; Peters, M. C.; Mooney, D. J., Bioadsorbable polymer scaffolds for tissue engineering capable of sustained growth factor delivery. *Journal of Controlled Release* **2000,** 64, (1-3), 91-102.
137. Murphy, W. L.; Dennis, R. G.; Kileny, J. L.; Mooney, D. J., Salt fusion: An approach to improve pore interconnectivity within tissue engineering scaffolds. *Tissue Engineering* **2002,** 8, (1), 43-52.
138. Irvine, D. J.; Stachowiak, A.; Jain, S., Engineering biomaterials for control of immune cell functions. In *Thermec'2003, Pts 1-5*, Trans Tech Publications Ltd: Zurich-Uetikon, 2003; Vol. 426-4, pp 3213-3218.
139. Stachowiak, A.; Irvine, D. J., Toward an in vitro model of the lymph node T zone. *Faseb Journal* **2004,** 18, (4), A429-A429.
140. Stachowiak, A. N.; Bershteyn, A.; Tzatzalos, E.; Irvine, D. J., Bioactive hydrogels with an ordered cellular structure combine interconnected macroporosity and robust mechanical properties. *Advanced Materials* **2005,** 17, (4), 399-+.
141. Velev, O. D.; Lenhoff, A. M., Colloidal crystals as templates for porous materials. *Current Opinion in Colloid & Interface Science* **2000,** 5, (1-2), 56-63.
142. Gates, B.; Xia, Y., Photonic band-gap properties of opaline lattices of spherical colloids doped with various concentrations of smaller colloids. *Applied Physics Letters* **2001,** 78, (21), 3178-3180.
143. Gates, B.; Lu, Y.; Li, Z. Y.; Xia, Y., Fabrication and characterization of photonic crystals with well-controlled thickness and stop-band attenuation. *Applied Physics a-Materials Science & Processing* **2003,** 76, (4), 509-513.
144. Xia, Y. N.; Gates, B.; Yin, Y. D.; Lu, Y., Monodispersed colloidal spheres: Old materials with new applications. *Advanced Materials* **2000,** 12, (10), 693-713.
145. Lu, Y.; Yin, Y. D.; Gates, B.; Xia, Y. N., Growth of large crystals of monodispersed spherical colloids in fluidic cells fabricated using non-photolithographic methods. *Langmuir* **2001,** 17, (20), 6344-6350.

146. Braun, P. V.; Zehner, R. W.; White, C. A.; Weldon, M. K.; Kloc, C.; Patel, S. S.; Wiltzius, P., Epitaxial growth of high dielectric contrast three-dimensional photonic crystals. *Advanced Materials* **2001,** 13, (10), 721-724.
147. Vlasov, Y. A.; Bo, X. Z.; Sturm, J. C.; Norris, D. J., On-chip natural assembly of silicon photonic bandgap crystals. *Nature* **2001,** 414, (6861), 289-293.

Biographical Note

Yuhua Hu

Education

Massachusetts Institute of Technology **Cambridge, MA**

Ph.D. in Chemical Engineering (08/2001–04/2008)

M.S. in Chemical Engineering Practice (08/2001–06/2003)

Tsinghua University **Beijing, PR China**

M.S. in Biochemical Engineering (08/1999–06/2001)

B.S. in Chemical Engineering (08/1995–06/1999)

Research Experience

Massachusetts Institute of Technology **Cambridge, MA**

Research Assistant in Biomaterials and Immune System Engineering Lab (11/2004–04/2008)

- Synthesizing and characterizing biodegradable nanoparticles, and studying their application as an intracellular drug delivery system for siRNA delivery, protein delivery in immunotherapy
- Synthesized pH-sensitive core–shell nanoparticles and characterized their physicochemical properties
- Synthesized pH-sensitive porous hydrogel scaffold for tissue engineering

Research Assistant in Nanomaterials Research Lab (NMRL) (08/2002–11/2004)

- Studied glucose-responsive insulin delivery hydrogel in animal model
- Designed and synthesized non-viral gene delivery system for liver cancer therapy
- Synthesized hydroxyapatite nanoparticles for bone remediation application
-

Practice School of MIT Chemical Engineering Department (06/2002–08/2002)

- Studied the viscosity effects of ultra-low molecular weight synthetic polymers in an insulin controlled release system (Alkermes Inc.)
- Modified the product line for wheat chex in pilot plant, and studied and simulated toaster behavior of wheat chex product line (General Mills, Inc.)

Tsinghua University Beijing, PR China

Research Assistant in Bioreactor and Bioengineering Lab (04/2000–07/2001)

- Designed and produced several kinds of Oral Osmotic Pumps with polymeric materials for sustained and controlled release
- Characterized the physicochemical properties of synthetic biomaterials

Research Assistant in Bioreactor and Bioengineering Lab (08/1998–06/1999)

- Studied the petrochemical industrial wastewater treatment with air-lifted column
- Characterized the removal of nitrogenous compounds in air-lifted column with porous carriers

Teaching Experience

Massachusetts Institute of Technology Cambridge, MA

Supervisor in Undergraduate Research Opportunity Program of MIT (03/2003–06/2008)

- Study of biodegradability of nanoparticles (03/2007– 06/2008)
- Synthesis of pH-sensitive nanoparticles by emulsion polymerization (05/2006–02/2007)
- Purification of insulin conjugates by HPLS (03/2004–11/2004)
- Synthesis of glucose-responsive hydrogel (02/2003–9/2003)

Teaching assistant (02/2004–05/2004), Chemical Engineering Department

Course: 10.26 Chemical Engineering Projects Laboratory

- Study of material properties for protection from chemical warfare agent
- Addition of ingredients to functional foods using nanoparticles

Tsinghua University **Beijing, PR China**

Teaching assistant (02/2000–07/2000), Chemical Engineering Department

Course: Principles of Chemical Engineering, Tsinghua, PR China

Honors and Awards

2007 Best Graduate Student Research Award, Biomedical Engineering Society

2007 Best Poster Winner in Chemical Engineering Department at MIT

2000 Guanghua Fellowship

2000 Excellent Undergraduate Thesis

1999 Excellent Undergraduate Honor

1998 Oriental Dong Fellowship

1997 Excellent Student Fellowship

1997 German Fellowship

1996 Excellent Student Scholarship

Publications

"Regulation of Intracellular delivery by core–shell nanoparticles via electrostatic surface binding of protein or siRNA cargos'' (Biomacromolecules, in preparation)

"Relationship between swelling and pore morphology in pH-sensitive inverse opal gel membranes'' (Soft Matter, in preparation).

A. Verma, O. Uzun, **Y. Hu**, Y. Hu, N. Watson, S. Chen, D.J. Irvine, F. Stellacci, "Nanoscale surface structure impacts the interaction of nanoparticles with living cells", *Nature Materials*, 2008, (accepted).

Y. Hu, T. Litwin, A. R. Nagaraja, B. Kwong, J. Katz, N. Watson, D. J. Irvine, "Cytosolic Delivery of membrane-impermeable molecules in dendritic cells using pH-sensitive core–shell nanoparticles", *Nano Letters,* 2007, 7(10) 3056–3064.

L. Ye, **Y. Hu**, J. Chen, "Study on delivery characteristics of oral osmotic pump system of verapamil hydrochloride", *Chinese Journal of Pharmaceuticals*, 2002, 33 (12) 590–592.

Y. Hu, F. Ding, Y. Fan, "Effects of organic carbon resource on process of simultaneous nitrification and denitrification", *Environmental Engineering*, 2001, 19(4) 17–20.

Scientific Presentations

Materials Research Society Fall meeting, Nov 2007, Boston, MA

Oral Presentation "Intracellular delivery of membrane-impermeable macromolecules using biodegradable pH-sensitive core–shell nanoparticles"

Biomedical Engineering Society annual meeting, Sept 2007, Los Angeles, CA

Oral Presentation "Cytosolic drug delivery in dendritic cells by pH-sensitive core–shell nanoparticles". Awarded **Best Graduate Student Research Awards**

American Chemical Society Spring meeting, Mar 2007, Chicago, IL

Oral Presentation "Intracellular drug delivery via pH-sensitive hydrogel nanoparticles".

Materials Research Society Fall meeting, Nov 2005, Boston, MA

Poster presentation "pH-sensitive inverse opal hydrogel for gene delivery". Nominated Best Poster Awards

3rd China-USA Joint Conference of Chemical Engineering, Jun 2000, Beijing, China

Oral presentation "Simultaneous nitrification and denitrification in a bubble column with porous carrier"

2nd Annual Symposium on Chemical Engineering and Material Science, Oct 1999, Beijing, China

Oral presentations "Degradation of petrochemical wastewater by activated sludge – I effects of the operation conditions" and "Degradation of petrochemical wastewater by activated sludge – II the study of dynamics"

Patent Pending

Y. Hu, D. J. Irvine, "Biodegradable pH-sensitive core–shell nanoparticles for intracellular drug delivery", US patent, (submitted to MIT Technology Licensing Office, Aug 2007).